2011

The Application of Two-photon Absorbing Probes in Lysosomal, Zinc Ion Sensing and Folate Receptor-targeted Bioimaging

Xuhua Wang
University of Central Florida

THE APPLICATION OF TWO-PHOTON ABSORBING PROBES IN LYSOSOMAL, ZINC ION SENSING AND FOLATE RECEPTOR-TARGETED BIOIMAGING

by

XUHUA WANG

M.S. Shanghai Institute of Material Medica, Chinese Academy of Sciences, 2007

A dissertation submitted in partial fulfillment of the requirements
for the degree of Doctor of Philosophy
in the Department of Chemistry
in the College of Sciences
at the University of Central Florida
Orlando, Florida

Spring Term
2011

Major Professor: Kevin D. Belfield

ABSTRACT

Two-photon fluorescence microscopy (2PFM) has become a powerful technique for bioimaging in non-invasive cancer diagnosis and also investigating the mechanization and original of a variety of diseases by tracking various biological processes. Because the fluorescence emission by two photon absorbing (2PA) is directly proportional to the square of the intensity of excitation light, this intrinsic property of 2PA provides 2PFM great advantages over traditional one-photon fluorescence microscopy (1PFM), including high 3D spatial localization, less photodamage and interference from biological tissue because of using longer wavelength excitation (700-1300 nm). However, most 2PA probes are hydrophobic and their photostabilities are questionable, severely limiting their biological and medical applications. In addition, probes with significant specificity for certain organelles for tracking cellular processes or metal ions for monitoring neural transmission are somewhat rare. Moreover, it is also very significant to deliver the probes to specific disease sites for early cancer diagnosis.

In order to increase the water solubility of probes, polyethylene glycol (PEG) was introduced to a fluorene-based 2PA probe LT1 for lysosomal 2PFM cell imaging. The 2PFM bioimaging application of the novel two-photon absorbing fluorene derivative LT1, selective for the lysosomes of HCT 116 cancer cells is described in Chapter II. Linear and nonlinear photophysical and photochemical properties of the probe were investigated to evaluate the potential of the probe for 2PFM lysosomal imaging. After the investigation of the cytotoxicity of this new probe, colocalization studies of the probe with commercial lysosomal probe Lysotracker Red in HCT 116 cells were conducted. A high colocalization coefficient (0.96) was achieved and

demonstrated the specific localization of the probe in lysosomes. A figure of merit, F_M, was introduced by which all fluorescent probes for 2PFM can be compared. LT1 was demonstrated to have a number of properties that far exceed those of commercial lysotracker probes, including much higher 2PA cross sections, good fluorescence quantum yield, and, importantly, high photostability, all resulting in a superior figure of merit. Consequently, 2PFM was used to demonstrate lysosomal tracking with LT1.

In addition to lysosomes, it is also very significant to investigate the physiological roles of free metal ions in biological processes, especially Zn^{2+}, because Zn^{2+} normally serves either as the catalytic elements in enzymatic activity centers or as structural elements in enzymes and transcription factors. However, biocompatible and effective Zn^{2+} probes for 2PFM bioimaging are infrequent. In Chapter III, 2PFM bioimaging with a hydrophilic 2PA Zn^{2+} sensing fluorescent probe, bis(1,2,3-triazolyl)fluorene derivative, is described. 2PFM bioimaging of the probe in living HeLa cancer cells was demonstrated. The results revealed a significant fluorescence increase upon introduction of Zn^{2+} into the cancer cells, and a reversible Zn^{2+} binding to the probe was also demonstrated, providing a robust probe for two-photon fluorescence zinc ion sensing.

Early cancer diagnosis is another critical application for 2PFM, but there are still huge challenges for this new technique in clinical areas. Most 2PA probes with large two-photon absorbing cross sections and fluorescence quantum efficiency are synthetically more accessible in hydrophobic forms. In order to increase the efficiency of the probes and minimize the effect of the probe on the human body, delivery of the probe specifically to cancer sites is desired. The

synthesis and characterization of narrow dispersity organically modified silica nanoparticles (SiNPs), diameter ~30 nm, entrapping a hydrophobic two-photon absorbing fluorenyl dye, are reported in Chapter IV. The surface of the SiNPs was functionalized with folic acid to specifically deliver the probe to folate receptor (FR) over-expressing HeLa cells, making these folate 2PA dye-doped SiNPs potential candidates as probes for two-photon fluorescence microscopy (2PFM) bioimaging. In vitro studies using FR over-expressing HeLa cells demonstrated specific cellular uptake of the functionalized nanoparticles. However, when the concentration of the dye in SiNPs increased for higher signal output, the fluorescence quantum efficiency of a probe normally decreases because of self-quenching. In Chapter V, a near-infrared (NIR) emitting probe is reported to overcome this limitation through both aggregate-enhanced fluorescence emission and aggregate enhanced two-photon absorption. The dye was encapsulated in SiNPs and the surface of the nanoparticles was functionalized with PEG followed by a folic acid derivative to specifically target folate receptors. NIR emission is important for deep tissue imaging. *In vitro* studies using HeLa cells that upregulate folate receptors indicated specific cellular uptake of the folic acid functionalized SiNP nanoprobe. Meanwhile, the probe was also investigated for live animal imaging by employing mice bearing HeLa tumors for *in vivo* studies. *Ex vivo* 2PFM tumor imaging was then conducted to achieve high quality 3D thick tissue tumor images.

PUBLICATIONS TO DATE FROM DISSERTATION WORK

1. Wang, X.; Nguyen, D. M.; Yanez, C. O.; Rodriguez, L.; Ahn, H.; Bondar, M. V.; Belfield, K. D. *J. Am. Chem. Soc.* **2010**, *132*, 12237-12239.

2. Wang, X.; Yao, S.; Ahn, H.; Zhang, Y.; Bondar, M. V.; Torres, J. A.; Belfield, K. D. *Biomedical Optics Express* **2010**, *1*, 453-462.

3. Yao, S.; Ahn, H.; Wang, X.; Fu, J.; Van Stryland, E. W.; Hagan, D. J.; Belfield, K. D. *J. Org. Chem.* **2010**, *75*, 3965-3974.

4. Nguyen, D. M.; Wang, X.; Ahn, H.; Rodriguez, L.; Bondar, M. V. Belfield, K. D. *ACS Applied Materials & Interfaces* **2010**, *2*, 2978-2981.

5. Biswas, S.; Wang, X.; Morales, A. R.; Ahn, H.; Belfield, K. D. *Biomacromolecules* **2011**, *12*, 441-449.

6. Belfield, K. D.; Bondar, M. V.; Hernandez, F. E.; Przhonska, O. V.; Wang, X.; Yao, S. *Physical Chemistry Chemical Physics* **2011**, *13*, 4303-4310.

7. Andrade, C. D.; Yanez, C. O.; Qaddoura, M. A.; Wang, X.; Arnett, C. L.; Coombs, S. A.; Yu, J.; Bassiouni, R.; Bondar, M. V.; Belfield, K. D. *Journal of Fluorescence.* **2011**, in press, DOI: 10.1007/s10895-010-0801-3.

8. Belfield, K. D.; Bondar, M. V.; Morales, A. R.; Padilha, L. A.; Przhonska, O. V.; Wang, X. *J. Am. Chem. Soc.* **2011**, submitted.

9. Wang, X.; Morales, A. R.; Urakami, T.; Zhang, L.; Bondar, M. V.; Komatsu, M.; Belfield, K. D. *J. Am. Chem. Soc.* **2011**, submitted.

To my family, especially to Xiaofang Jiang, my wife, who has accompanied me in my entire academic research experience and provided me with great love.

ACKNOWLEDGMENTS

First of all, I would like to thank my advisor Prof. Kevin D. Belfield who gave me this great opportunity to work with so many bright and diligent colleagues in this exciting research area. Dr. Belfield's constant support, encouragement, and valuable guidance have led me to consolidate this dissertation. Because of his enthusiasms for diverse research areas, I was motivated to explore the magic applications by investigating the interrelationship of Optics & Photonics, Material Science, and Biological Science. His valuable suggestions and insightful discussions were also greatly appreciated.

I would also like to thank my colleagues from Dr. Belfield's research group for their enjoyable friendship and constant advice throughout my research experience. Especially, I would like to thank Dr. Sheng Yao, Dr. Alma R. Morales, and Dr. Dao M. Nguyen for their generous advice and sharing their precious compounds. I would also like to acknowledge Hyo-yang Ahn for her helping in nonlinear spectroscopy and Dr. Mykhailo Bondar for his valuable suggestions in photostability experiments. In addition, I am also grateful for Dr. Cicerone O. Yanez who taught me how to use the home-built two-photon laser-scanning microscope for two-photon bioimaging and shared his biological research experiences, and Dr. Sanchita Biswas who taught me how to use gel permeation chromatography (GPC) and entrusted me with her dye and biomolecular conjugated block copolymer. Finally, I want to acknowledge Dr. Takeo Urakami and Dr. Masanobu Komatsu form Sanford-Burnham Medical Research Institute for their help in the *in vivo* work.

Finally, I would like to thank my parents and my parents in law, my sister, my brother and sister in law, and especially my wife. Without their support and endless love, I could not finish

my research work. I am also grateful to all my best friends and the people who helped me in my research life.

TABLE OF CONTENTS

LIST OF FIGURES

LIST OF TABLES

LIST OF SCHEMES

LIST OF ACRONYMS AND ABREVIATIONS

^{1}H	Hydrogen 1 isotope
1PFM	One-photon fluorescence Microscopy
2PA	Two-photon absorption
2PFM	Two-photon fluorescence microscopy
2F-FLIM	Two-photon fluorescence lifetime microscopy
3D	Three-dimension(al)
^{13}C	Carbon 13 isotope
CAN	Acetonitrile
AF	Alex Fluor 555
AOT	Aerosol OT
APTES	(3-aminopropyl)triethoxysilane
Ar	Argon or aromatic system
ATCC	America Type Culture Collection
$CDCl_3$	Deuterated chloroform
cm^{-1}	Wavenumber
CT	Computed tomography

d	Doublet
DCC	Dicyclohexylcarbodiimide
DCM	Dichloromethane
DBF	4,4'-(1E,1'E)-2,2'-(9,9-didecyl-9H-fluorene-2,7-diyl)bis(ethene-2,1-diyl)bis(N,N-dibutylaniline)
DETA	N’ [3-(trimethoxysilyl)-propyl]diethylenetriamine
DFP	2-(2,6-bis((E)-2-(7-(diphenylamino)-9,9-diethyl-9H-fluoren-2-yl)vinyl)-4H-pyran-4-ylidene)malononitrile
DLS	Dynamic light scattering
DMSO	Dimethyl sulfoxide
EPR	Enhanced Permeability and Retention
EtOH	Ethanol
FA	Folic acid
FA-SH	(S)-2-(2-(4-((2-amino-4-hydroxypteridin-6-yl)methylamino)phenyl)

	acetamido)-5-(2-mercaptoethylamino)-5-oxopentanoic acid
FBS	Bovine serum
FRs	Folate receptors
F_M	Figure of Merit
fs	Femtosecond (10^{-15} s)
g	Gram
GM	Goppert-Mayer unit for the 2PA cross-section (1×10^{-50} cm^4 s $photon^{-1}$ $molecule^{-1}$)
GPC	Gel permeation chromatography
h	Hour
IR	Infrared
L	Liter
Lit.	Literature
LT1	4,4'-(9,9-di(2,5,8,11,14,17,20,23,26,29-decaoxahentriacontan-31-yl)-9H-fluorene-2, 7-diyl) bis (ethyne-2,1-diyl) bis (N, N-

	dimethylaniline)
LT Red	LysoTracker Red
m	Multiplet
μM	Micromole pre liter (10^{-6} moles/liter)
MAL-PEG-SCM	Maleimide-poly(ethylene glycol)-succinimidyl carboxymethyl, average M.W. 3400
min	Minute
mL	Milliliter (10^{-3} L)
mmole	Millimoles (10^{-3} moles)
MRI	Magnetic resonance imaging
MS	Mass spectrum
ms	Millisecond
MT	MitoTracker Red FM
mW	Mill watts
NA	Numerical aperture
NIR	Near infrared
nm	Nanometer (10^{-9} m)
nmole	Nan mole (10^{-9} mole)
NMP	N-methyl-2-pyrrolidinone

NMR	Nuclear magnetic resonance
OD	Optical density
ORMOSIL	Organically modified silica
PdI	Polydisperse Index
PEG	Polyethylene glycol
ppm	Parts per million
PMMA	Polymethylmethacrylate
pTHF	Polytetrahydrofuran
r. t.	Room temperature
RES	Reticuloendothelial system
RSP	Reflection short pass
s	Seconds or singlet
S_1	First excited state, singlet
S_0	Ground state, singlet
SiNPs	Silica nanoparticles
t	Triplet
TEA	Triethylamine
TEM	Transmission electron microscopy
THF	Tetrahydrofurane
TMS	Tetramethylsilane
TPEN	N,N,N’,N’-tetrakis(2-

	pyridylmethyl)ethylenediamine
UV	Ultraviolet
VTES	Triethoxyvinylsilane
W	Watts
wt%	Weight percentage
δ	ppm or 2PA cross section
Δ	Conventional heating
ε	Molar absorption coefficient
λ_{max}	Wavelength of maximum absorption
τ_f	Fluorescence life
Φ_f	Fluorescence quantum yield
Φ_d	Photodecomposition quantum yield

CHAPTER I: BACKGROUD AND INTRODUCTION

I.1 Background

Cancer is going to surpass heart disease to become the leading cause of morbidity and mortality in the United States, and the incidences are expected to continue on an upward trend for the near future (Figure I-1).[1] In 2009, it was estimated that 12.9 million new cases of cancer occurred worldwide, with an estimated economic cost of US $286 billion.[2] Because early cancer detection can increase the survival rates dramatically and save money, no mention increase quality of life, investment in the research of developing new techniques for early cancer detection is of paramount interest.[3]

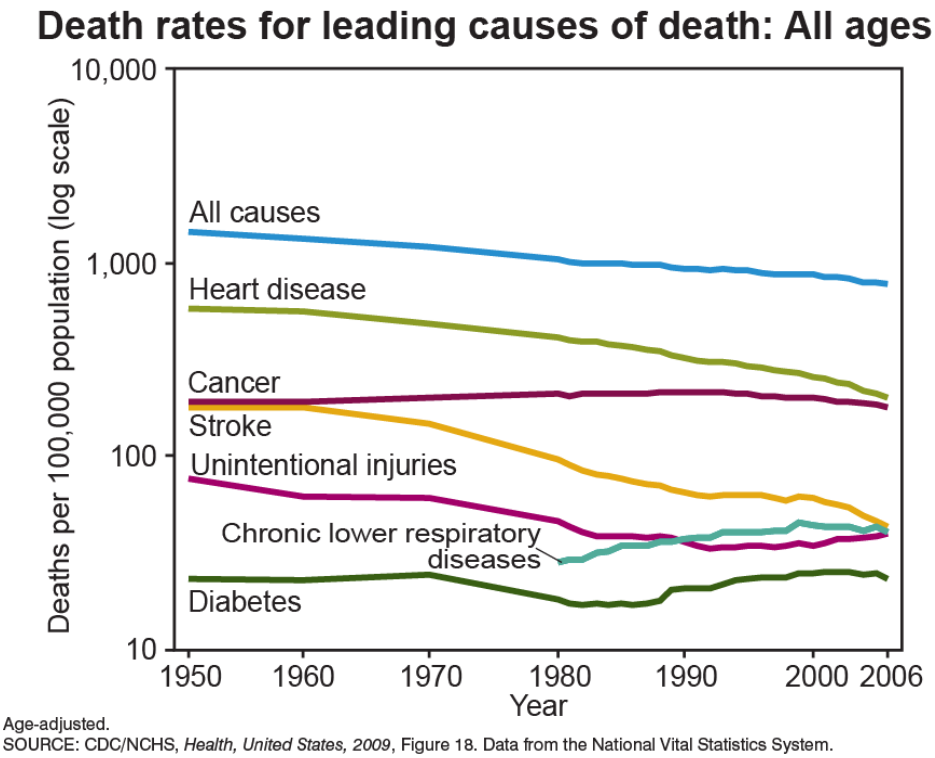

Figure I-1. Death rates for leading causes of death for all ages: United States, 1950–2006.

Conventional imaging technologies for cancer detection — x-ray, magnetic resonance imaging (MRI) and computed tomography (CT) — can serve as proxies for proximity, but the pictures they offer are often incomplete and obscured.[4] One of the exciting areas of research is the application of the fluorescence-based two photon fluorescence microscopy (2PFM) for cancer diagnostics. This technique provides a series of advantages over conventional imaging technologies including: (a) providing images in three-dimension (3D) with submicrometer resolution; (b) large tissue depth penetration compared to traditional one-photon fluorescence microscopy (1PFM); (c) allowing high-sensitivity imaging by eliminating contamination of the fluorescence signal by the excitation light; (d) reduced specimen photodamage that facilitates imaging of living specimens.[5, 6] However, a lack of biocompatible two-photon absorbing (2PA) probes with large 2PA and fluorescence efficiency in physiological environment, good photostability and high biological specificity limited their application in bioimaging.[7]

To introduce organic-based 2PA probes into physiological environments, one strategy is to incorporate hydrophilic moieties and targeting biomolecules directly on the organic chromophore. However, this method generally involves tremendous efforts in synthesis and biomolecular conjugation for targeting bioimaging. Another strategy is by employing hydrophilic nanoparticles to encapsulate hydrophobic 2PA dyes in their nonpolar cores and, thus, bring the dyes into aqueous media. In addition, the surface of the nanoparticles can further be functionalized with targeting agents. The *in vivo* application of this class of nanoprobes as diagnostic agents is of intense interest owing to their unique properties, such as large specific capacity for chromophore loading and sufficient fluorescence efficiency. This concept aims to provide a path for the development of probes for early detection of cancer.

Bioconjugated nanoprobes are attractive candidates because of their: (a) enhanced permeation and retention (EPR) effects that may result in increased concentration in tumor tissue; (b) ligand-mediated active targeting of the tumor site by modifying the surface of the nanoparticles with bimolecular; (c) increased circulation time and enhanced the accumulation of the probe in targeted tumor sites; (d) increased photostability; and (e) decreased nephrotoxicity, bone-marrow toxicity, cardiotoxicity, mucositis, and gastrointestinal toxicity or neurotoxicity.[8-11]

I.2 Introduction

I.2.1 Lysosomal bioimaging

Lysosomes are membranous organelles of ~500 nm that normally function as the terminal degradation compartment of the endocytic pathway, while the abnormal accumulation of lysosomes may cause autosomal recessive storage disease.[12-14] In addition, cancer invasion and metastasis are frequently accompanied with altered lysosomal trafficking and increased lysosomal enzyme expression and activity.[15, 16] A few fluorescent-based techniques for labeling lysosomes of cancer cells and solid tumor models have been investigated to study lysosomal trafficking and their role in invasion.[17, 18] Hence, developing effective probes to label lysosomes with fluorescent tags and monitor the lysosomal trafficking in cells and solid tumors are critical to study the role of lysosomes in cancer invasion and metastasis.

I.2.2 Folate receptor targeted bioimaging

Folate receptors (FRs), glycosylphosphatidylinositol-anchored proteins that bind to both folic acid and folate-linked probes or drugs with high affinity (K_d ~ 100 pM), are significantly upregulated in a variety of human cancers (ovaries, breast, endometrium, lungs, kidneys, colon, brain, and myeloid cells of hematopoietic origin) but few express to any large degree in most healthy tissues.[19, 20] The use of folic acid-conjugated PET agents, MRI contrast agents, and fluorescent probes to target FRs overexpressed cancers for the purpose of early diagnosis and imaging cancers with high specificity and sensitivity were reported recently.[21-23] However, there are few reports of FR targeted two-photon fluorescence microscopy (2PFM) bioimaging.[24]

I.2.3 Reticuloendothelial system (RES)

The reticuloendothelial system (RES), which is divided into primary and secondary lymphoids organs, is a part of the immune system and normally accumulates in lymph nodes and the spleen. It consists of phagocytic cells located in reticular connective tissue, primarily monocytes and macrophages. In addition, the Chuffer cells of the liver and tissue histiocytes are part of the RES.[25, 26] The RES in the animal body always functions through poisonings, which are any molecules that act as a binding enhancer for the process of phagocytosis, and can bind to circulating particles and remove them from the circulation within seconds to minutes.[27] The RES can recognize and sequester intravenously injected colloidal carriers, such as liposome and multifunctional nanoprobes rapidly and subsequently clear them from the circulation. Hence, the RES has hampered nanoprobes or drugs from efficient accumulation in pathological sites.[28, 29]

I.2.4 Influence of particle surface and size-mechanism for passive targeting

To avoid RES uptake and consequently prolong their circulation time, the particle surface and particle size of nanoparticles are two significant parameters for optimization. Imparting a stealth-shielding on the surface of the nanoparticle is a convenient strategy to prevent recognition of the circulating particles by RES cells. PEGylation has proven to be the most effective method among several strategies to modify the surface of the nanomaterials and impart them with shielding properties.[30] Because of a loss of conformational entropy of bound PEG chains upon the approach of serum opsonins in terms of PEG steric hindrance, it prevents the deposition of particle surfaces, thereby reducing the uptake by RES cells.[31]

In addition, because of the enhanced permeation and retention (EPR) effect of cancerous tumors, reducing the particle size below 100 nm was demonstrated to decrease the clearance of

nanomaterials by the RES effectively.[32] Long-circulating nanomaterials with the appropriate particle size have more frequent opportunities to encounter 'leaky tumor capillaries' and extravasate into the tumor tissue via the EPR effect.[33] Therefore, passive targeting to cancerous tumors can be obtained by tuning the size of nanomaterials.

I.2.5 Ligand-mediated active targeting

A variety of disease-specific ligand-receptor pairs, e.g., ligands based on antibodies, antibody fragments, proteins, and peptides have been identified with the development of cell biology.[34] Those ligands based on antibodies, antibody fragments, proteins, and peptides were fervently investigated for specific drug and probe delivery in term of their highly selective towards specific cell receptors.[35] Therefore, in addition to passive targeting through the EPR effect, delivery of particles to smaller solid tumor and metastatic cells can be achieved by modifying particle surfaces with moieties directed at cell surface markers unique to the cell types.

I.2.6 Enhanced specificity via a synergistic combination of passive and active targeting strategies

An optimal platform for *in vivo* nanoprobe delivery and significant enhancement of the efficacy of a diagnostic protocol can be achieved by combining passive and active targeting strategies synergistically. By optimizing the particle size to best suit the pathophysiology of a particular cancer, one can maximize accumulation of nanoprobe at the pathological sites. Additionally, appropriate selection of the targeting ligand and control over nanoparticle modification can lead to enhanced cellular accumulation of specific targeting nanoprobe. It was suggested that the physiological properties of nanoparticle carriers can largely determine their pharmacokinetics and biodistribution; meanwhile, the presence of targeting ligands can lead to

enhancement of intracellular accumulation.[36] Nanoparticles first extravasate into the tumor stroma through the fenestrations of the angiogenic vasculature, demonstrating targeting by enhanced permeation and retention. Nanoprobes can carry multiple targeting biomolecular, which can further target them to their receptors upregulated in cancer tissues, resulting in nanoprobes accumulation the tumors suitable for bioimaging.

I.3 Organization of the Dissertation

After a brief background introduction in Chapter I, the application of a novel two-photon absorbing fluorene derivative LT1, selective for the lysosomes of cancer cells is described in Chapter II. In order to increase the water solubility of the lysosomal probe, polyethylene glycol (PEG) was introduced to a fluorene based two-photon absorbing (2PA) probe LT1 for lysosomal two-photon fluorescence microscopy (2PFM) cell imaging. Linear and nonlinear photophysical and photochemical properties of the probe were investigated to evaluate the potential of the probe for 2PFM lysosomal imaging. After the investigation of the cytotoxicity of this new probe, colocalization studies of the probe with the commercial lysosomal probe Lysotracker Red in HCT 116 cells were conducted. A high colocalization coefficient (0.96) was achieved and supporting specific localization of the probe in lysosomes. To compare the properties of the novel between probes, a figure of merit, F_M, was introduced. LT1 was demonstrated to have a number of properties that far exceed those of commercial lysotracker probes, including much higher 2PA cross sections, good fluorescence quantum yield, and, importantly, high photostability, all resulting in a superior figure of merit. Consequently, 2PFM was used to demonstrate lysosomal tracking with LT1.

In Chapter III, the 2PFM bioimaging application of a 2PA Zn^{2+} sensing fluorescent probe bis(1,2,3-triazolyl)fluorene derivative is described. After investigating the cytotoxicity, 2PFM bioimaging of the probe in living HeLa cancer cells was demonstrated. The results revealed a significant fluorescence increase upon introduction of Zn^{2+} into the cancer cells, and a reversible

Zn^{2+} binding to the probe was also demonstrated, providing a robust zinc ion sensing probe for future studies.

In Chapter IV, the synthesis and characterization of narrow dispersity organically modified silica nanoparticles (SiNPs), average diameter ~30 nm, entrapping a hydrophobic two-photon absorbing fluorenyl dye were reported. The surface of the SiNPs were functionalized with a folic acid derivative to specifically deliver the probe to folate receptor (FR) overexpressing HeLa cells, making these folate two-photon dye-doped SiNPs potential candidates as probes for two-photon fluorescence microscopy (2PFM) bioimaging. *In vitro* studies using FR overexpressing HeLa cells demonstrated specific cellular uptake of the functionalized nanoparticles. However, when the concentration of the dye in SiNPs increased, the fluorescence quantum efficiency of probes normally decreased because of self-quenching, making a strategy to overcome this limitation an important objective.

Consequently, a 2PA and aggregation-enhanced emission NIR dye was proposed to overcome the limitation of self-quenching at high dye loading and is described in Chapter V. The dye was encapsulated by SiNPs and the surface of the nanoparticles was functionalized with maleimide-terminated PEG. In addition, the NIR emission property of the dye was beneficial for deep tissue imaging. The surface of the 2PA and aggregation-enhanced emission nanoprobe was modified with a folic acid derivative for folate receptor-targeted *in vitro* and *in vivo* bioimaging. *In vitro* studies using HeLa cells, that upregulate folate receptors, indicated specific cellular uptake of the folic acid functionalized nanoprobe. Meanwhile, the probe was also investigated for live animal

imaging by employing mice bearing HeLa tumors for *in vivo* imaging. *Ex vivo* 2PFM tumor imaging was then conducted to achieve high quality 3D thick tissue tumor images.

I.4 References

[1] National Center for Health Statistics (US), Hyattsville (MD): National Center for Health Statistics (US), January 2010, 48-49.

[2] A report from the Economist Intelligence Unit. The global burden of cancer—challenges and opportunities.

[3] Smith, R. A.; Cokkinides, V.; Eschenbach, A. C.; Levin, B.; Cohen, C.; Runowicz, C. D.; Sener, S.; Saslow, D.; Eyre, H. J. *CA Cancer J Clin*. **2002**, *52*, 8-22.

[4] Weisseleder, R. *Nature Reviews Cancer* **2002**, *2*, 11-18.

[5] So, P. T. C.; Dong, C. Y.; Masters, B. R.; Berland, K. M. *Annu. Rev. Biomed. Eng.* **2000**, *2*, 399-429.

[6] Helmchen, F.; Denk, W. *Nature Method* **2005**, *2*, 932-940.

[7] Alberto, D. Confocal and two-photon microscopy, foundation, applications and advances, Lavoisier, 2002.

[8] Sharma, P.; Brown, S.; Walter, G.; Santra, S.; Moudgil, B. *Advances in Colloid and Interface Science* **2006**, *123-126*, 471-485.

[9] Weissleder, R.; Ntziachristos,V. *Nature Medicine* **2003**, *9*, 123-128.

[10] Tallury, P.; Payton, K.; Santra, S. *Nanomedicine* **2008**, *3*, 579-592.

[11] De, M.; Ghosh, P. S.; Rotello, V. M. *Adv. Mater.* **2008**, *20*, 4225-4241.

[12] Glunde, K.; Guggino, S. E.; Solaiyappan, M.; Pathak, A. P.; Ichikawa, Y.; Bhujwalla, Z. M. *Neoplasia* **2003**, *5*, 533-545.

[13] Chen, C.; Bach, G.; Pagano, R. E. *Proc. Natl. Acad. Sci. USA* **1998**, *95*, 6373-6378.

[14] Ohmi, K.; Kudo, L. C.; Ryazantsev, S.; Zhao, H.; Karsten, S. L.; Neufeld, E. F. *Proc. Natl. Acad. Sci.USA* **2009**, *106*, 8332-8337

[15] Groth-Pedersen, L.; Ostenfeld, M. S.; Høyer-Hansen, M.; Nylandsted, J.; Jäättelä, M. *Cancer Res.* **2007**, *67*, 2217-2225.

[16] Fehrenbacher, N.; Bastholm, L.; Kirkegaard-Sørensen, T.; Rafn, B.; Bøttzauw, T.; Nielsen, C.; Weber, E.; Shirasawa, S.; Kallunki, T.; Jäättelä, M. *Cancer Res.* **2008**, *68*, 6623-6633.

[17] Glunde, K.; Foss, C. A.; Takagi, T.; Wildes, F.; Bhujwalla, Z. M. *Bioconjugate Chemistry* **2005**, *16*, 843-851.

[18] Li, C.; Greenwood, T. R; Glunde K. *Neoplasia* **2008**, *10*, 389-98.

[19] Sega, E. I.; Low, P. S. *Cancer Metastasis Rev.* **2008**, *27*, 655-664.

[20] Antomy, A. C. *Annual Review of Nutrition* **1996**, *16*, 501-521.

[21] Mathias, C. J.; Lewis, M. R.; Reichert, D. E.; Laforest, R.; Sharp, T. L.; Lewis, J. S.; Yang, Z. Waters, D. J.; Snyder, P. W.; Low, P. S.; Welch, M. J.; Green, M. A. *Nuclear Medicine and Biology* **2003**, *30*, 725-731.

[22] Kalber, T. L.; Kamaly, N.; Hussein, M. O.; Jorgensen, M. R.; So, P.; Bell, J. D.; Miller, A. D. *Proc. Intl. Soc. Mag. Reson. Med.* **2007**, *15*, 1156.

[23] Bharali, D. J.; Lucey, D. W.; Jayakumar, H.; Pudavar, H. E.; Prasad, P. N. *J. Am. Chem. Soc.* **2005**, *127*, 11364-11371.

[24] Wessels, J. T.; Busse, A. C.; Mahrt, J.; Dullin, C.; Grabbe, E.; Mueller, G. A. *Cytometry Part A* **2007**, *71A*, 542-549.

[25] Old, L. J.; Benacerraf, B.; Clarke, D. A.; Carswell, E. A.; Stockert, E. *Cancer Res.* **1961**, *21*, 1281-1300

[26] Reticuloendothelial system, http://en.wikipedia.org/wiki/Reticuloendothelial_system

[27] Jenkin, C. R.; Rowley, D. *The Journal of Experimental Medicine* **1961**, *114*, 363-374.

[28] Torchilin, V. P. *Nature Reviews Drug discovery* **2005**, *4*, 145-160.

[29] Moghimi, S. M.; Hunter, A. C.; Murray, J. C. *Pharmacological Reviews* **2001**, *53*, 283-318.

[30] Harris, J. M.; Chess, R. B. *Nature Reveiws Drug Discovery* **2003**, *2*, 214-221.

[31] Veronese, F. M.; Mero, A. *BioDrugs* **2008**, *22*, 315-329.

[32] Maeda, H.; Wu J.; Sawa, T.; Matsumura, Y.; Hori, K. *Journal of Controlled Release* **2000**, *65*, 271-284.

[33] McDonald, D. M.; Baluk, P. *Cancer Res.* **2002**, *62*, 5382-5385.

[34] Brigger, I.; Dubernet, C.; Couvreur, P. *Advanced Drug Delivery Reviews* **2002**, *54*, 631-651.

[35] Tomlinson, E. *Advanced Drug Delivery Reviews* **1988**, *1*, 271-272.

[36] De, M.; Ghosh, P. S.; Rotello, V. M. *Advanced Materials* **2008**, *20*, 4225-4241.

CHAPTER II: HIGH FIDELITY HYDROPHILIC PROBE FOR TWO-PHOTON FLUORESECENCE LYSOSOMAL IMAGING

Reproduced with permission from: Wang, X.; Nguyen, D. M.; Yanez, C. O.; Rodriguez, L.; Ahn, H.; Bondar, M. V.; Belfield, K. D. *J. Am. Chem. Soc.* **2010**, *132*, 12237-12239.

II.1 Abstract

The synthesis and characterization of a novel two-photon absorbing fluorene derivative LT1, selective for the lysosomes of HCT 116 cancer cells was reported. Linear and nonlinear photophysical and photochemical properties of the probe were investigated to evaluate the potential of the probe for 2PFM lysosomal imaging. The cytotoxicity of the probe was investigated to evaluate the potential of using this probe for live two-photon fluorescence biological imaging applications. Colocalization studies of the probe with commercial Lysotracker Red in HCT 116 cells demonstrated the specific localization of the probe in the lysosomes with an extremely high colocalization coefficient (0.96). A figure of merit, F_M, was introduced to allow comparison between probes. LT1 has a number of properties that far exceed those of commercial lysotracker probes, including higher 2PA cross sections, good fluorescence quantum yield, and, importantly, high photostability, all resulting in a superior figure of merit. 2PFM was used to demonstrate lysosomal tracking with LT1.

II.2 Introduction

Lysosomes are membrane-bound organelles of ~ 500 nm diameter that are terminal degradative compartments of mammalian cells.[1] Lysosomes are involved in a numerous physiological processes, such as bone and tissue remodeling, plasma membrane repair, cholesterol homeostasis along with cell death and cell signalling.[2] In addition, tumor invasion and metastasis are largely associated with altered lysosomal trafficking and increased lysosomal enzyme expression and activity.[3] Effective techniques to fluorescently label lysosomes of cancer cells and solid tumor models are therefore of significant interest to study lysosomal trafficking and its role in invasion.[4]

In order to understand the biological activities of lysosomes, a variety of fluorescent probes derived from neutral red and acridine orange have been developed and commercialized.[5] However, most of the commercial probes require a rather short excitation wavelength, seriously limiting their use in tissue imaging due to low penetration depth, the need to be conjugated with bimolecular, suffer from pH sensitivity, poor water solubility, and poor photostability.[6] These limitations motivated us to search for two-photon absorbing dyes for two-photon fluorescence microscopy imaging, due to the longer wavelength (700 - 1300 nm) light and a quadratic dependence on laser intensity of two-photon absorption (2PA) provide advantages such as localized excitation and prolonged observation time.[7] A biocompatible, photostable and water soluble lysosomal marker with high 2PA cross section will provide a strong tool to study lysosomal trafficking and its role in invasion with high resolution spatial images.

II.3 Result and Discussion

Herein, wie describe a symmetric hydrophilic fluorene derivative 4,4'-(9,9-di(2, 5,8,11,14,17,20,23,26,29-decaoxahentriacontan-31-yl)-9H-fluorene-2, 7-diyl) bis (ethyne-2,1-diyl) bis (N, N-dimethylaniline) (LT1) and demonstrate ins use as an efficient 2PA fluorophore to perform noninvasive labeling of lysosomes *in vitro*. The new fluorene derivative LT1 was specifically designed to contain a pair of 10-unit polyethylene glycol (PEG) groups in the 9-position of the fluorene ring, which made the probe highly water soluble and imparted very low cytotoxicity. The hydrophilic fluorene derivative LT1 was synthesized from 2, 7-diiodofluorene 2 and 4-ethynyl-N, N-dimethylaniline 3 through a Sonogashira cross-coupling reaction using a $PdCl_2P(Ph_3)_2$/CuI catalytic system at 72% yield (Scheme II-1).[8]

Scheme II-1. Synthesis of the fluorene derivative LT1.

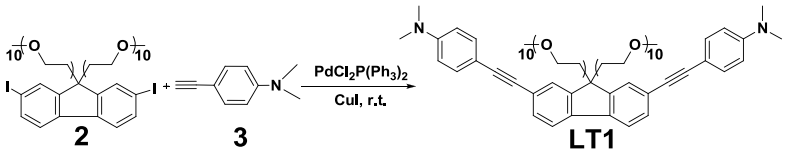

The linear and nonlinear photophysical properties of probe are reported to investigate specific fluorescence properties which are important for nonlinear optical applications. The absorption and emission spectra of LT1 were sensitive to solvent polarity, and the emission spectra exhibited large bathochromic shifts in the order of toluene < THF < EtOH < H_2O. The emission spectra showed much greater solvatochromic shifts than absorption spectra (79 nm vs. 7 nm), suggestive of the potential of LT1 as a polarity-sensitive probe.

In addition, the excitation anisotropy spectra (dot) and anisotropy values, r, for LT1 in polytetrahydrofuran (pTHF) are shown in Figure II-1, along with the linear absorption spectra for

LT1 in PBS buffer. Probe LT1 displayed a constant value of r ≈ 0.37, for excitation in the spectral range λ ≈ 374 – 455 nm, corresponding to the first electronic transition $S_0 \rightarrow S_1$. And a higher electronic transition, $S_0 \rightarrow S_2$, was observed in the wavelength range λ ≈ 289 – 326 nm (r ≈ 0.24). Because the pH of lysosomes is around 4.8, the pH stability in slight acidic environment is essential for lysosomal probes. The pH stability of the LT1 was investigated by measuring the absorbance and emission of LT1 in a series of buffers with different pH values from 4.16 to 10.0. The results, illustrated in Figure II-4, indicated that LT1 was very stable over this entire pH range.

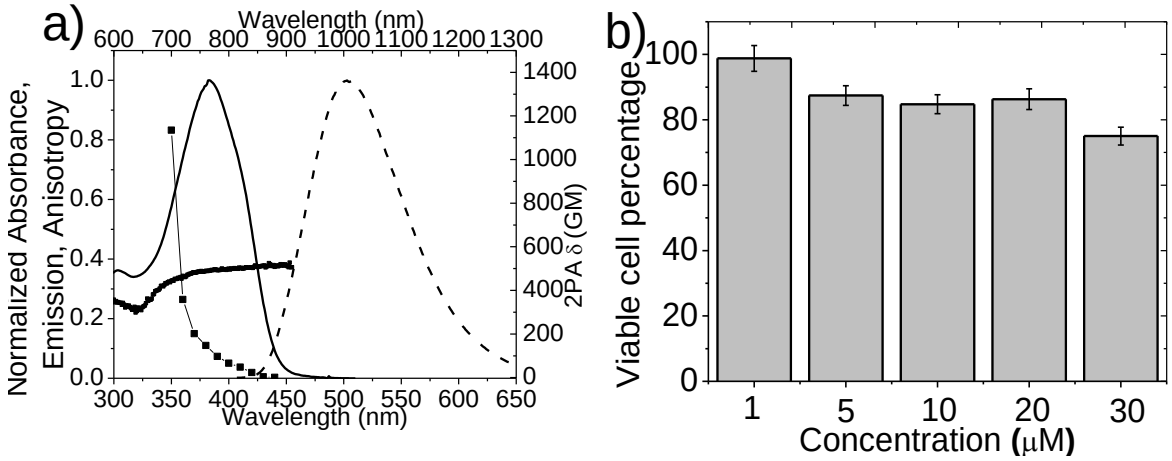

Figure II-1. (a) Normalized absorption (solid) (in PBS), emission (dish) (in PBS), anisotropy (dot) spectra (in pTHF) and two-photon absorption cross section (square) (in toluene) of LT1; (b) Viability of HCT 116 cells with LT1.

By employing a standard two-photon induced fluorescence method with a femtosecond laser system, probe LT1 afforded a maximum 2PA cross section of ~ 1100 GM (1 GM = 10^{-50} cm^4 s $photon^{-1}$) at 700 nm (Figure II-1, square), which is a much higher than commercial probes of those reported by others < 10 - 200 GM for two-photon fluorescence microscopy (2PFM)

bioimaging.[9] In addition, the photostability and 2PA cross sections of LT1 were compared with the commercially available Lysosomal markers Lysotracker Red (LT Red) and Lysotracker Green (LT Green) by photodecomposition experiments and 2PA cross-section measurements. Herein, we define a Figure of Merit (F_M) by which probes for 2PFM can be compared; the product of their fluorescence quantum yield (Φ_f) and 2PA cross section (δ) normalized by their photodecomposition quantum yield (Φ_d), i.e., $F_M = \Phi_f\delta/\Phi_d$. The F_M of LT1 was two orders of magnitude higher than LT Green and LT Red (Table II-1), strong support for the fidelity of LT1 relative to the commercial LT Red and LT Green for 2PFM biological imaging.

Table II-1. Photophysical data for LT1, Lysotracker Green, and Lysotracker Red.[a]

Probes	$\lambda_{max}^{(1)}/\lambda_{max}^{(2)}$ [b]	ε [c]	Φ_f [d]	δ [e]	$\Phi_d \times 10^6$ [f]	$\Phi_f\delta$ [g]	$F_M \times 10^{-6}$ [h]
LT1	387/501	7.7	0.38	1135	0.94	431.3	458.8
LT Green	502/510	6.3	1.0	17	3.70	17	4.6
LT Red	575/591	4.9	0.07	33	5.31	2.3	0.4

[a] Except for 2PA cross section measurements, all other measurements were performed in PBS buffer. [b] λ_{max} values of the one-photon absorption and emission spectra in nm. [c] Molar absorbance in 1×10^4 $M^{-1} \cdot cm^{-1}$. [d] Fluorescence quantum yield, ±15%. [e] 2PA cross-section (LT1 in toluene at 700 nm, LT Green in DMSO at 700 nm and LT Red in DMSO at 740 nm) in 10^{-50} cm^4 s $photon^{-1}$(GM), ±15%. [f] Photobleaching decomposition quantum yield. [g] Two-photon action cross section in GM. [h] Figure of merit in GM.

In order to demonstrate the potential utility of LT1 for 2PFM cellular imaging, cytotoxicity or cell viability must be assessed. To address this, viability assays in an epithelial colorectal

carcinoma cell line, HCT 116, was conducted via the MTS assay.[10] Figure II-1 (b) showed the viability data for HCT 116 cells after treating with several concentrations of LT1 for 24 h. The data indicated that LT1 has low cytotoxicity (~85% viability) over a concentration range from 1–20 μM, appropriate for cell imaging. This bodes well for the utility of this hydrophilic probe, particularly for live cell imaging application for lysosomal tracking via 2PFM.

Subsequently, in order to assess whether LT1 can be efficiently uptaken by cancer cells, the efficiency of LT1 uptake by HCT 116 cells was evaluated. The one photon fluorescence microscopy (1PFM) and 2PFM images showed LT1 can be effectively taken by HCT 116 cells and the optimum concentration of LT1 for the cellular uptake was determined by comparing the image of HCT 116 treated with 5, 10, 20, and 30 μM for 2 h. The results showed that HCT 116 treated 20 μM can provide bright images with negligible toxicity. In addition, to determine the location of the probes in the cells, a colocalization study of LT1 with several well known one-photon fluorescence (1PF) probes in HCT 116 cells was conducted. 1PFM images of HCT 116 cells co-stained with LT1 and lysosomal marker Lysotracker Red (LT Red), mitochondrion marker Mitotracker Red FM (MT) or Golgi apparatus marker Alexa Fluor 555 (AF) (Figure II-2 and Figure II-7) individually demonstrated that the localization of LT1 in the cells was nearly identical to Lysotracker Red. The 1PFM images of HCT 116 cells were taken with two different channels; Fluor out (Ex: 377/50; DM: 409; Em: 525/40) for LT1 and Texas Red (Ex: 562/40; DM: 593; Em: 624/40) for commercial markers under the same conditions. The colocalization coefficient, A, was calculated by Slidebook 5.0 software with Pearson's method to evaluate the colocalization of LT1 relative to the commercial probes. The data in Table II-2 showed that the

colocalization coefficient of LT1 with Lysotracker Red was much higher than the others (0.96 vs. 0.45, 0.46), indicating that LT1 possesses lysosomal specificity.

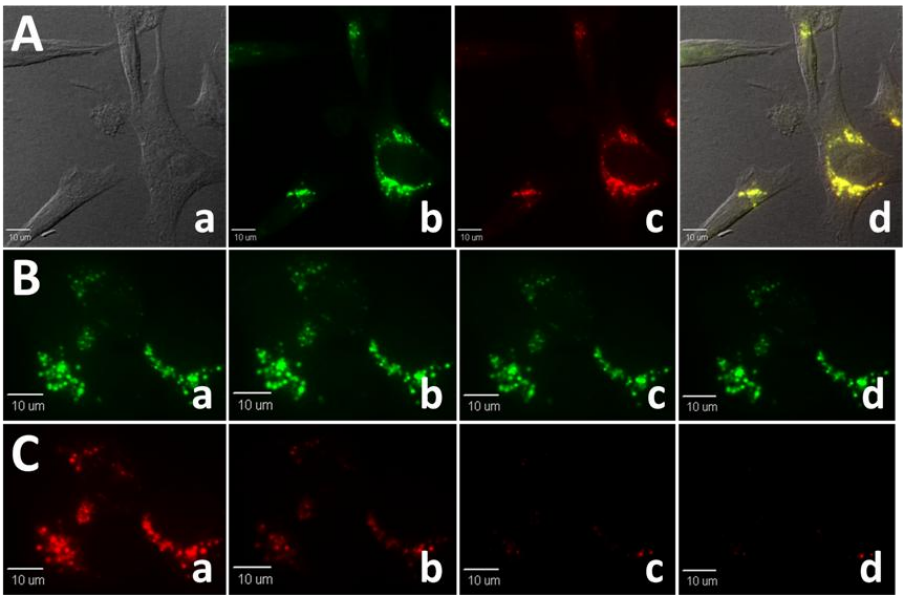

Figure II-2. Colocalization images of HCT 116 cells incubated with LT1 (20 μM, 2 h) & Lysotracker Red (LT Red, 75 nM, 2 h) and photostability comparison of LT1 and Lysotracker Red as lysosome markers in HCT 116 cells. (A) (a) DIC (b) one-photon confocal probe LT1 fluorescence image using a custom made Fluor out filter cube (Ex: 377/50; DM: 409; Em: 525/40; (c) one-photon confocal LT Red fluorescence image using a Texas Red filter cube (Ex: 562/40; DM: 593; Em: 624/40); (d) merged image of DIC and two channels of fluorescence images. One-photon confocal microscopy images of HCT 116 cells co-stained with (B) LT1 and (C) Lysotracker Red. The images were taken at (a) 0 min (b) 6 min (c) 12 min, and (d) 15 min under successive irradiation (the power on the focus plane is ~ 9 mW). All the images were acquired with a 60×, oil immersion objective.

Moreover, the photostability of LT1 and Lysotracker Red in the HCT 116 cells was also compared (Figure II-2 and Figure II-10), and were consistent with the photodecomposition

experiments in PBS buffer. The fluorescence intensity of Lysotracker Red decreased by ca. 50% in the first 3 min under successive irradiation using a 100 W mercury lamp (the power on the focal plane is ~ 9 mW), resulting in only 10% of the initial fluorescence intensity after 15 min irradiation. In contrast, the fluorescence intensity of LT1 decreased very slowly, decreased to ca. 70% of the initial fluorescence intensity after 15 min irradiation. In order to evaluate if LT1 can be used as a long-term lysosome tracking probe, a long-term lysosome tracking assay was conducted. The results (Figure II-11) revealed that after 9 h postincubation, the images still showed the probe was lysosome-specific, with a Pearson's colocalization coefficient of 0.78. This result demonstrates the potential for LT1 as a stable lysosome marker for two-photon fluorescence microscopy.

In addition, to get an initial sense of the lysosomal specificity of LT1 in other cell lines, COS-7 (African green monkey kidney fibroblast-like) cells were employed using the same method described above for the HCT 116 cells. The colocalization images (Figure II-8) and colocalization coefficient data (Table II-2) indicated that LT1 can also specifically stain lysosomes of other cells and significantly avoid staining other organelles such as the Golgi apparatus and mitochondria, suggesting broad, general utility for this new probe. An endocytosis process is proposed (Figure II-9) for a possible pathway of LT1 cellular uptake, consistent with the literature.[11]

To demonstrate the advantage of using probe LT1 as a lysosomal marker for 2PFM imaging, two-photon fluorescence imaging of HCT 116 cells was conducted. The HCT 116 cell images (Figure II-3) indicate that the 1PFM and 2PFM images are similar, with higher 3D resolution and contrast realized by 2PFM, to the point of visualizing individual lysosomes.

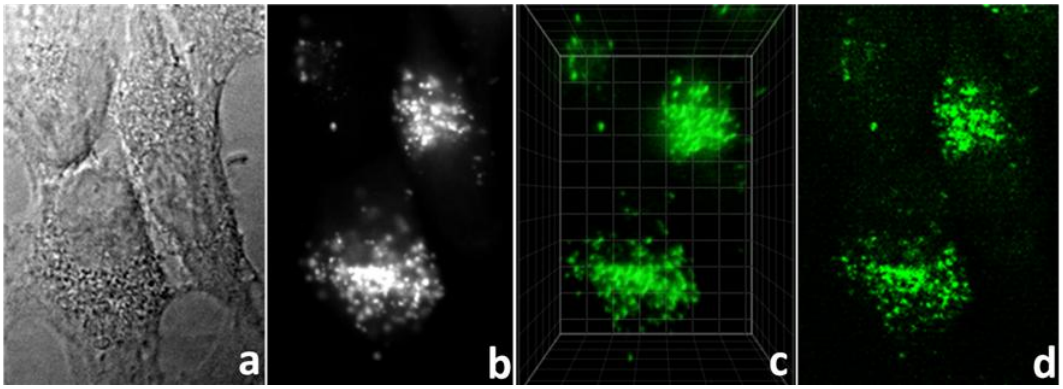

Figure II-3. Images of HCT 116 cells incubated with fluorescence probe LT1 (20 μM, 2h) all taken with 60x, oil immersion objective. a) DIC, 500 ms. b) One photon fluorescence image, 150 ms (filter cube Ex: 377/50 DM: 409 Em: 525/40). c) 3D reconstruction from overlaid two-photon fluorescence images (Ex: 700 nm; Em: long-pass filter 690 nm) 5 μm grid. d) two-photon fluorescence images (Ex: 700 nm; Em. long-pass filter 690 nm).

II.4 Conclusion

In conclusion, we report a very effective hydrophilic fluorene derivative, LT1, as a lysosomal marker for two-photon fluorescence cell imaging. A figure of merit, F_M, was introduced to allow a meaningful comparison between any probes designed for two-photon fluorescence imaging. The new probe has a number of properties that far exceed those of commercial lysotracker probes, including higher 2PA cross sections, high lysosomal selectivity, good fluorescence quantum yield, and, importantly, high photostability, all resulting in a superior figure of merit relative to commercial lysosomal probes. 2PFM was used to demonstrate lysosomal tracking with LT1, paving the way for future studies with LT1 to detect aberrant lysosomal trafficking. This may eventually lead to a new agent for studying lysosome related diseases such as Tay-Sachs disease, mucopolysaccharidosis III B, and Niemann-Pick disease.[12]

II.5 Experimental

II.5.1 General

The ^{1}H and ^{13}C NMR spectroscopic measurements were performed using a Varian 500 NMR spectrometer, at 500 MHz for ^{1}H and 125 MHz for ^{13}C, with tetramethysilane (TMS) as internal reference; ^{1}H (referenced to TMS at $\delta = 0.0$ ppm) and ^{13}C (referenced to $CDCl_3$ at $\delta = 77.0$ ppm). Chemical shifts of ^{1}H and ^{13}C spectra were interpreted with the support of CS ChemDraw Ultra version 5.0. Lysotracker Red, Alexa Fluor 555 conjugate and Mitotracker Red FM were purchased from Invitrogen (Carlsbad, CA, USA). Promega CellTiter 96® AQueous One Solution Reagent was purchased from Fisher. The epithelial colorectal carcinoma cell line HCT 116 and African green monkey kidney fibroblast-like cell line COS-7 were purchased from ATCC (America Type Culture Collection, Manassas, VA, USA). All cells were incubated in Dulbecco's modified Eagle's Medium (DMEM, Invitrogen, Carlsbad, CA, USA), supplemented with 10% fetal bovine serum (FBS, Atlanta Biologicals, Lawrenceville, GA, USA), 100 units / mL penicillin-streptomycin (Atlanta Biologicals, Lawrenceville, GA, USA) and incubated at 37 °C in a 95% humidified atmosphere containing 5% CO_2. The steady-state absorption spectra were obtained with an Agilent 8453 UV/Vis spectrophotometer in 10 mm path length quartz cuvettes with dye concentrations ~ 1×10^{-5} M. The steady-state fluorescence, excitation and excitation anisotropy spectra were measured with PTI QuantaMaster spectrofluorimeter in 10 mm spectrofluorometric quartz cuvettes, with dye concentrations ~ $(1–1.5) \times 10^{-6}$ M. All measurements were performed at room temperature.

II.5.2 pH sensitivity measurements

The steady-state absorption spectra of probe ~1.5 μM LT1 at various pH in 10 mM EMS buffer were obtained with an Agilent 8453 UV/Vis spectrophotometer in 10 mm path length quartz cuvettes. The emission spectra of probe LT1 at various pH in 10 mM EMS buffer were measured on the PTI QuantaMaster spectrofluorimeter. As can be seen in Figure II-4, the probe LT1 is very stable with no observable changes in either the absorption or emission spectra.

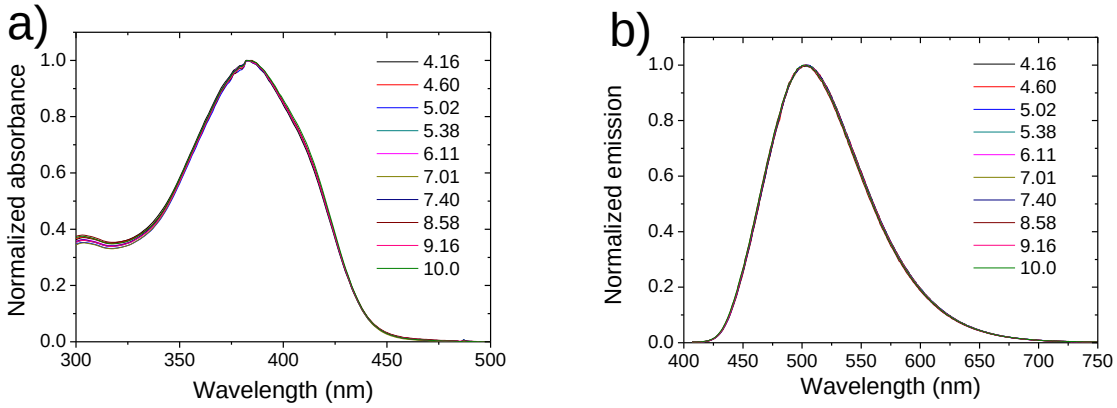

Figure II-4. (a) Normalized absorption and (b) emission spectra of ~1.5 μM LT1 at various pH in 10 mM EMS buffer (excited at 397 nm).

II.5.3 Photostability of LT1 in PBS buffer (pH = 7.4)

The photostability of LT1 was determined by the absorption method previously described in ref.16. For LT1, a solution of LT1 in PBS buffer (pH = 7.4) was irradiated in 1 mm path length quartz cuvettes with a 405 nm diode laser at 20 mW. The photostability of Lysotracker Red was measured by irradiating a solution in PBS buffer (pH = 7.4) in 1 mm path length quartz cuvettes with a 534 nm diode laser at 20 mW. The photostability of Lysotracker Green was measured by irradiating a solution in PBS buffer (pH = 7.4) in 1 mm path length quartz cuvettes with a 501 nm argon ion laser filtered with a band pass filter (490-510 nm) at 20 mW. The values of photodecomposition quantum yields, Φ_d, were calculated according to equation II-2, and the

results listed in Table II-1 are the average of ten pairs of adjacent absorbance maxima (Figure II-5).

$$\Phi_d = \frac{(A_1 - A_0)N_A}{1000 \times \varepsilon \times I \times (1 - 10^{-(A_1+A_0)/2}) \times (t_1 - t_0)} \quad \text{(II-2)}$$

where Φ_d is the photobleaching decomposition quantum yield, A_1 is absorbance maxim at t_1, A_0 is absorbance max at t_0, N_A is Avogadro's number, ε is molar absorbance, t_1-t_0 is time exposed (s), and I is the intensity of laser in photon cm^{-2} s^{-1}.

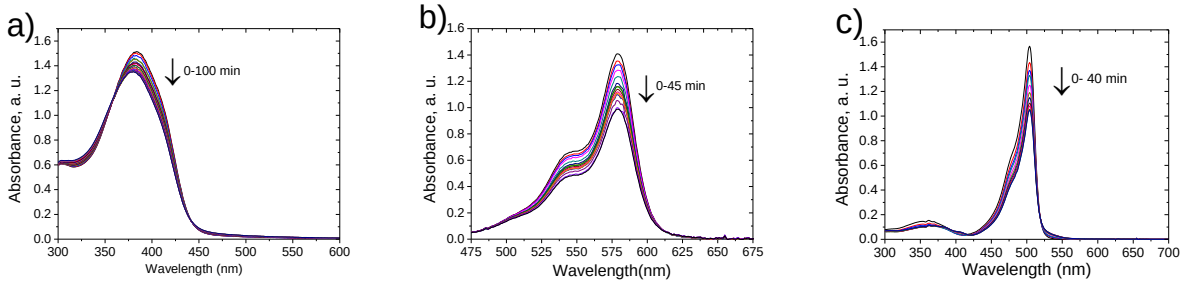

Figure II-5. Absorbance spectra of (a) LT1, (b) Lysotracker Red and (c) Lysotracker Green in PBS buffer (pH = 7.4) by irradiation at 405, 534, and 501 nm, respectively.

II.5.4 Cytotoxicity Assay

To assess the cytotoxicity of fluorene derivative LT1, 5×10^3 per well of HCT 116 cells in 96-well plates were incubated in 90 µL of DMEM medium without phenol red, supplemented with 10% FBS and 100 units / mL penicillin-streptomycin for 24 h. The cells were then incubated with various amounts of fluorene derivative LT1 (30, 20, 10, 5, and 1 µM) for an additional 20 h. Subsequently, 20 µL of CellTiter 96® AQueous One Solution reagent was added to each well, followed by further incubation for 4 h at 37 °C. The relative viability of the cells incubated with fluorene derivative to untreated cells was determined by measuring the MTS-formazan absorbance on a Kinetic microplate reader (Spectra Max M5, Molecular Devices, Sunnyvale, CA,

USA) at 490 nm with subtraction of the absorbance of the cell-free blank volume at 490 nm. The results from three individual experiments were averaged.

II.5.5 Uptake of LT1 by cancer cells

HCT 116 cells or COS-7 cells were placed onto poly-D-lysine coated glasses in 24-well plates (40,000 cells per well), and the cells were incubated for 48 h before incubating with fluorescent probes. A stock solution of fluorescent probe LT1 dissolved in H_2O was prepared as a 1.7 mM solution. The solution was diluted to 5, 10, 20, or 30 μM solutions by complete growth medium, Dulbecco's modification of Eagle's medium (DMEM), and freshly placed over the cells for a 2 h incubation period. After incubation, the cells were washed with PBS (3 – 5×) and fixed using 3.7% formaldehyde solution for 15 min at 37 °C. Then 0.5 mL / well $NaBH_4$ (1 mg / mL) solution in PBS (pH = 8.0), which was prepared by adding few drops of 6N NaOH solution into PBS (pH = 7.2), was used for treating the fixed cells for 15 min (2×). The plates were then washed twice with PBS and once with H_2O. Finally, the glass covers were mounted with Prolong gold mounting media for microscopy.

II.5.6 Colocalization study

HCT 116 cells or COS-7 cells were placed onto poly-D-lysine coated glasses in 24-well plates (40,000 cells per well), and the cells were incubated for 48 h before incubating with fluorescent probes. A stock solution of fluorescent probe LT1 dissolved in water was prepared as a 1.7 mM solution. Stock solutions of Lysotracker Red (LT Red) and Mitotracker Red FM (MT Red) in DMSO were purchased as 1.0 mM solutions. A stock solution of Alexa Fluor 555 (AF) in DMSO was prepared as a 10 μg / mL solution. For co-staining the cells with LT1 and LT Red, the solution was diluted to 20 μM LT1 and 75 nM LT Red with complete growth medium,

DMEM, and then freshly placed over the cells for a 2 h incubation period. For co-staining the cells with LT1 and MT Red, the solution was diluted to 20 μM LT1 and 500 nM MT Red with complete growth medium, DMEM, and then freshly placed over the cells for a 2 h incubation period. For co-staining the cells with LT1 and AF, the cells were first incubated with 20 μM LT1 solution for 100 min, followed by incubation with LT1 (20 μM) and AF (10 μg / ml) for 20 min. After incubation, the cells were washed with PBS (3–5×) and fixed using 3.7% formaldehyde solution for 15 min at 37 °C, followed by treatment with 0.5 mL / well $NaBH_4$ (1 mg / mL) solution in PBS (pH = 8.0) for 15 min. The last step was repeated. The plates were then washed twice with PBS and once with H_2O. Finally, the glass coverslips were mounted with Prolong gold mounting media for microscopy.

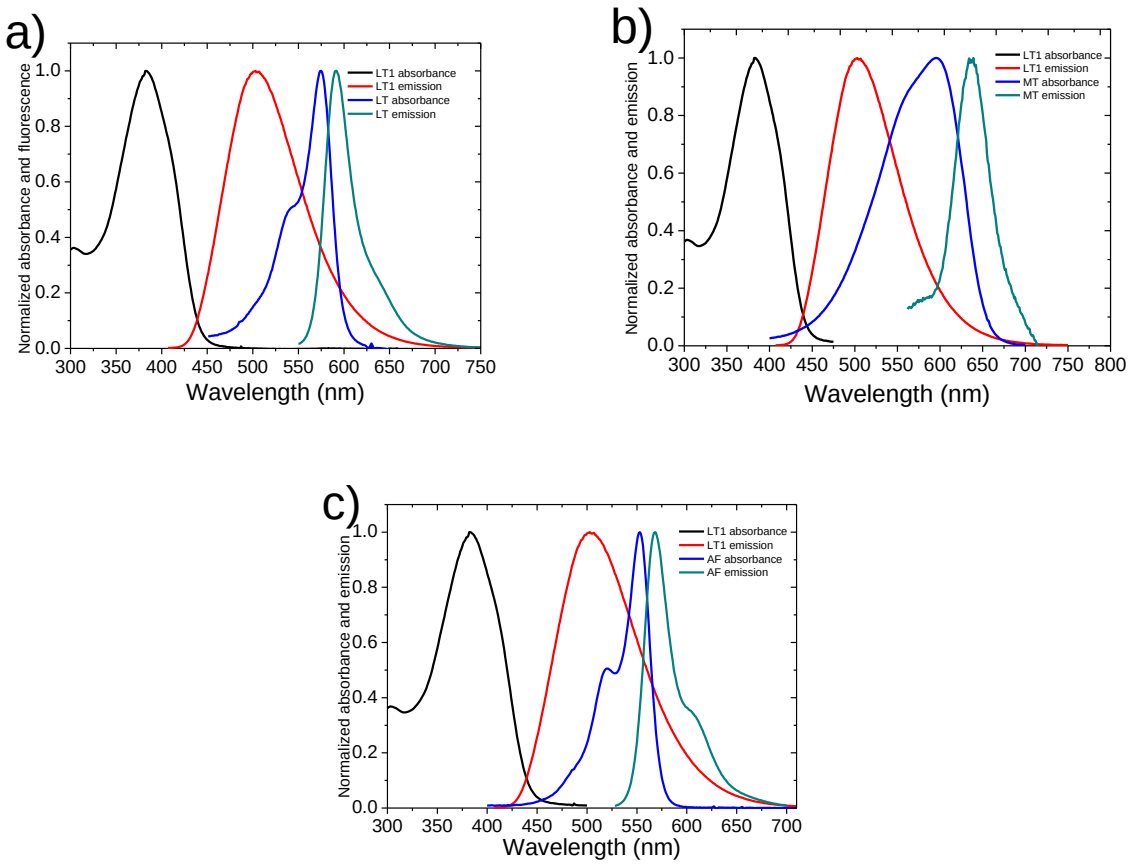

Figure II-6. Normalized absorption and emission spectra of (a) LT1 and Lysotracker Red (LT Red) (excited at 397 and 540 nm), (b) LT1 & Mitotracker Red FM (MT Red) (excited at 397 and 545 nm) and (c) LT1 and Alexa Fluor 555 (AF) (excited at 397 and 515 nm) in PBS (pH = 7.4) buffer.

Conventional single-photon fluorescence images were obtained using inverted microscope (Olympus IX70) equipped with a QImaging cooled CCD (Model Retiga EXi) and a 100 W mercury lamp. In order to improve the fluorescence background-to-image ratios, one-photon confocal fluorescence images of the fixed cells were taken using a custom made filter cube referred to as Fluor out (Ex: 377/50; DM: 409; Em: 525/40) and a Texas Red filter cube (Ex: 562/40; DM: 593; Em: 624/40) for LT1 and Lysotracker Red, Alexa Fluor 555, and Mitotracker

Red FM, respectively. The specifications of the filter cube were tailored to match the excitation wavelength of the probes and to capture most of their emission (Figure II-6). After that, the Slidebook 5.0 program was employed to calculate the Pearson's colocalization coefficients of images acquired in the two channels; Fluor out and Tex Red channels. First, the background of the images was subtracted, and then a mask fitting the area of cells was used to calculate the Pearson's colocalization coefficients. The Pearson's colocalization coefficients are listed in Table II-2.

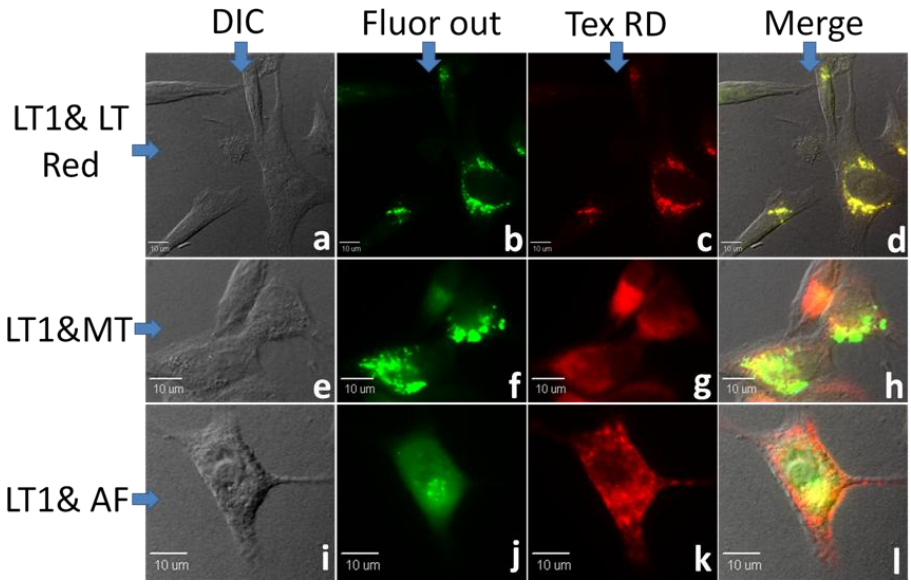

Figure II-7. Colocalization images of HCT 116 cells incubated with LT1 (20 μM, 2 h) and Lysotracker Red (LT Red, 75 nM, 2 h) (top row), LT1 (20 μM, 2 h) and Mitotracker Red FM (MT, 500 nM, 2 h) (middle row), and LT1 (20 μM, 2 h) and Alexa Fluor 555 (AF, 10 μg / mL, 20 min) (bottom row). All the images were acquired with a 60×, oil immersion objective. Left column: DIC, 500 ms. Second column (from left): one-photon confocal fluorescence image of probe LT1 using a custom made Fluor out filter cube (Ex: 377/50; DM: 409; Em: 525/40), 150 ms. Third column (from left): one-photon confocal fluorescence image of LT Red, MT, or AF using a Texas Red filter cube (Ex: 562/40; DM: 593; Em:

624/40) 150 ms. Right column: merged image of DIC and two channels of fluorescence images. The scar bar is 10 μm.

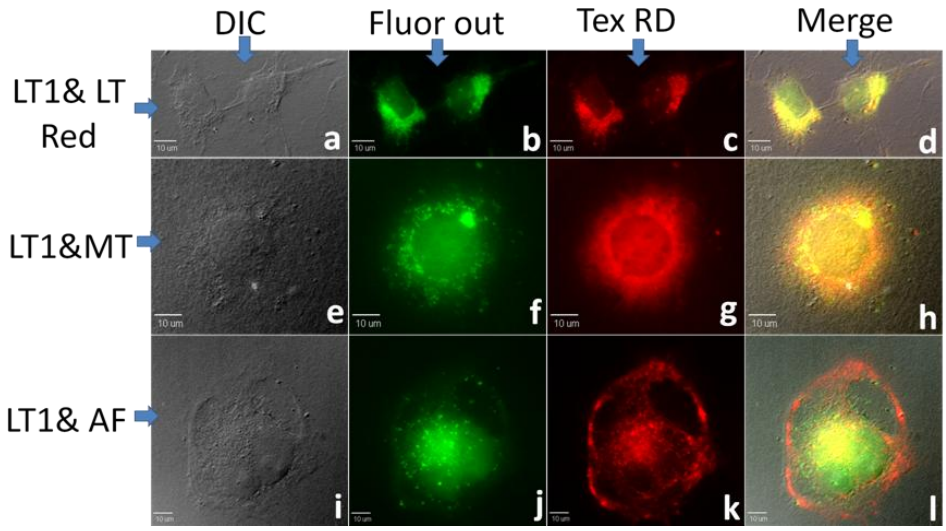

Figure II-8. Colocalization images of COS-7 cells incubated with LT1 (20 μM, 2 h) and Lysotracker Red (LT Red, 75 nM, 2 h) (top row), LT1 (20 μM, 2h) and Mitotracker Red FM (MT, 500 nM, 2 h) (middle row), and LT1 (20 μM, 2 h) and Alexa Fluor 555 (AF, 10 μg/mL, 20 min) (bottom row). All the images were acquired with a 60×, oil immersion objective. Left column: DIC, 500 ms. Second column (from left): one-photon confocal fluorescence image of probe LT1 using a custom made Fluor out filter cube (Ex: 377/50; DM: 409; Em: 525/40), 150ms. Third column (from left): one-photon confocal fluorescence image of LT Red, MT, or AF using a Texas Red filter cube (Ex: 562/40; DM: 593; Em: 624/40) 150 ms. Right column: merged image of DIC and two channels of fluorescence images. The scar bar is 10 μm.

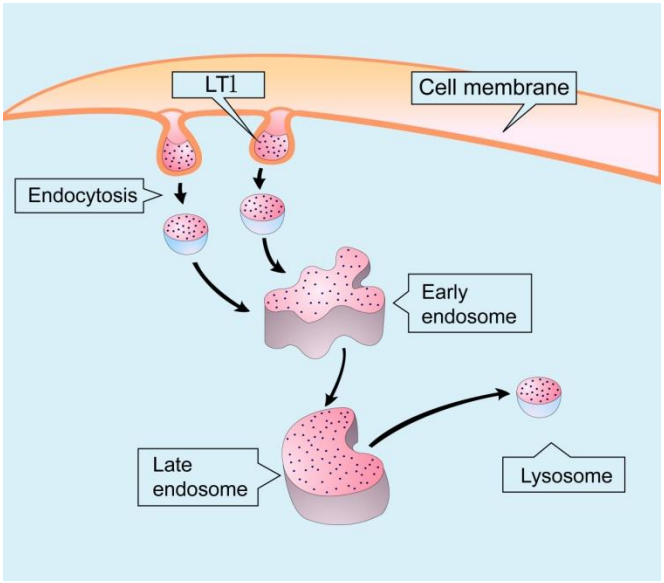

Figure II-9. Proposed LT1 uptake pathway via endocytosis process in cell.

Table II-2. Pearson's colocalization coefficient.

Cell types	A, Pearson's colocalization coefficient		
	LT1&LT Red	LT1&MT	LT1&AF
HCT 116	0.96	0.45	0.46
COS -7	0.92	0.51	0.45

II.5.7 Photostability of LT1 as a lysosome marker in cancer cells

In order to test the photostability of LT1 as lysosome marker in cancer cells, HCT 116 cells were co-stained with LT1 (20 μM, 2 h) and Lysotracker Red (75 nM, 2 h). After incubation, all the cells were washed with PBS (3–5×) and fixed using 3.7% formaldehyde solution for 15 min at 37 °C. Then the fixed cells were treated with 0.5 mL / well $NaBH_4$ (1 mg / mL) solution in PBS (pH = 8.0) for 15 min. The last step was repeated. The plates were then washed twice with PBS and once with H_2O. Finally, the glass coverslips were mounted with Prolong gold mounting media for microscopy. The same cells were excited for 15 min by successive irradiation using a 100 W mercury lamp (the power on the focal plane is ~ 9 mW). The one-photon fluorescence

images were collected every 3 min in the Fluor out channel (Ex: 377/50; DM: 409; Em: 525/40) for LT1 and the Texas Red channel (Ex: 562/40; DM: 593; Em: 624/40) for Lysotracker Red. The fluorescence intensity of the images was calculated by the Slidebook 5.0 program and normalized to track the change in fluorescence intensity from the two channels.

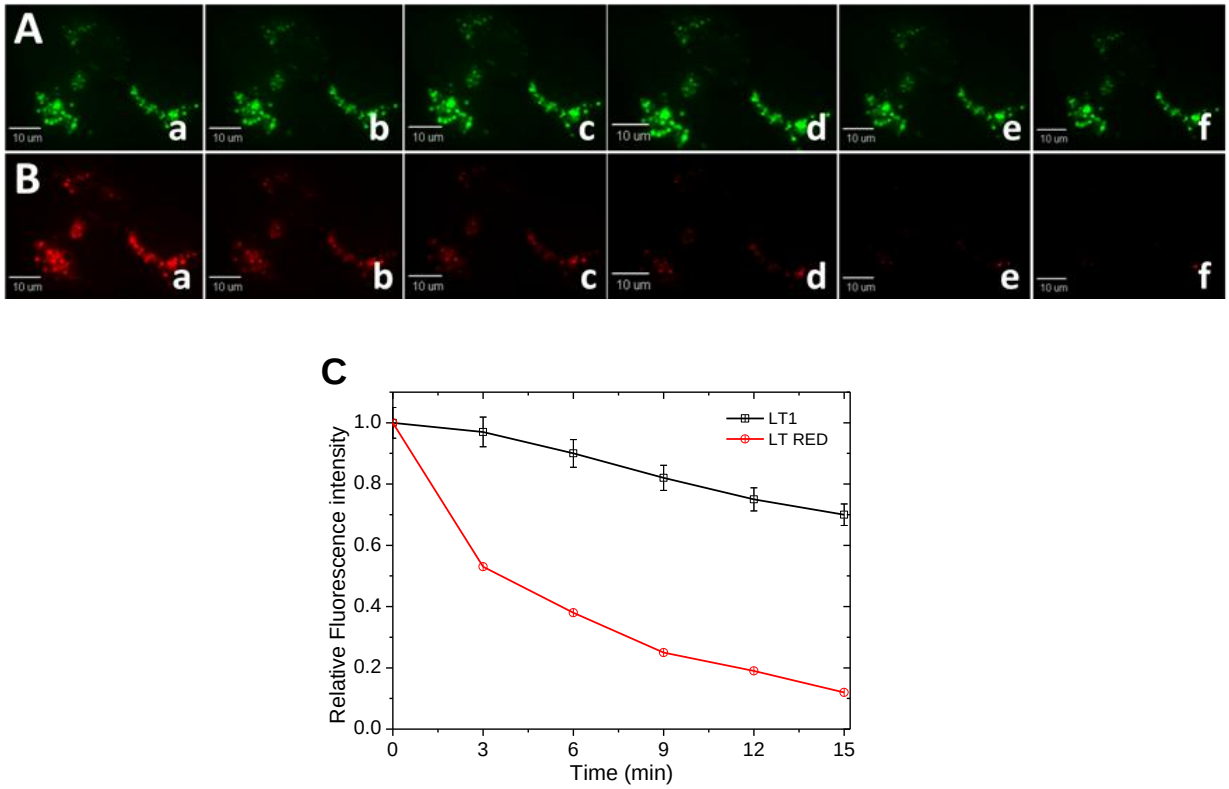

Figure II-10. Photostability comparison of LT1 and Lysotracker Red as lysosome markers in HCT 116 cells. One-photon confocal microscopy images of HCT 116 cells co-stained with (A) LT1 and (B) Lysotracker Red. The images were acquired at (a) 0 min (b) 3 min (c) 6 min (d) 9 min (e) 12 min, and (f) 15 min under successive irradiation (the power on the focal plane is ~ 9 mW). (C) Normalized fluorescence intensity curves of LT1 and Lysotracker Red. All the images were acquired under the same conditions.

II.5.8 Long-term lysosome tracking assays

HCT 116 cells were placed onto poly-D-lysine coated glasses in a 5 cm-diameter dish (400,000 cells per well), and the cells were incubated for 48 h before incubating with fluorescent probe LT1. In order to track the lysosome in cancer cells, the HCT 116 cells were co-stained with LT1 and LT Red, the solution was diluted to 20 μM LT1 and 75 nM Lysotracker Red solution by complete growth medium, DMEM, and then freshly placed over the cells for a 2 h incubation period. The cells were then washed thoroughly and incubated by new DMEM medium for an additional 3, 6, and 9 h. After incubation, the cells were washed with PBS (3–5×) and fixed using 3.7% formaldehyde solution for 15 min at 37 °C. The fixed cells were then treated with 0.5 mL / well $NaBH_4$ (1 mg / mL) solution in PBS (pH = 8.0) for 15 min. The last step was repeated. The plates were then washed twice with PBS and once with H_2O. Finally, the glass coverslips were mounted with Prolong gold mounting media for microscopy. The one-photon cell images were taken with an inverted microscope (Olympus IX70) equipped with a QImaging cooled CCD (Model Retiga EXi) and 100 W mercury lamp. The one-photon confocal fluorescence images of the HCT 116 cells were taken using a custom-made filter cube Fluor out (Ex: 377/50; DM: 409; Em: 525/40) for LT1 and a Texas Red filter cube (Ex: 562/40; DM: 593; Em: 624/40) for Lysotracker Red.

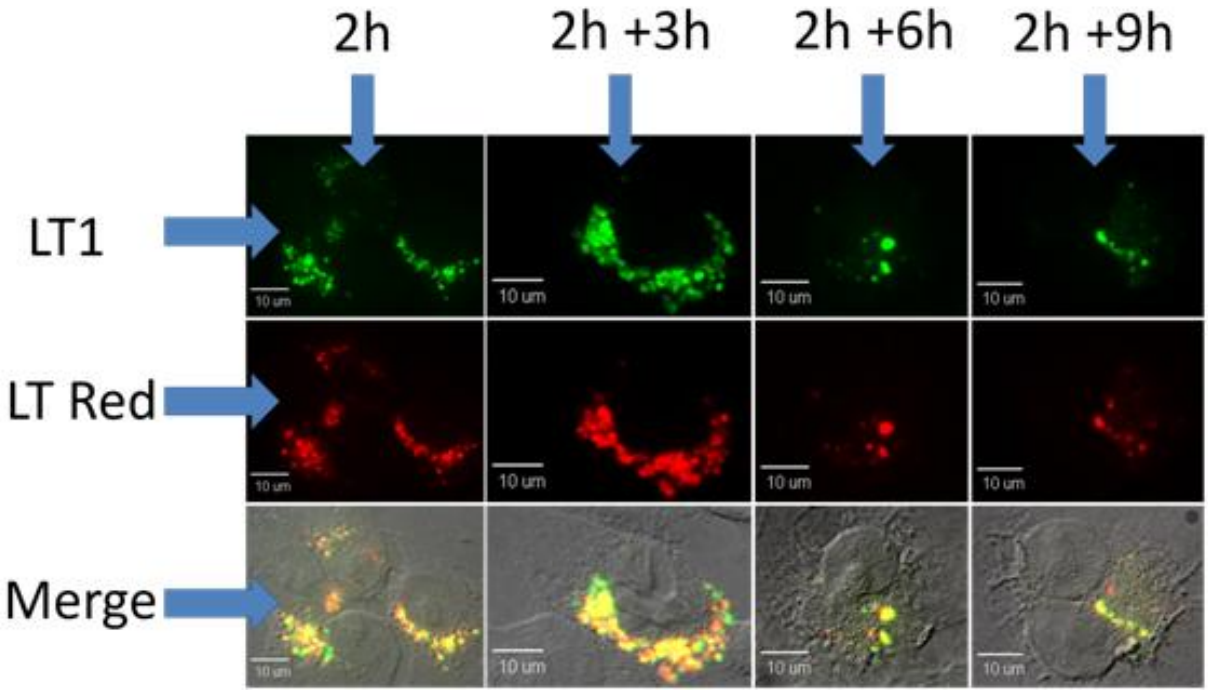

Figure II-11. Long-term lysosome tracking assay for LT1 as a lysosome marker. Left line: colocalization images of HCT 116 cells incubated with LT1 (20 μM, 2 h) & Lysotracker Red (LT Red, 75 nM, 2 h). Second to fourth line: colocalization images of HCT-116 cells incubated with LT1 (20 μM, 2 h) first and then postincubated with fresh DMEM medium for an additional 3, 6, and 9 h, respectively. Lysotracker Red (75 nm, 2 h) was used to label lysosomes just before cell imaging.

II.5.9 Two-photon image of cells

Two-photon fluorescence microscopy (2PFM) images were collected on a modified Olympus Fluoview FV300 microscope system coupled to a tunable Coherent Mira 900F Ti: sapphire, 76 MHz, modelocked, femtosecond laser tuned to 700 nm. An emission short-pass filter (cutoff 690 nm) was placed in the microscope scanhead to avoid background irradiance from the excitation source. Consecutive layers, separated by approximately 0.15 μm, were recorded to create a 3D reconstruction from overlaid two-photon fluorescence images. The two-photon induced

fluorescence was collected with a 60× microscope objective (UPLANSAPO 60x, NA=1.35, Olympus).

II.6 References

[1] Luzio, J. P.; Pryor P. R.; Bright N. A. *Nature Reviews* **2007**, *8*, 622-632.

[2] Safig, P.; Klumperman J. *Nature Reviews* **2009**, *10*, 623-635.

[3] Fehrenbacher, N.; J äättel ä, M. *Cancer Res.* **2005**, *65*, 2993-2995.

[4] Glunde, K.; Foss, C. A.; Takagi, T.; Wildes, F.; Bhujwalla, Z. *Bioconjugate Chem.* **2005**, *16*, 843-851.

[5] Anderson, R. G. W.; Orci, L. *J. Cell Biol.* **1988**, *106*, 539-543.

[6] (a) Lemieux, B.; Percival, M. D.; Falgueyret, J. *Analytical Biochemistry* **2004**, *327*, 247-251. (b) Griffiths, G.; Hoflack, B.; Simons, K.; Mellman, I.; Kornfeld, S. *Cell* **1988**, *52*, 329-341.

[7] Morales A. R.; Yanez C. O.; Schafer-Hales K. J.; Marcus A. I.; Belfield K. D. *Bioconjugate Chem.* **2009**, *20*, 1992-2000.

[8] Liang Y.; Xie ,Y.-X.; Li , J.-H. *J. Org. Chem.* **2006**, *71*, 379-381.

[9] (a)Kim, M. K.; Lim C. S.; Hong, J. T.; Han J. H.; Jang, H. Y.; Kim, H. M.; Cho, B. R. *Angew. Chem. Int. Ed.* **2010**, *49*, 364-367. (b) Gao, Y.; Wu, J.; Li, Y.; Sun, P.; Zhou, H.; Yang, J.; Zhang, S.; Jin, B.; Tian, Y. *J. Am. Chem. Soc.* **2009**, *131*, 5208-5213. (c) Picot, A.; D'Ale´ o, A.; Baldeck, P. L.; Grichine, A.; Duperray, A.; Andraud, C.; Maury, O. *J. Am. Chem. Soc.* **2008**, *130*, 1532-1533.

[10] Malich, G.; Markovic, B.; Winder, C. *Toxicology* **1997**, *124*, 179-192.

[11] (a) Jr, D. W. *J Cell Biol.* **1990**, *110*, 1923-1933. (b) Helenius, A.; Mellman, I.; Wall, D.; Hubbard, A. *Trends Biochem. Sci.* **1983**, *8*, 245-250 (c) Lawrence, B. P.; Brown, W. J. J. *Cell Science* **1992**, *102*, 515-526.

[12] (a) Ohmi, K.; Kudo, L. C.; Ryazantsev, S.; Zhao, H.; Karsten, S. L.; Neufeld, E. F. *PNAS* **2009**, *106*, 8332-8337. (b) Kirkegaard, T.; Roth, A. G.; Petersen, N. H. T.; Mahalka, A. K.; Oslen, O. D.; Moilanen, I.; Zylicz, A.; Knudsen, J.; Sandhoff, K.; Arenz, C.; Kinnunen, P. K. J.; Nylandsted, J.; Jäättelä, M. *Nature* **2010**, *463*, 549-554

[13] Belfield, K. D.; Bondar, M.V.; Prazhonska, O.V.; Shafer, K. J. *J. Fluoresc.* **2002**, *12*, 449-454.

[14] Lakowicz, J. R. Principles of Fluorescence Spectroscopy, Kluwer Academic/Plenum: New York, 1999; p53.

[15] Lakowicz, J. R. Principles of Fluorescence Spectroscopy, Kluwer Academic/Plenum: New York, 1999; p188-189.

[16] Corredor, C. C.; Belfield, K. D.; Bondar, M. V.; Przhonska, O.V.; Yao, S. *Journal of photochemistry and photobiology A: Chemistry* **2006**, *184*, 105-112.

[17] Belfield, K. D.; Bondar, M. V.; Yanez, C. O.; Hernandez, F. E.; Przhonska, O. V. *J. Phys. Chem.* **2009**, *113*, 7101-7106.

CHAPTER III: *IN VITRO* TWO-PHOTON FLUORESCENCE ZINC ION SENSING WITH A BIS (1, 2, 3-TRIAZOLYL) FLUORENYL PROBE

Reproduced in part with permission from: Nguyen, D. M.; Wang, X.; Ahn, H.; Rodriguez, L.; Bondar, M. V.; Belfield, K. D. *ACS Appl. Mater. Interfaces* **2010**, *2*, 2978-2981.

III.1 Abstract

A bis(1,2,3-triazolyl)fluorene derivative was synthesized as a multiphoton absorbing, zinc ion sensing fluorescent probe. Two-photon fluorescence microscopy imaging revealed a significant fluorescence increase upon introduction of Zn^{2+} into HeLa cells, demonstrating reversible Zn^{2+} binding.

III.2 Introduction

Zinc is the second most abundant element *in vivo* and plays a significant role in the metabolic regulation, ion channels and receptors, neuronal transmission, and certain metalloenzymes.[1,2] In neurophysiology, zinc ion is thought to participate in the formation of β-amyloid in Alzheimer's disease.[3] Zinc ion release also causes hypoglycemia-induced neuronal death.[4] The zinc ion is relatively inert with a closed shelf of $3d^{10}$ electronic configuration, hence fluorescence methods are advantageous for detection of Zn^{2+}.[5, 6]

Fluorescent probes for Zn^{2+} sensing *in vitro* and *in vivo* in biological environments should exhibit selectivity for Zn^{2+} over other relevant heavy metal ions. The probe should have high affinity, as well as bind rapidly and reversibly. Zinc ion sensing utilizing fluorescein and porphyrin derivatives have been reported.[7-9] Since the advent of two-photon absorption (2PA) and techniques that rely on 2PA, a number of advantages have been identified for 2PA, e.g., molecules can be excited at a long wavelength, usually in the near infrared (NIR) region, deeper penetration and less scattering, and reduced photodamage and photobleaching.[10] Recently, our laboratory developed 2PA fluorescent probes for targeting cellular proteins[11, 12] and other biological applications. The fluorene-based construct is employed for its generally high fluorescence quantum yield, reasonably large 2PA cross section, and high photostability.[13-18]

III.3 Result and Discussion

The cytotoxicity of probe **1** was evaluated by the Alamar Blue cytotoxicity assay to assess its suitability for *in vitro* imaging. Relative low cytotoxicity of **1** in HeLa cells was demonstrated with optimal concentrations for imaging at 5-15 μM (Figure III-1).

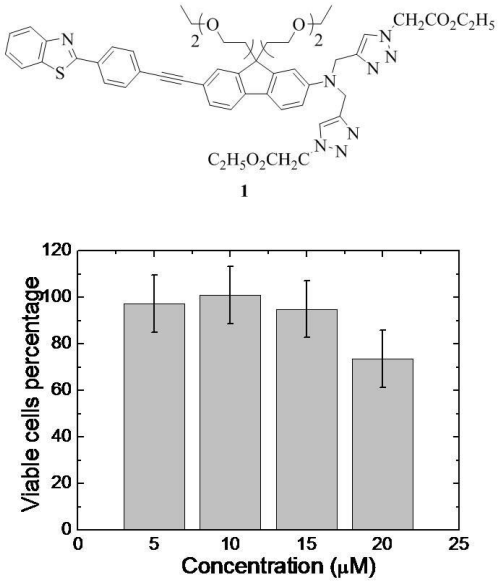

Figure III-1. Structure of Zn^{2+} probe **1** and viability of HeLa cells incubated with **1**. Error bars represent standard error of the mean of 3 replicates.

In vitro Zn^{2+} sensing and 2PFM imaging was investigated for probe **1** in live HeLa cells; cells were maintained on a stage incubator and images were acquired before and after a zinc containing medium was introduced into cells. Next, N,N,N',N'-tetrakis(2-pyridylmethyl)ethylenediamine (TPEN) was introduced as a chelator[19] to displace Zn^{2+} in the zinc complex of **1**, resulting in a decrease in fluorescence (Figure III-2B, D) *in vitro*.

The new probe exhibited both good two-photon absorption and fluorescence enhancement upon Zn^{2+} binding, had low cytotoxicity, had high Zn^{2+} binding constants, and, importantly, was

soluble in aqueous media. Bis(1,2,3-triazolyl)fluorene **1** proved useful for *in vitro* zinc ion sensing by 2PFM, suggesting future potential for *in vivo* Zn^{2+} sensing and imaging, a subject of future investigation.

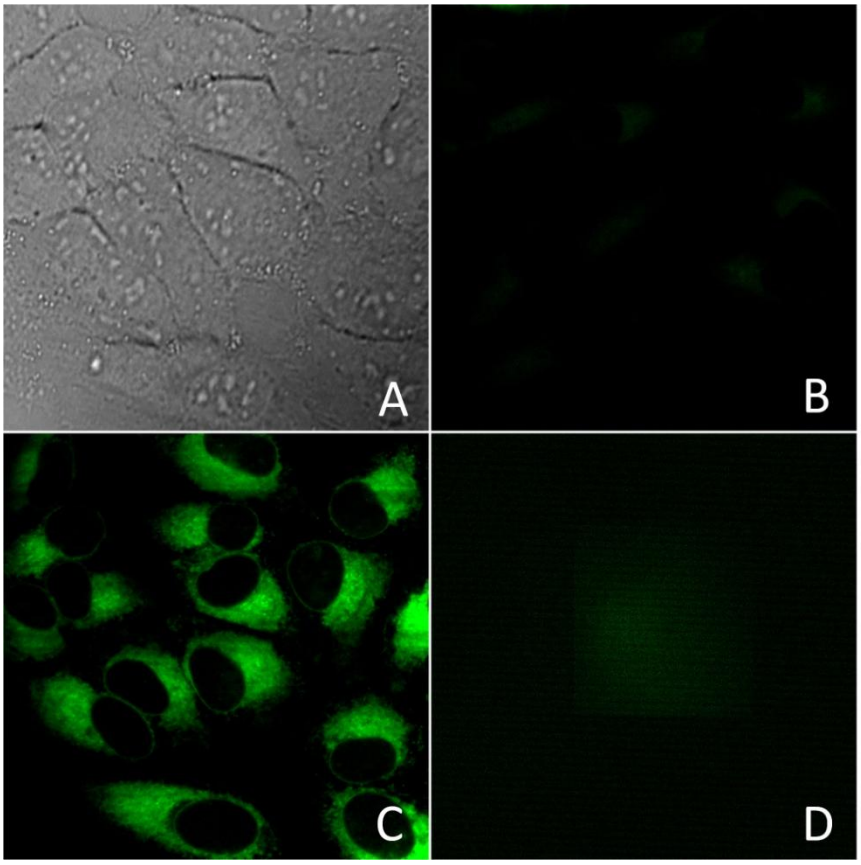

Figure III-2. (A) DIC image of HeLa cells incubated with 15 μM of probe **1** for 2 h. (B) 2PFM image at λ_{ex} = 740 nm and power = 50 mW. (C) 2PFM image after 15 min treatment with zinc sulfate (50 μM). (D) 2PFM image after further incubation with 50 μm TPEN for 15 min.

III.4 Conclusion

A high two-photon absorbing hydrophilic fluorene derivative **1** was demonstrated as a zinc ion sensing fluorescent probe. 2PFM imaging revealed a significant fluorescence increase upon introduction of Zn^{2+} into living HeLa cells, demonstrating reversible Zn^{2+} binding.

III.5 Experimental

III.5.1 Materials and general methods

N,N,N',N'-tetrakis(2-pyridylmethyl) ethylenediamine (TPEN) were purchased from commercial sources (Acros and Aldrich) and used as received. The HeLa cells were purchased from ATCC (America Type Culture Collection, Manassas, VA, USA). All cells were incubated in RPMI-1640 medium (Invitrogen, Carlsbad, CA), supplemented with 10% fetal bovine serum (FBS, Atlanta Biologicals, Lawrenceville, GA, USA), 100 units / mL penicillin-streptomycin (Atlanta Biologicals, Lawrenceville, GA, USA) and incubated at 37 ℃ in a 95% humidified atmosphere containing 5% CO_2.

III.5.2 Cell viability assay

HeLa cells (ATCC) were incubated for 24 h in 96-black wall well plates (20,000 cells per well) with RPMI medium (GIBCO) supplemented with 10% fetal bovine serum and 1% penicillin-streptomycin in a humidified atmosphere of 5% CO_2 at 37 ℃. Probe **1** was added into the wells and incubated for a period of 24 h prior to the Alamar Blue viability protocol (Invitrogen). Briefly, Alamar Blue (20 μL) was added to culture medium at 10% volume and kept at 37 ℃ in an incubator. Fluorescence emission was then recorded at 590 nm upon excitation at 560 nm with a SpectraMax M5 (Molecular Devices) after 6 h of incubation. For a control, Alamar Blue was added to the cell medium without fluorescent probe. The experiment was performed in triplicate for data analysis.

III.5.3 Cell incubation and imaging

HeLa cells were placed into a poly-D-lysine (Invitrogen) coated glass coverslip in 5 cm diameter plates (200,000 cells per well). The cells were grown for 36 h before incubation with

probe **1**. A stock solution of **1** in DMSO was prepared as 1 mM solutions, and then diluted to 15 μM dye solution with the cell medium. The dye solution was freshly prepared and placed over the cells for 2 h. After incubation with **1**, the cells were washed with the PBS solution (3 to 5 times) and put in a Biophotonics stage incubator chamber on a fluorescence microscope stage at 37 ℃ with continuous flow of medium for live cell imaging. An inverted microscope (Olympus IX70) equipped with a QImaging cooled CCD (Model Retiga EXi) was utilized, where the output of a filtered 100 W mercury lamp was employed as the light excitation source. A customized filter cube (Ex 377/50, DM 409, Em 460/50) was used. Two-photon fluorescence microscopy (2PFM) images were collected on a modified Olympus Fluoview FV300 microscope system coupled to a tuneable laser at 740 nm. An emission short-pass filter (cutoff 690 nm) was placed in the microscope scanhead to avoid background irradiance from the excitation source. The two-photon induced fluorescence was collected with a 60× microscope objective (UPLANSAPO 60x, NA = 1.35, Olympus).

III.6 References

[1] Bush, A. I. *Curr. Opin. Chem. Biol.* **2000**, *4*, 184-191.

[2] Maret, W. *Biometals* **2001**, *14*, 187-190.

[3] Bush, A. I. *Trends. Neurosci.* **2003**, *26*, 207-214.

[4] Suh, S. W.; Garnier, P.; Aoyama, K.; Chen, Y.; Swanson, R. A. *Neurobiol. Disease* **2004**, *16*, 538-545.

[5] Valeur, B.; Leray, I.; *Coord. Chem. Rev*. **2000**, *205*, 3-40.

[6] Barrios, A. M. *ACS Chem. Biol.* **2006**, *1*, 67-68.

[7] Walkup, G. K.; Burdette, S. C.; Lippard, S. J.; Tsien, R. Y. *J. Am. Chem. Soc.* **2000**, *122*, 5644-5645.

[8] Nolan, E. M.; Lippard, S. J. *Acc. Chem. Res.* **2009**, *42*, 193-203.

[9] Zhang, X. A.; Lovejoy, K. S.; Jasanoff, A.; Lippard, S. J. *Proc. Natl. Acad. Sci. USA* **2007**, *104*, 10780-10785

[10] Denk, W.; Strickler, J. H.; Webb, W. W. *Science* **1990**, *248*, 73-76.

[11] Morales, A. R.; Schafer-Hales, K. J.; Marcus, A. I.; Belfield, K. D. *Bioconjugate Chem.* **2008**, *19*, 2555-2567.

[12] Morales, A. R.; Yanez, C. O.; Schafer-Hales, K. J.; Marcus, A. I.; Belfield, K. D. *Bioconjugate Chem.* **2009**, *20*, 1992-2000.

[13] Belfield, K. D.; Hagan, D. J.; Stryland, E. W.; Schafer, K. J.; Negres, R. A. *Org. Lett.* **1999**, *1*, 1575-1578.

[14] Schafer, K. J.; Belfield, K. D.; Yao, S.; Frederiksen, P. K.; Hales, J. M.; Kolattukudy, P. E. *J. Biomed. Opt.* **2005**, *10*, 514021-514028.

[15] Corredor, C. C.; Belfield, K. D.; Bondar, M. V.; Przhonska, O. V.; Yao, S. *J. Photochem. Photobiol. A Chem.* **2006**, *184*, 105-112.

[16] Belfield, K. D.; Bondar, M. V.; Przhonska, O. V.; Schafer, K. J. *J. Photochem. Photobiol. A Chem.* **2004**, *162*, 489-496.

[17] Belfield, K. D.; Bondar, M. V.; Przhonska, O. V.; Schafer, K. J. *J. Photochem .Photobiol. A Chem.* **2004**, *162*, 569-574.

[18] Belfield, K. D.; Bondar, M. V.; Przhonska, O. V.; Schafer, K. J. *J. Photochem. Photobiol. Sci.* **2004**, *3*, 138-141.

[19] C. A. Blindauer, M. T. Razi, S. Parsons, P. J. Sadler, *Polyhedron* **2006**, *25*, 513-520.

CHAPTER IV: FOLATE RECEPTER TARGETING SILICA NANOPARTICLE PROBE FOR TWO-PHOTON FLUORESCENCE BIOIMAGING

Reproduced with permission of the Optical Society of America from: Wang, X.; Yao, S.; Yang Ahn, H.; Zhang, Y.; Bondar, M. V.; Torres, J. A.; Belfield, K. D. *Biomedical Optics express* **2010**, *1*, 453–462.

IV.1 Abstract

Narrow dispersity organically modified silica nanoparticles (SiNPs), diameter ~30 nm, entrapping a hydrophobic two-photon absorbing fluorenyl dye, were synthesized by hydrolysis of triethoxyvinylsilane and (3-aminopropyl) triethoxysilane in the nonpolar core of Aerosol-OT micelles. The surface of the SiNPs were functionalized with folic acid, to specifically deliver the probe to folate receptor (FR) over-expressing HeLa cells, making these folate two-photon dye-doped SiNPs potential candidates as probes for two-photon fluorescence microscopy (2PFM) bioimaging. *In vitro* studies using FR overexpressing HeLa cells and low FR expressing MG63 cells demonstrated specific cellular uptake of the functionalized nanoparticles. One-photon fluorescence microscopy (1PFM) imaging, 2PFM imaging, and two-photon fluorescence lifetime microscopy (2P-FLIM) imaging of HeLa cells incubated with folate-modified two-photon dye-doped SiNPs were demonstrated.

IV.2 Introduction

Two-photon fluorescence microscopy (2PFM) has several advantages in biological imaging over conventional one-photon fluorescence microscopy (1PFM), including high three-dimensional (3D) spatial localization due to the inherent nonlinear dependence of two-photon fluorescence (2PF) on the illumination intensity [1, 2], deeper penetration into optically thick tissue, and improved tissue viability because of using near-IR excitation. [3, 4] We have reported a number of fluorene-based molecules that undergo good two-photon absorption (2PA). However, 2PA fluorenyl fluorophores with high fluorescence quantum efficiency are synthetically more accessible in hydrophobic forms.[5-7] The incompatibility to aqueous biological systems limits their application in biological imaging area. Our efforts are directed to overcome these limitations as described herein.

Nanomaterials are beginning to revolutionize the fields of medicine, bioimaging, and photonics due to their chemical and biological resilience, safety, and multimodality of the surface.[8-10] In the past few years, ceramic-based nanomaterials have proven to be innocuous and have been widely investigated in the application of gene delivery as DNA carriers[11], photodynamic therapy as carriers of photosensitizers [12, 13], and bioimaging as nanoprobes [14, 15]. In this paper, organically modified silica (ORMOSIL) nanoparticles were employed to encapsulate hydrophobic fluorenyl dyes to provide a stable aqueous dispersion of the fluorescent probe and improve the fluorophore's photostability. Narrow dispersity ORMOSIL nanoparticles (diameter ~25 nm), entrapping a hydrophobic two-photon absorbing fluorenyl dye 4,4'-(1E,1'E)-2,2'-(9,9-didecyl-9H-fluorene-2,7-diyl)bis(ethene-2,1-diyl)bis(N,N-dibutylaniline) (DBF), were synthesized in the nonpolar core of Aerosol-OT micelles by hydrolysis of triethoxyvinylsilane

and (3-aminopropyl)triethoxysilane. To introduce targeting specificity, the surface of the SiNPs was further functionalized by a cell receptor targeted ligand.

With the development of cell biology, a variety of disease-specific ligand-receptor pairs have been identified, e.g., ligands based on antibodies, antibody fragments, proteins, and peptides. Because of their high selectivity towards specific cell receptors, those biomolecules were conjugated to nanoparticles and investigated for specific targeting delivery.[16] One example of such a ligand-receptor pair is folate ligand and folate receptor (FR). FR is found overexpressed in a number of human cancer cell while the distribution in normal tissues is minimal. The folate ligand, which is a member of vitamin B family, plays an important role in cell survival by its participation in the biosynthesis of nucleic and amino acids.[17] It is also a high affinity ligand that enhances conjugated anti-cancer drugs by targeting folate receptor (FR) positive cancer cells.[18] In this work, a most commonly used folate ligand, folic acid, was introduced on the surface of dye-doped SiNPs, not only because it can efficiently internalize into the cell through receptor mediated endocytosis when conjugated with a variety of biomolecules, but, significantly, folic acid is stable and low cost.[19]

The nanoparticle probes were structurally characterized while spectroscopic analyses demonstrated that the optical properties of the incorporated dye were retained. Moreover the photostability of the dye improved significantly by encapsulation within the SiNPs. *In vitro* studies using Hela cells that overexpress FRs revealed cellular uptake of the folate nanoparticles. Meanwhile MG63 cells, which do not express FR, did not uptake the folate SiNPs efficiently.[20] Furthermore, Hela cells, whose FRs were first blocked by free folic acid, were incubated with the folic acid conjugated SiNPs, resulting in a dramatic decrease in the uptake of the folic acid

conjugated SiNPs. These finding demonstrated that the folic acid functionalized SiNPs have *in vitro* cell specificity, while maintaining good 2PA, fluorescence, and photostability properties, making these 2PA modified SiNPs useful tools as for two-photon optical bioimaging.[21]

IV.3 Results and discussion

The morphology and size of the DBF-doped SiNPs were determined by TEM images (Figure. IV-1). The particle size distribution determined by the TEM images indicated that they were of narrow dispersity, with a diameter range of 25-40 nm. The average particle size of the dye-doped amino-terminated silica nanoparticles (SNP-DBF-NH_2) was 30 nm. After the particles were conjugated with folic acid, their average particle size increased to 34 nm. The increase in particle size is apparently attributed to the shielding of their surface by folic acid. In addition, the absorbance of 272 nm in the folic acid functionalized nonlabeled silica nanoparticles (SNP-NHFA) and folate dye-doped silica nanoparticles (SNP-DBF-NHFA) also indicated successful conjugation of the folic acid with the silica nanoparticles (Figure. IV-2a). Moreover, the presence of the folic acid on the surface of the SiNPs was demonstrated by comparing the anisotropy, excitation, and emission spectra of the nonlabeled amino-terminated silica nanoparticles (SNP-NH_2) and SNP-NHFA in water. The concentration of dye in SNP-DBF-NHFA was determined by absorbance at 410 nm ($\varepsilon_{410\ nm} = 7.1 \times 10^4\ M^{-1}cm^{-1}$ in water). The final concentration of SNP-DBF-NHFA in water was 2.3 mg/mL, determined by vaporization.

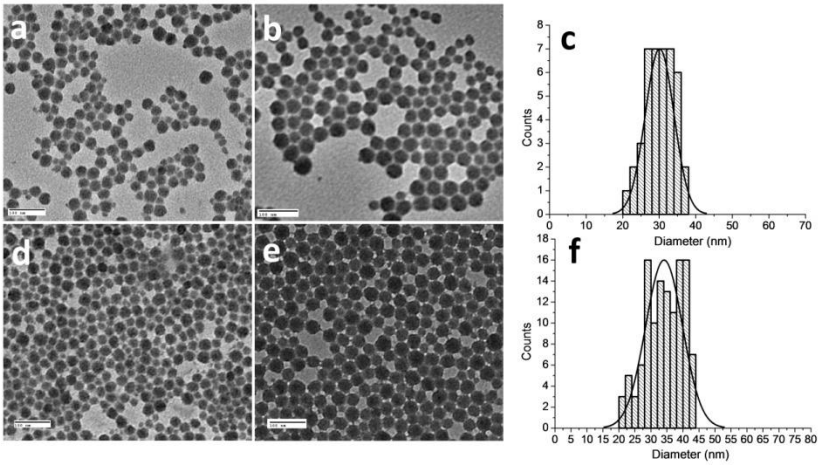

Figure IV-1. TEM images of silica nanoparticles (a) SNP-NH_2, (b) SNP-DBF-NH_2, and (c) their particle size distribution, (d) SNP-NHFA, (e) SNP-DBF-NHFA, and (f) their particle size distribution. Scale bar: 100 nm.

The linear and nonlinear photophysical properties of the SiNPs were investigated to assess their potential for two-photon bioimaging. The absorption, excitation, and fluorescence spectra of the SiNPs suspended in water, as well as the free DBF dye in THF, are shown in Figure IV-2. The spectra of dye-doped SiNPs were similar to the spectra of the free DBF in THF, except for the expected absorbance of folic acid at 272 nm in the folate SiNPs. The spectra of unlabeled folate silica nanoparticles (SNP-NHFA) exhibited absorbance and excitation of folic acid at 272 and 360 nm, and very weak fluorescence of the folic acid with maximum emission at 476 nm, which was not present in the spectra of folic acid-free unlabeled silica nanoparticles (SNP-NH_2).

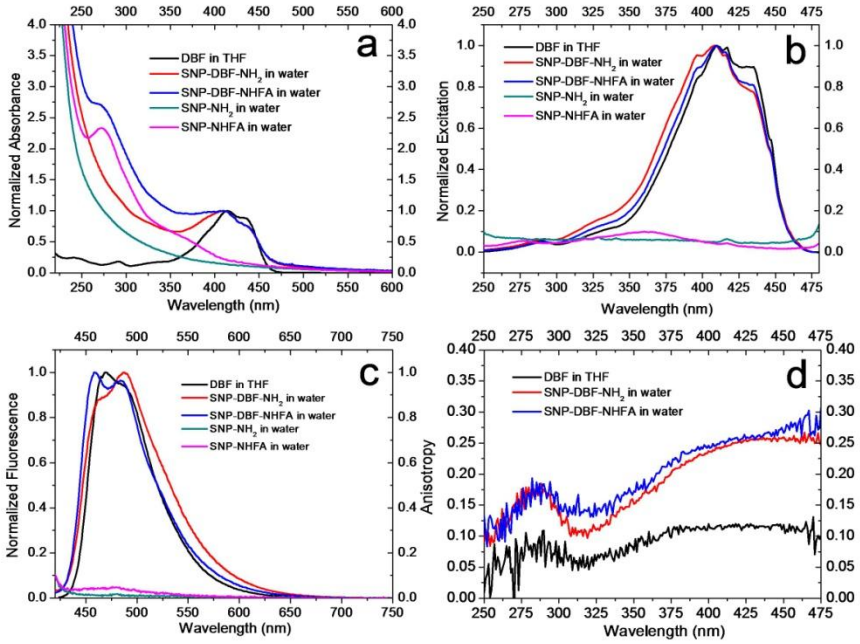

Figure IV-2. (a) Normalized absorption of DBF in THF and SiNPs in water, (b) normalized excitation spectra of DBF in THF and SiNPs in water, the maximum excitation of SNP-NH_2 and SNP-NHFA were normalized to 0.1 (Em: 490 nm), (c) normalized fluorescence emission spectra of DBF in THF and SiNPs in water, the maximum fluorescence of SNP-NH_2 and SNP-NHFA were normalized to 0.1 (Ex: 410 nm), and (d) fluorescence anisotropy of DBF in THF and SiNPs in water (Em: 490 nm).

The fluorescence anisotropy of SNP-DBF-NH_2, SNP-DBF-NHFA suspended in water and the free dye in THF (Figure IV-2d) indicates that the fluorescence of the dye doped in the particles manifests relative high anisotropy, just as in very viscous solvent pTHF [15] while the free dye in THF exhibited much lower fluorescence anisotropy. This result can be explained by the fact that the rotational mobility of the dye molecules within the SiNPs was limited. Although the fluorescence quantum yield, Φ_f, of the dye in SiNPs suspended in water decreased to 0.49 from 1.0 in organic solvent, due to likely aggregation, its photostability improved nearly 7 times when

it was encapsulated in the SiNPs. The photostability of the dye-doped SiNPs nanoparticles and free dye in THF were compared with the common fluorescent dye fluorescein. The photobleaching decomposition quantum yield of fluorescein was 7.3×10^{-6}, approximately 4 times higher than DBF in THF and 28 times higher than SNP-DBF-NHFA in water. The photostability results and the photophysical properties of SNP-DBF-NHFA suspended in water and the free dye in THF are summarized and compared with fluorescein in Table IV-1. The florescence decays of the free dye in THF and SNP-DBF-NHFA suspended in water were characterized by a single exponential process. The fluorescence life time, $\tau \approx 1.2$ ns, of DBF remained almost the same after encapsulation in SiNPs. The efficiency 2PA for free DBF in relatively high polarity solution, THF, which is close to water, was investigated. The 2PA cross sections were determined in the range of 700-940 nm, a useful range for 2PFM, and are presented in Figure IV-3a. The dye showed a maximum 2PA cross section value of ~400 GM at 740 nm, which is quite suitable for 2PFM bioimaging using commercially available femtosecond lasers.

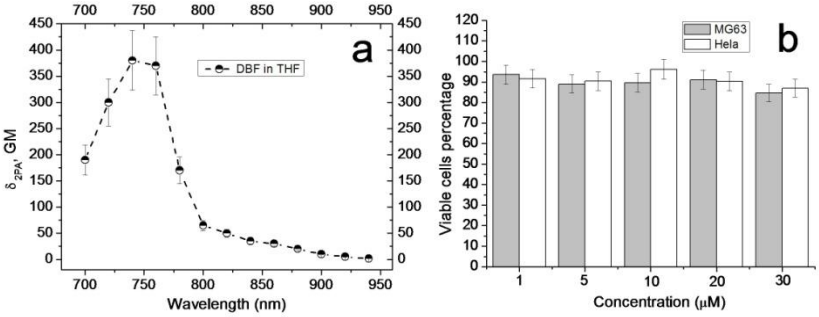

Figure IV-3. (a) 2PA cross sections of DBF (fs excitation). (b) Viability of Hela and MG63 cells with SNP-DBF-NHFA.

Table IV-1. Photophysical properties of the DBF in THF, SNP-DBF-NHFA in water and fluorescein in 0.1 M NaOH aqueous solution.

Materials	$\lambda_{max}^{(ex)} / \lambda_{max}^{(fl)}$ [a]	$\varepsilon \cdot 10^{-4}$ [b]	T [c]	Φ_f [d]	$\Phi_d \times 10^6$ [e]
DBF	410/470	10.1	1.25 ± 0.08	1.0	1.9
SNP-DBF-NHFA	409/458	7.1	1.20 ± 0.08	0.49	0.26
Fluorescein	491/521	8.8	n.d.[f]	0.95	7.3

[a] λ_{max} values of the one-photon excitation and emission spectra in nm; [b] molar absorbance in M^{-1} cm^{-1}; [c] fluorescence lifetime in ns; [d] fluorescence quantum yield, ±15%; [e] photodecomposition quantum yield, ±15%; [f] Not determined.

Cytotoxicity of the SiNPs must be minimized if the particles are to be used as probes for 2PFM imaging in living cells. An MTS viability test with Hela and MG63 cells was performed to determine the cytotoxicity of the folate dye-doped SiNPs The results presented in Figure IV-3b indicates that the toxicity of the nanoparticles is very low (~ 90% viability) over a concentration range from 1 – 30 μM, after treating the HeLa and MG63 cells with a variety of concentrations of nanoparticles for 24 h. The concentrations were determined by the absorbance of the SiNPs at 410 nm.

To test the selectivity of the folate dye-doped SiNPs *in vitro*, HeLa cells, known to overexpress FRs, were employed as a positive control while low folate receptor expressing cancer cells MG63 were selected as a negative control.[17] One-photon and two-photon fluorescence microscopy was used to study the selective uptake of the folate silica nanoparticles SNP-DBF-NHFA between Hela and MG63 cells. The fluorescence images of HeLa and MG63

cells incubated with folate silica nanoparticles SNP-DBF-NHFA, shown in Figure IV-4, indicated that SNP-DBF-NHFA was specifically taken by FR overexpressing Hela cells. However, the low FR expressing MG63 cells (Figure IV-4 middle row) did not take the folate nanoparticles effectively. To confirm that the uptake of the folate nanoparticles by Hela cells is mediated by the FR, HeLa cells whose FR were initially blocked by free folic acid were used to incubate with SNP-DBF-NHFA. The result (bottom row of Figure IV-4) indicated that the Hela cells did not uptake the folate silica nanoparticles to any large degree after their FRs were blocked by folic acid. This enhanced efficiency is attributed to receptor-mediated uptake of these folate nanoparticles with the FR of HeLa cells.

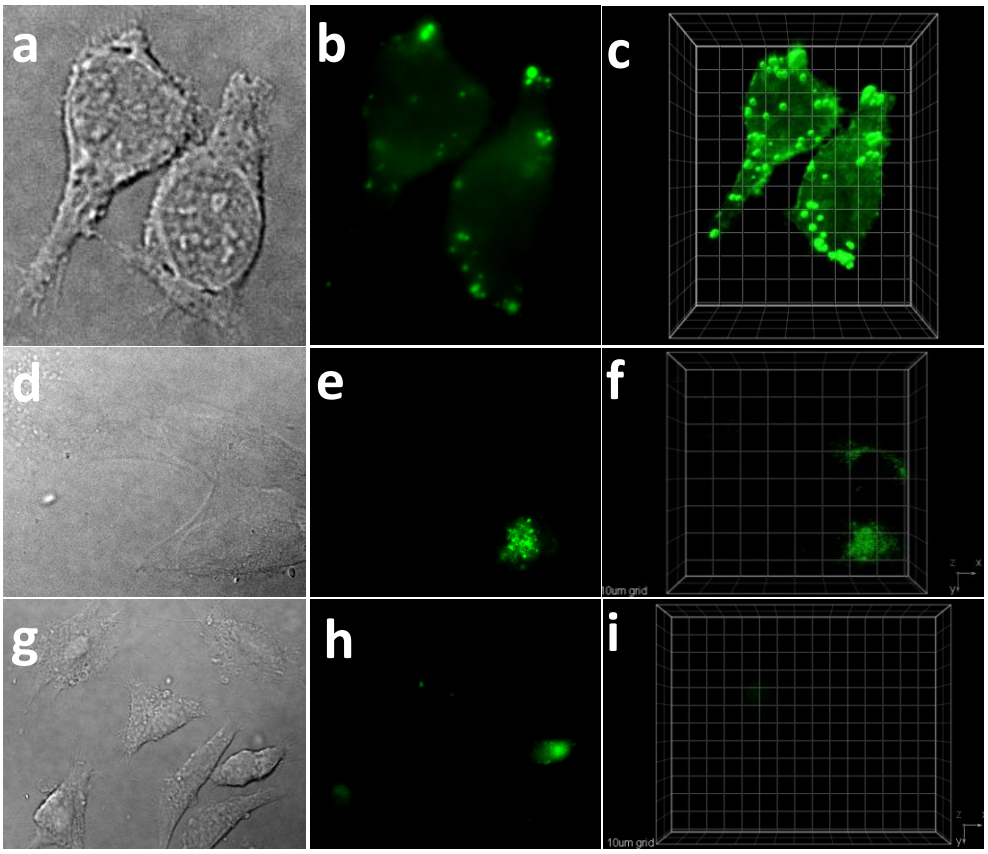

Figure IV-4. Images of HeLa cells (top row), MG63 cells (middle row), and folate receptor blocked HeLa cells (bottom row) incubated with SNP-DBF-NHFA (20 μM, 2 h). Left column: DIC, 40 ms. Middle column: one-photon fluorescence image, 200 ms (filter cube Ex: 377/50 DM: 409 Em: 525/40). Right column: 3D reconstruction from overlaid two-photon fluorescence images (Ex: 740 nm; Power: 30 mW; Em. short-pass filter 690 nm) 10 μm grid.

Moreover, 2PFM and 2P-FLIM images (Figure IV-5) of HeLa cells incubated with SNP-DBF-NHFA were performed to show the distribution of nanoparticles in the cells. The resulting 2PFM and 2P-FLIM images clearly illustrate organelles in the cytoplasm of cells. The organelles are spherical in shape with an average diameter of ~600 nm, likely lysosomes or endosomes in term of their size and morphology.[22] The average fluorescence lifetime of the SiNP probe within

the organelles was ~ 1.2 ns, consistent with that observed for the dye-doped SiNPs in water, further confirming successful SNP-DBF-NHFA up take by HeLa cells.

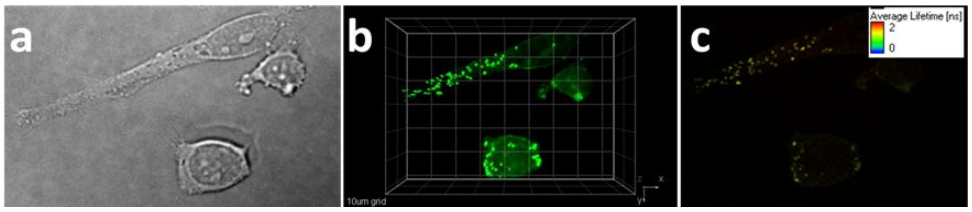

Figure IV-5. Images of HeLa cells incubated with SNP-DBF-NHFA (20 μM, 2 h). (a) DIC, 20 ms, (b) 3D reconstruction from overlaid two-photon fluorescence images (Ex: 740 nm; Power: 30 mW; Em. short-pass filter 690 nm) 10 μm grid, (c) 2P-FLIM image (Ex: 740 nm; Power: 30 mW).

IV.4 Conclusion

Narrow dispersity organically-modified SiNPs, entrapping a hydrophobic 2PA fluorescent dye, were synthesized and characterized. In order to specifically deliver the two-photon fluorescent SiNPs to cancer cells, the surface of the nanoparticles were functionalized with folic acid. Significantly, the photostability of the fluorescent silica nanoparticles was seven times greater than the free dye and 28 times greater than the commercially available dye fluorescein. Cytotoxicity of the folate-modified dye-containing SiNPs was low. The folate-modified dye-containing SiNPs were selectively taken by folate receptor overexpressing HeLa cells, as determined by 1PFM, 2PFM, and 2P-FLIM imaging experiments. Thus, these folate-modified dye-containing SiNPs are candidates as efficient probes for 2PFM and 2P-FLIM bioimaging applications, and have prospective application for earlier diagnosis of folate receptor overexpressed cancers, including breast, ovary, endometrium, and lung cancer.

IV.5 Experimental

IV.5.1 Materials

Triethoxyvinylsilane (VTES, 97%), cosurfactant 1-butanol (99%), surfactant Aerosol OT (AOT, 98%). Dioctylsulfosuccinate sodium salt and (3-aminopropyl)triethoxysilane (APTES) were purchased from Sigma-Aldrich. N-methyl-2-pyrrolidinone (NMP, 99%) was purchased from Acros Organic. Thermo Slide-A-Lyzer® 10K cut off dialysis cassettes and 0.22 μm cutoff membrane filter were purchased from Fisher Inc. All the above chemicals were used as received without further purification unless noted. HeLa and MG63 cells were purchased from ATCC (America Type Culture Collection, Manassas, VA). All cells were incubated in RPMI-1640 medium (Invitrogen, Carlsbad, CA), supplemented with 10% fetal bovine serum (FBS, Atlanta Biologicals, Lawrenceville, GA), 100 units / mL penicillin-streptomycin (Atlanta Biologicals, Lawrenceville, GA), and incubated at 37 ℃ in a 95% humidified atmosphere containing 5% CO_2. Details of fluorenyl derivative DBF, including preparation and characterization, were described in ref. 23.[23]

IV.5.2 Synthesis of dye-encapsulated amine-terminated silica nanoparticles

Amine-terminated SiNPs, with or without fluorenyl derivative DBF, were synthesized according to the method described by P. N. Prasad et al.[15] The synthesis of silica nanoparticles and their bioconjugation with folic acid was schematically described by Figure IV-6. Briefly, the nanoparticles were synthesized in the nonpolar core of AOT / 1-butanol micelles in deionized water. NMP was used as a hydrophilic solvent which has unlimited water miscibility as well as suitable solubility for DBF. First, 0.22 g of the surfactant AOT, 300 μL of the cosurfactant 1-butanol, and 100 μL of NMP were dissolved in 10 mL deionized water with magnetic stirring,

forming an oil-in-water microemulsion. To the microemulsion system, 100 μL of neat NMP or NMP solutions containing DBF dye (2 mg / mL) was added, followed by addition 100 μL of neat VTES. After stirring the reaction mixture for one additional hour, the polymerization reaction was initialized by the addition of 20 μL neat APTES. To ensure completion of polymerization within the coprecipitated nanoparticles, the mixtures were further stirred at room temperature for 20 h. Nanoparticle purification was conducted by dialysis against deionized water in a 10 kDa cutoff cellulose membrane to remove surfactant, cosurfactant, and other unreacted molecules for 48 h. The dialyzed solution was then filtered through a 0.22 μm cutoff membrane filter and stored at 5 ℃ for later use.

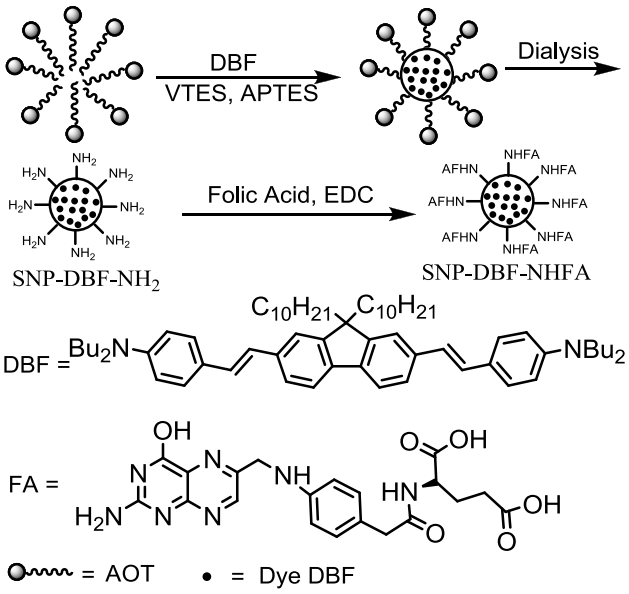

Figure IV-6. Schematic illustration of the synthesis of silica nanoparticles and their bioconjugation with folic acid.

IV.5.3 Conjugation of amine-terminated silica nanoparticles with folic acid

To a 5 mL portion of stock solution of amine-terminated DBF dye-doped or unlabeled nanoparticles, 200 μL of 0.1 M EDC solution was added, and the mixture was stirred at r. t. for 30 min. Then, an excess of folic acid (2 mg) was added, and the reaction between folic acid and amino groups was allowed to proceed for 3 h. The reaction mixture was dialyzed against deionized water for 50 h to remove unreacted molecules. Finally, all the samples were filtered through a 0.22 μm cutoff membrane filter and stored at 5 °C for later use.

IV.5.4 Characterization of dye-encapsulated silica nanoparticles

Transmission electron microscopy (TEM) images were obtained using a JEOL-JEM 1011 Transmission electron microscope (Manufacturer: JEOL, Ltd., Japan.) operating at 100 kV n bright field for the SiNPs. A drop of nanoparticles dispersed in water was placed on a holey carbon film copper grid and left to evaporate. The bioconjugation of the SiNPs with folic acid was confirmed by comparing the optical spectra of the SiNPs.

IV.5.5 Linear photophysical characterization

Linear photophysical properties of DBF and the SiNPs, including absorption, fluorescence, excitation, anisotropy, and fluorescence lifetime, were investigated in spectroscopic grade THF or ultrapure deionized water at room temperature. The steady-state absorption spectra were measured with an Agilent 8453 UV-visible spectrophotometer in 10 mm path length quartz cuvettes. The steady-state fluorescence, excitation, and fluorescence anisotropy spectra were measured with PTI QuantaMaster spectrofluorimeter in 10 mm spectrofluorometric quartz cuvettes, with dye concentrations ~ (1–1.5) $\times 10^{-6}$ M. Fluorescence lifetimes of the free dye and nanoparticles were measured with a single photon counting system PicoHarp 300 under 76 MHz

femtosecond excitation (MIRA 900, Coherent) with time resolution of ≈ 80 ps. The values of fluorescence quantum yield of DBF in THF and SiNPs in water were determined relative to 9, 10-diphenylanthracene in cyclohexane (Φ_f = 0.90) as a standard.[24] All optical densities of the dye DBF, silica nanoparticles, and standard were less than 0.1.

IV.5.6 Photostability measurement

The photostabilities of DBF in THF and SiNPs suspended in water were measured by irradiation of solutions of DBF in THF or SiNPs in water in 1 mm path length quartz cuvettes using a 405 nm diode laser at 20 mW.[25] Irradiation time-dependent absorption spectra were obtained with an Agilent 8453 UV/Vis spectrophotometer with an initial OD of ~ 1.5. For comparison, the photostability of fluorescein was measured by irradiation of solutions of fluorescein in 0.1 M NaOH(aq) in 1 mm path length quartz cuvettes by a 501 nm argon ion laser at 2.1 mW. Absorption spectra were recorded with an initial OD of ~ 1.6. Photodecomposition quantum yields, Φ_d, were calculated according to equation IV-1, and the result shown in Table I-1 is the average of ten pairs of adjacent maximum absorption values.

$$\Phi_d = \frac{(A_1 - A_0)N_A}{1000 \times \varepsilon \times I \times (1 - 10^{-(A_1+A_0)/2}) \times (t_1 - t_0)} \qquad \text{(IV-1)}$$

where Φ_d is the photodecomposition quantum yield, A_1 is absorbance maximum at t_1, A_0 is absorbance maximum at t_0, N_A is Avogadro's number, ε is molar absorbance, t_1-t_0 is exposure time (s), and I is the intensity in photon $\cdot sec^{-1} \cdot cm^{-2}$.

IV.5.7 Determination of two-photon cross section

The 2PA spectrum of DBF was determined over a broad spectral region by the typical two-photon induced fluorescence (2PF) method relative to Rhodamine B in methanol as a standard.[26]

A PTI QuantaMaster spectrofluorimeter and femtosecond Ti: sapphire laser (Mira 900F, 220 fs pulse width, 74 MHz repetition rate, Coherent, USA), tuning range 700–940 nm, were used. Two-photon fluorescence measurements were performed in 10 mm fluorometric quartz cuvettes with dye concentrations ~ 1.5×10^{-5} M in THF. The experimental fluorescence excitation and detection conditions were conducted with negligible reabsorption. The quadratic dependence of two-photon induced fluorescence intensity on the excitation power was verified for each excitation wavelength.

IV.5.8 Cytotoxicity Assay

To test the cytotoxicity of the folate-modified SiNPs, 4×10^3 per well of HeLa cells or MG63 cells in 96-well plates were incubated for 24 h in 90 μL of RPMI-160 medium without phenol red, supplemented with 10% FBS and 100 units / mL penicillin-streptomycin. Then cells were then incubated with various amounts of silica nanoparticles SNP-DBF-NHFA (30 μM, 20 μM, 10 μM, 5 μM, 1 μM) for an additional 20 h. Subsequently, 20 μL of CellTiter 96® AQueous One Solution reagent was added into each well, followed by incubation for an additional 4 h at 37 ℃. The relative viability of the cells incubated with the SiNPs relative to untreated cells was determined by measuring the MTS-formazan absorbance on a Kinetic microplate reader (Spectra Max M5, Molecular Devices, Sunnyvale, CA, USA) at 490 nm with a subtraction of the absorbance of cell-free blank volume at 490 nm. The results from three individual experiments were averaged.

IV.5.9 Uptake of silica nanoparticles by cancer cells

HeLa cells or MG63 cells were placed onto poly-D-lysine coated glasses in 24-well plates (40,000 cells per well), and the cells were incubated for 48 h before incubating with dye-doped

SiNPs. A stock solution of dye-doped SiNPs suspended in water was prepared as 0.5 mM solution. The solution was diluted to a 10 μM, 20 μM, and 50 μM by complete growth medium, RPMI-1640, and then freshly placed over the cells for a 2 h period. After incubation, cells were washed with PBS (3–5×) and fixed using 3.7% formaldehyde solution for 15 min at 37 ℃. To reduce autofluorescence, a fresh solution of $NaBH_4$ (1 mg / mL) in PBS (pH = 8.0), which was prepared by adding few drops of 6N NaOH solution into PBS (pH = 7.2), was used for treating the fixed cells for 15 min (2×). The plates were then washed twice with PBS and finally water. Subsequently, glass covers were mounted with Prolong gold mounting medium for microscopy.

IV.5.10 1PFM, 2PFM and two-photon FLIM imaging

Conventional single-photon fluorescence images were obtained using an inverted microscope (Olympus IX70) equipped with a QImaging cooled CCD (Model Retiga EXi) and excitation with a 100 W mercury lamp. In order to improve the fluorescence background-to-image ratios, one-photon confocal fluorescence images of the fixed cells were obtained using a custom made filter cube (Ex: 377 / 50; DM: 409; Em:525 / 40) for the dye-doped SiNPs. The specifications of the filter cube were tailored to match the excitation wavelength of probes and to capture most of its emission profile. 2PFM and 2P-FLIM imaging were performed by a modified Olympus Fluoview FV300 microscope system coupled to a tunable Coherent Mira 900F Ti: sapphire (76 MHz, modelocked, femtosecond laser tuned to 740 nm), and a compact FLIM system from PicoQuant. An emission short-pass filter (cutoff 690 nm) was placed in the microscope scanhead to avoid background irradiance from the excitation source. Consecutive layers, separated by approximately 0.15 μm, were recorded to create a 3D reconstruction from overlaid 2PFM images. The two-photon induced fluorescence was collected with a 60× microscope objective

(UPLANSAPO 60×, NA=1.35, Olympus). For 2P-FLIM imaging, the output fluorescence was delivered to an avalanche photodiode (APD) detector (PicoQuant, Germany). A band-pass filter (500nm -700 nm) was placed in front of the APD detector. Data were acquired using the Time Harp 300 module and software package *SymPhoTime* (PicoQuant, Germany).

IV.6 References

[1] Denk, W.; Strickler, J. H.; Webb, W. W. *Science* **1990**, *249*, 73-76.

[2] Williams, R. M.; Zipfel, W. R.; Webb, W. R. *Curr. Opin. Chem. Biol.* **2001**, *5*, 603-608.

[3] Centonze, V.E.; White, J. G. *Biophys. J.* **1998**, *75*, 2015-2024.

[4] Squirrell, J. M.; Woksin, J. G.; Bavister, B. D. *Nat. Biotechnol.* **1999**, *17*, 763-767.

[5] Morales, A. R.; Schafer-Hales, K. J.; Marcus, A. I.; and Belfield, K. D. *Bioconjugate Chem.* **2008**, *19*, 2559-2567.

[6] Andrade, C. D; Yanez, C. O.; Rodriguez, L. and Belfield, K. D. *J. Org. Chem.* **2010**, *75*, 3975-3982.

[7] Morales, A. R.; Yanez, C. O.; Schafer-Hales, K. J.; Marcus, A. I.; Belfield, K. D. *Bioconjugate Chem.* **2009**, *20*, 1992-2000.

[8] Ferrari, M. *Nature Reviews* **2005**, *5*, 161-170.

[9] Ruoslahti, E.; Bhatia, S. N.; Sailor, M. J. *J. Cell. Biol.* **2010**, *188*, 756-768.

[10] Ohulchanskyy, T. Y.; Roy, I.; Yong, K.; Pudavar, H. E.; Prasad, P. N. *WIREs Nanomedicine and Nanobiotechnology* **2010**, *2*, 162-175.

[11] Bharali, D. J.; Klejbor, I.; Stachowiak, E. K.; Dutta, P.; Roy, I.; Kaur, N.; Bergey, E. J.; Prasad, P. N.; Stachowiak, M. K. *Proc. Natl. Acad. Sci. U.S.A.* **2005**, *102*, 11539-11544.

[12] Ohulchanskyy, T. Y.; Roy, I.; Goswami, L. N.; Chen, Y. H.; Bergey, E. J.; Pandey, R. K. Oseroff, A. R.; Prasad, P. N. *Nano Lett.* **2007**, *7*, 2835-2842.

[13] Kim, S.; Ohulchanskyy, T. Y.; Pudavar, H. E.; Pandey, R. K.; Prasad, P. N. *J. Am. Chem. Soc.* **2007**, *129*, 2669-2675.

[14] Qian, J.; Li, X.; Wei, M.; Gao, X.; Xu, Z.; He, S. *Optics express* **2008**, *16*, 19568-19578.

[15] Kumar, R.; Roy, I.; Ohulchanskyy, T. Y.; Goswami, L. N.; Bonoiu, A. C.; Bergey, E. J.; Tramposch, K. M.; Maitra, A.; Prasad, P. N. *ACSnano* **2008**, *2*, 449-456.

[16] Brigger; I.; Dubernet, C.; Couvreur, P. *Advanced Drug Delivery Reviews* **2002**, *54*, 631-651.

[17] Antony, A. C, *Annu. Rev. Nutr.* **1996**, *16*, 501-521.

[18] Lemon, C. P.; Reddy, J. A., *Adv. Drug Delivery Rev.* **2004**, *56*, 1127-1141.

[19] Lu, Y.; Low, P. S. *Advanced Drug Delivery Reviews* **2002**, *54*, 675–693.

[20] Sun, C.; Sze, R.; Zhang, M. *Journal of Biomedical Material Research Part A* **2006**, *78A*, 550-557.

[21] Park, J.; Gu, L.; Maltzahn, G. V.; Ruoslahti, E.; Bhatia, S. N.; Sailor, M. J. *Nature Materials* **2009**, *8*, 331 – 336.

[22] Shi, H.; He, X.; Yuan, Y.; Wang, K.; Liu, D. *Anal. Chem.* **2010**, *82*, 2213-2220.

[23] Yao; S.; Ahn, H.; Wang, X.; Fu, J.; Van Stryland, E. W.; Hagan, D. J.; Belfield, K. D. *J. Org. Chem.* **2010**, *75*, 3965-3975.

[24] J. R. Lakowicz, Kluwer Academic / Plenum Publisher, New York, Second Edition, 52-53, 1999.

[25] Corredor, C. C.; Belfield, K. D.; Bondar, M. V.; Przhonska, O. V.; Yao S. *J. of Photochemistry and photobiology A: Chemistry* **2006**, *184*, 105- 112.

[26] Belfield, K. D.; Bondar, M. V.; Yanez, C. O.; Hernandez, F. E.; Przhonska, O. V. *J. Phys. Chem.* **2009**, *113*, 7101-7106.

[27] Sega, E. I.; Low, P. S. *Cancer Metastasis Rev.* **2008**, *27*, 655-664.

CHAPTER V: FOLATE RECEPTOR-TARGETED AGGREGATION-ENHANCED NEAR-IR EMITTING SILICA NANOPROBE FOR ONE-PHOTON *IN VIVO* AND TWO-PHOTON *EX VIVO* FLUORESCENCE BIOIMAGING

Reproduced with permission from: Wang, X.; Morales, A. R.; Urakami, T.; Zhang, L.; Bondar, M. V.; Komatsu, M.; Belfield, K. D. *J. Am. Chem. Soc.* **2011**, submitted for publication.

V.1 Abstract

A two-photon absorbing (2PA) and aggregation-enhanced near infrared (NIR) emitting pyran derivative, encapsulated in and stabilized by silica nanoparticles (SiNPs), is reported as a nanoprobe for two-photon fluorescence microscopy (2PFM) bioimaging that overcomes fluorescence quenching associated high chromospheres loading. The new SiNP probe exhibited aggregate-enhanced emission producing nearly twice as strong signal as the unaggregated dye, a three-fold increase in two-photon absorption relative to the DFP in solution and approx. four-fold increase in photostability. The surface of the nanoparticles was functionalized with a folic acid (FA) derivative for folate-mediated delivery of the nanoprobe for 2PFM bioimaging. Surface modification of SiNPs with the FA derivative was supported by zeta potential variation and ^{1}H NMR spectral characterization of the SiNPs as a function of surface modification. *In vitro* studies using HeLa cells expressing folate receptor (FR) indicated specific cellular uptake of the functionalized nanoparticles. The nanoprobe was demonstrated for FR targeted one-photon *in vivo* imaging of HeLa tumor xenograft in mice upon intravenous injection of the probe. The FA-

targeting nanoprobe not only exhibited highly selective tumor targeting but also readily extravasated from tumor vessels, penetrated into the tumor parenchyma and was internalized by the tumor cells. Two-photon florescence microscopy bioimaging provided three-dimensional (3D) cellular-level resolution imaging up to 350 μm deep in the HeLa tumor.

V.2 Introduction

In comparison with conventional bioimaging techniques, such as computed tomography (CT) or magnetic resonance imaging (MRI), fluorescence-based optical bioimaging affords much higher resolution and has been widely exploited to track biological processes.[1-4] Two-photon fluorescence microscopy (2PFM), one of the advanced fluorescence imaging techniques, has been investigated as a powerful tool for fundamental studies, cancer diagnosis, and oncologic drug development.[5-9] This technique has a number of advantages over traditional one-photon fluorescence microscopy (1PFM), including highly localized 3D spatial excitation, lower photo-induced damage, longer possible observation time, less interference by autofluorescence, and deeper penetration in tissue and thick samples.[10-13] However, one major challenge to the development and implementation of 2PFM for molecular bioimaging is a lack of biocompatible probes with sufficient two-photon absorption (2PA) cross section, high fluorescence quantum yield, and high photostability in physiological environments.[10, 14] For 2PFM applications, 2PA dyes are required to be hydrophilic or dispersible in aqueous media while maintaining high fluorescence efficiency.[15-17] Generally, organic materials with large 2PA cross sections are synthetically more accessible in hydrophobic forms and their fluorescence efficiencies are dramatically reduced in aqueous media due to self-aggregation-induced fluorescence quenching.[18, 19]

Recently, ceramic-based nanoparticles encapsulating hydrophobic dyes have been reported as biocompatible fluorescent probes for bioimaging.[20-22] Although the strategy to disperse hydrophobic dyes in aqueous media has been relatively successful in improving photostability, the amount of dye remained at quite a low concentration, limiting the intensity of the

fluorescence signal from individual nanoparticles due to aggregation-induced fluorescence quenching at high chromospheres loading.[23] Typically, fluorescence quantum yields of organic dyes are decreased by self-quenching in the aggregated stage. However, a series of organic dyes with a self-distorted structure were reported to exhibit fluorescence enhancement via aggregation rather than the customary decrease.[24-28] This phenomenon was exploited to develop a high-signal output silica nanoprobe for 2FPM imaging.[29] Although enhanced two-photon fluorescence was achieved, surface modification of the nanoparticles for *in vivo* targeting bioimaging have rarely been reported and the 2PA cross section of the dyes employed were generally low. A series of compounds, were reported to exhibit aggregation-enhanced emission,[30] but their two-photon based optical properties and application for 2PFM have not been reported. The development of silica nanoparticles (SiNPs) encapsulating an aggregation-enhanced emitting dye with a large 2PA cross section and high photostability as a nanoprobe for 2PFM would be significant.

To increase the stability of SiNPs for *in vivo* imaging, polyethylene glycol (PEG) is often introduced to their surface, since PEGylation of a drug or therapeutic protein can "mask" the agent from the host's immune system (reduced immunogenicity and antigenicity), increase the hydrodynamic size (size in solution) of the agent which prolongs its circulatory time by reducing renal clearance, decrease the toxicity of the system, and provide water solubility to hydrophobic drugs and proteins.[31] The PEG group has also been used to reduce normal tissue uptake of various materials, decrease toxicity, and increase tumor accumulation.[32] Beyond passive targeting through the enhanced permeability and retention (EPR) effect, delivery of particles to smaller solid tumors and metastatic cells can be achieved by modifying particle surfaces with moieties directed at cell surface markers unique to these cell types.[33] With developments in cell

biology, a variety of disease-specific ligand-receptor pairs have been identified, e.g., ligands based on antibodies, antibody fragments, proteins, and peptides.[34] Because of their high selectivity to specific cell receptors, ligands based on antibodies, antibody fragments, proteins, and peptides were fervently investigated for drug and bioimaging agent delivery.[35] Among the receptors of interest, the folate receptor (FR) is overexpressed by a spectrum of malignant tumors, including cancers of lung, ovary, breast, brain, kidney, colon and endometrium.[36] Recently, folic acid conjugated nanoparticles were investigated as carriers for delivering magnetic agents for MRI bioimaging,[37] photosensitizes for photodynamic therapy,[38] anti-cancer drugs for cancer therapy,[39] and quantum dots for two-photon fluorescence microscopy.[40] Folic acid was widely used for selective delivery of attached imaging and therapeutic agents to cancer tissues and sites because of its high affinity for the folate receptor ($K_d = 10^{-10}$ M).[41] However, the cellular-level understanding of how nanoparticles distribute within a solid tumor has not been thoroughly investigated due to the lack of fluorophores suitable for high resolution 3-d analysis in deep tissues. Herein, a two-photon absorbing, aggregation-enhanced near infrared (NIR) emitting and folate receptor-targeting silica nanoprobe is reported to probe the cellular distribution of folate nanoprobe within a solid tumor. The FR-targeted, highly selective tumor accumulation of the new SiNP probe was demonstrated by *in vivo* one-photon fluorescence imaging of tumor-bearing mice and *ex vivo* two-photon fluorescence imaging of whole-mounted tumors. Our study presents a critical development in SiNP technology for disease diagnostics and therapeutics.

V.3 Results and discussion

V.3.1 Aggregation enhanced emission of DFP

To study and exploit the potential utility of pyran derivatives, which were reported to exhibit aggregation-enhanced emission,[30] a pyran derivative 2-(2,6-bis((E)-2-(7-(diphenylamino)-9,9-diethyl-9H-fluoren-2-yl)vinyl)-4H-pyran-4-ylidene)malononitrile (DFP) (Figure V-1, left) was prepared and its photophysical properties were investigated herein for 2PFM bioimaging. A simple precipitation method was employed to prepare the stable DFP nanoaggregates dispersed in water, [24, 26] with THF as a water-miscible solvent for DFP. The roles of water in the organic nanoparticle preparation by precipitation included lowering the solubility of DFP and stabilizing a colloidal dispersion by promoting surface charge. Figure V-11 shows a representative transmission electron microscopy (TEM) image of the nanoaggregates made from 90% v/v of water in THF, having a diameter of 20 ± 6 nm. The results pictured in Figure V-1 (right) indicated that the relative fluorescence quantum yield (Φ_f) of DFP with the same concentration of 5×10^{-6} mol·L^{-1} decreased dramatically from 0.067 to 0.003 when the volume fraction of the water increased from 0 to 40%. Bulk precipitation occurred in the range of 50-60% water volume fraction, possibly because this amount of water decreased the solubility of DFP but did not stabilize the colloid enough by promoting surface charge.[24] The relative fluorescence quantum yield, Φ_f, of DFP at 50-60% was not measured due to bulk precipitation. After the volume fraction of the water was increased above 60%, stable nanoaggregates of DFP formed, and the relative Φ_f of DFP under the same conditions varied from 0.09 to 0.15 with the volume fraction of water increasing from 70 to 90%. It is apparent that the fluorescence of DFP was intensified by aggregation. Figure V-1 (middle) illustrates that the relative fluorescence intensity of DFP

with the same concentration at the aggregate state was much stronger than it was in THF solution under 500 nm laser excitation. The absorption and emission spectra of DFP in different water fraction solutions are presented in Figure V-12. The emission spectra showed that the fluorescence intensity was enhanced by aggregation with a minimal shift, whereas the absorption of DFP broadened and the intensity decreased with increasing water.

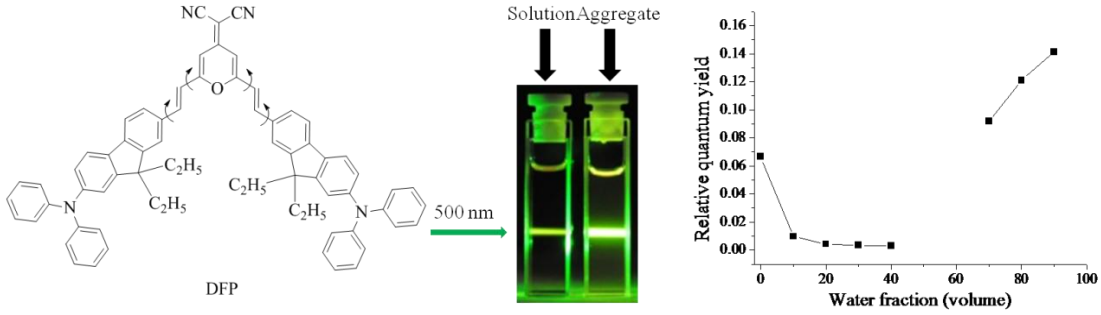

Figure V-1. Molecular structure of DFP (left), the florescence emission of DFP (5×10^{-6} mol·L^{-1}) in THF and THF/water mixture (90% volume fraction of water, nanoparticle suspension) under 500 nm laser excitation (middle), and the relative fluorescence quantum yields (Φ_f) of DFP (5×10^{-6} mol·L^{-1}) vs. water fraction in THF (right).

This relatively abnormal phenomenon exhibited by DFP may be explained by rotation upon the axes of the olefinic double bonds adjacent to the fluorenyl rings and pyramid ring in DFP (Figure V-1, left) so the conformational flexibility may result in the molecule being relatively nonemissive in dilute solution. However, when the molecule formed nanoaggregates in more hydrophilic solution, the intramolecular rotations were restricted and the molecular conformation was stiffened, resulting in aggregation-enhanced emission (i.e., the favored conformations were radiative).[30, 42] This presumption was supported by the blue-shifted monomer fluorescence in a

dilute solid solution of DFP in a polymethylmethacrylate (PMMA) film, where isolated molecules are stiffened and distorted by the rigid matrix (Figure V-4a). The DFP emission is red-shifted without quenching at concentrations that normally would be high enough to induce self-quenching, because the intermolecular steric hindrance between DFP molecules not only extends the π-conjugation but also diminishes intermolecular quenching effects.[43]

V.3.2 Synthesis, characterization and photophysical properties of amine-terminated DFP doped SiNPs

To apply the observed aggregation-enhanced emission property of the hydrophobic 2PA dye DFP for 2PFM bioimaging, dye-doped SiNPs encapsulating different amounts of DFP were prepared according to a moderately modified reported method.[29] Dye-doped SiNPs have been reported to be biocompatible,[44, 45] stable without releasing encapsulated hydrophobic molecules,[46] and facile to be modified with biomolecules.[47] The synthesis and surface modification of the dye-doped SiNPs are schematically described in Scheme V-1. To prepare the high loading dye-doped or no labeled SiNPs, a prepolymerized triethoxyvinylsilane (VTES) sol solution was first prepared. Then the sol solution and a solution with or without a certain amount of DFP were mixed and co-precipitated within the nonpolar interior of aqueous Tween-80 micelles through a solvent displacement process.[48] N'-[3-(Trimethoxysilyl)propyl]diethylenetriamine (DETA) was the added to the reaction mixture to introduce free amine groups on the SiNP surface for subsequent bioconjugation.

Scheme V-1. Synthesis and surface modification of DFP-doped SiNPs with FA surface modification.

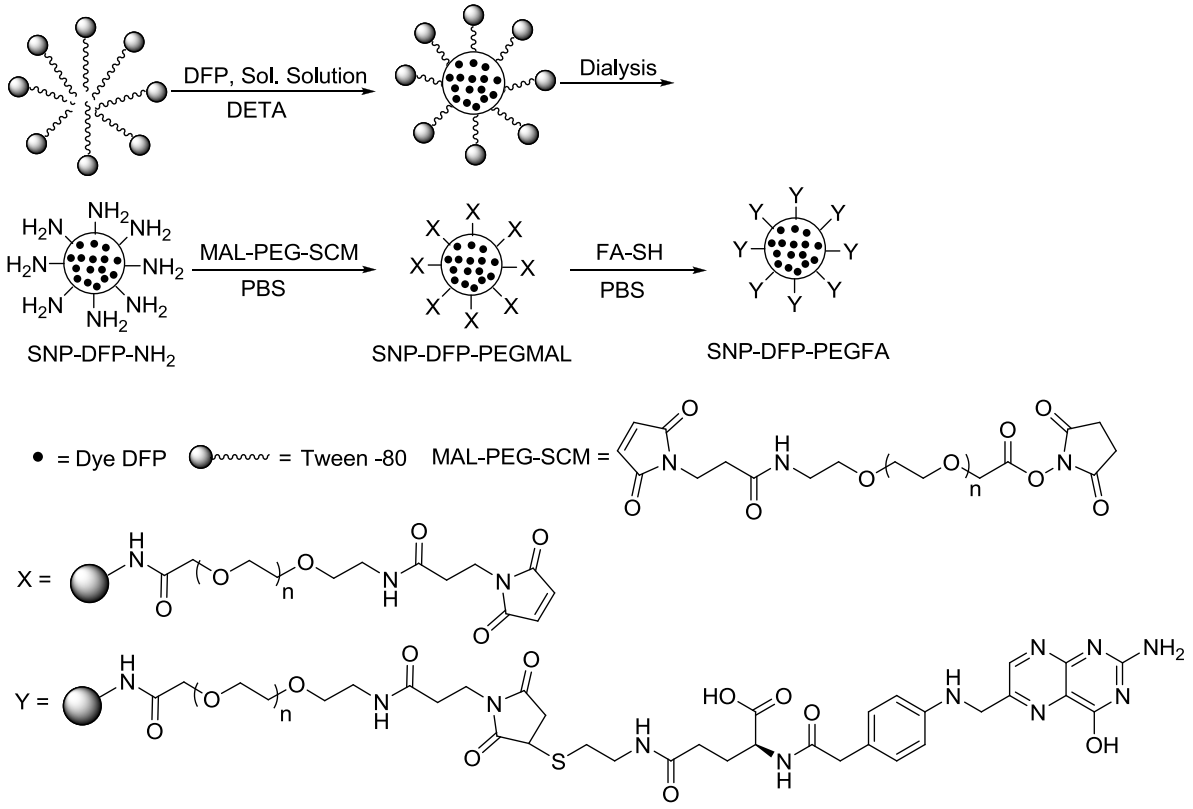

The zeta potential was analyzed to determine the change in surface charge of the SiNPs. Results in Figure V-2a indicated that the nonlabeled SiNPs presented an overall positive charge with a zeta potential value of +10.4 ± 0.5 mW, presumably because of the presence of amine moieties on the surface of the SiNPs.[48] With increasing dye loading, the overall surface charge of the SiNPs became more and more negative, and the 30 wt% (defined as DFP/[DFP+VTES] by weight) loading SiNPs exhibited a zeta potential of +2.14 ± 0.4 mV. The overall surface charge of SiNPs encapsulating different amounts of DFP varied possibly due to increasing surface hydrophobicity that promoted preferential adsorption of anions (OH^-) on the surface. The SiNP particle size was analyzed by transmission electron microscopic (TEM) and dynamic light

scattering (DLS). The results from DLS (Figure V-2b) indicated the particle size of SiNPs increased with increased loading ratios of DFP in the particles. A representive TEM image of 20 wt% SiNPs (Figure V-2c) was in good agreement with their number-averaged size distribution in water. The diameters were in the range of 20-30 nm with an average diameter of ca. 25 nm. This size is small enough to minimize the clearance of the host's immune system, prolong the circulation time of the SiNPs in live animals, and, hence, increase accumulation of the SiNPs in the targeted tumor.

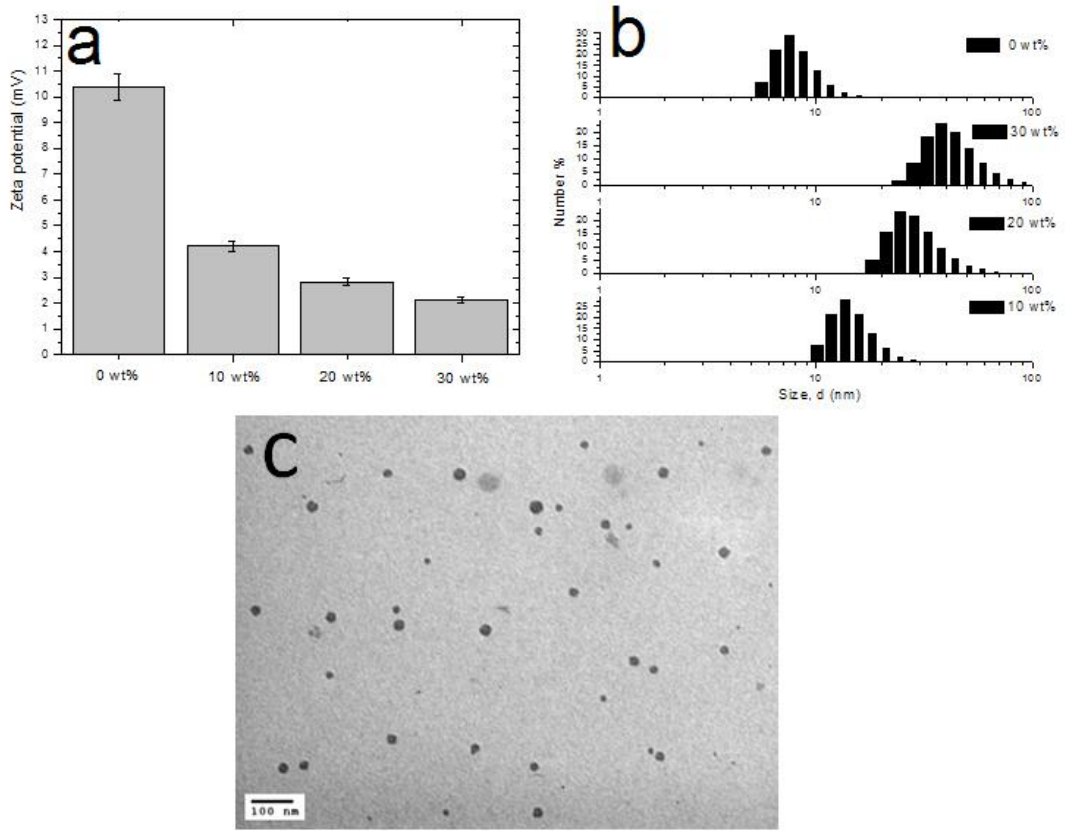

Figure V-2. (a) Zeta potential, (b) number-averaged particle size distribution by light scattering, and (c) and representative TEM image (20 wt% SiNPs) of SiNPs encapsulating different amounts of DFP; the scar bar is 100 nm.

The fluorescence quantum yield, Φ_f, and luminescence lifetime, τ_f, of the dye-doped SiNPs encapsulating various amounts of DFP, dispersed in water, were analyzed to optimize conditions for their use in 2PFM bioimaging. The results shown in Figure V-3a indicate that the fluorescence quantum yield, Φ_f, achieved a highest value of 0.19 ± 0.02 at a 20 wt% DFP concentration. According to the fluorescence decay presented in Figure V-3b, the fluorescence

lifetime of the SiNPs reached the highest value (2.32 ± 0.08 ns) at 20 wt% DFP and lowest value (1.81 ± 0.08 ns) at 10 wt% DFP, consistent with fluorescence quantum yield measurements.

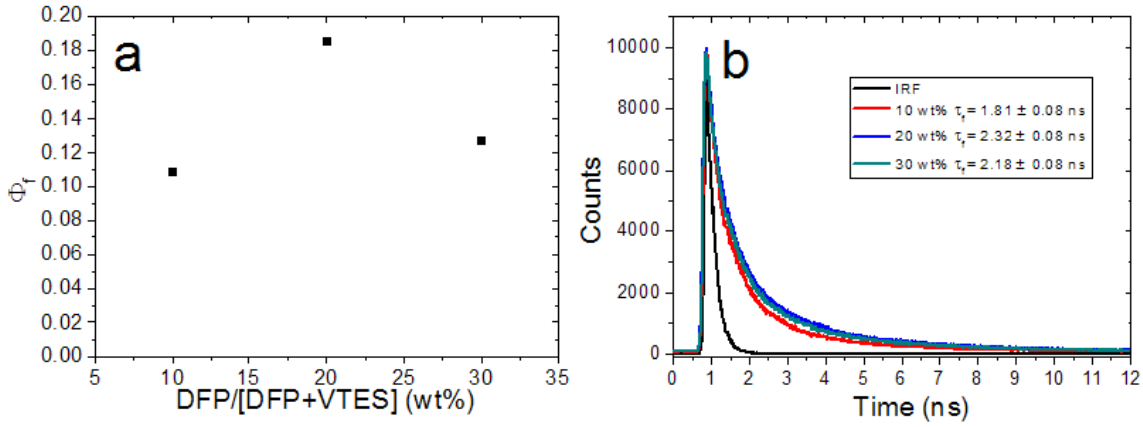

Figure V-3. (a) Fluorescence quantum yield and (b) fluorescence lifetime decay of SiNPs encapsulating differing quantities of DFP.

The 20 wt% SiNPs was chosen for the 2PFM bioimaging, not only because of their higher fluorescence quantum yield but also due to their suitable particle size for *in vivo* bioimaging. The linear and nonlinear photophysical properties of silica nanoprobe were investigated in phosphate buffered saline (PBS, 1×) to determine the potential utility of the silica nanoprobe for 2PFM bioimaging applications. The emission spectra of the 20 wt% SiNPs matrix was close to the emission spectra of 20 wt% DFP in PMMA (Figure V-4a), indicating that DFP in 20 wt% SiNPs was in the same aggregate state as DFP in PMMA solid solution. The absorption, emission, excitation, 2PA cross section, as well as the excitation anisotropy spectra of the silica nanoprobe in PBS (1×) are shown in Figure V-4b. The linear absorption spectrum (dark) and excitation spectrum (green) were sufficiently close to each other, and the emission spectrum (red) showed a maximum emission in the red (~650 nm), extending into the near-IR. The values of excitation anisotropy (Figure V-4b, blue) were not constant in the range of the main 1PA band (450 - 550

nm), indicating its relatively complex nature. Presumably, this band corresponds to at least two electronic transitions with different orientations of its transition dipoles.

By employing a standard z-scan method[49] with a femtosecond laser system, the silica nanoprobe afforded an impressive maximum 2PA cross section (δ) of ~2100 GM (1 GM = 10^{-50}·cm^4·s·$photon^{-1}$) at 980 nm (Figure V-4b, triangle), which was ca. three times higher than free DFP in THF (Figure V-4b, star). The aggregation enhanced two-photon absorption of DFP in SiNPs may be due to the considerably hindered internal rotation of the dye molecule in the solid silica matrix.[24] The 2PA efficiency of our nanoprobe is much higher than those previously reported, typically < 300 GM, for two-photon fluorescence microscopy (2PFM) bioimaging.[50]

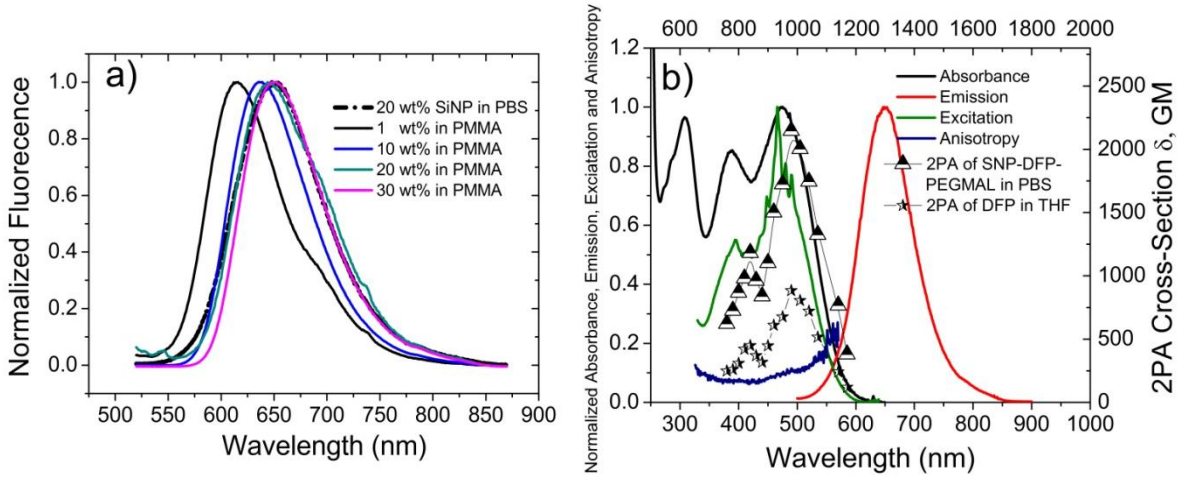

Figure V-4. a) Fluorescence emission spectra of DFP with different concentration in PMMA and 20 wt% SiNPs dispersed in PBS (1×). b) Absorption, emission, excitation, 2PA spectra of 20 wt% SiNPs (SNP-DFP-PEGMAL) and anisotropy spectrum in PBS (1×), as well as 2PA spectra of DFP in THF.

V.3.3 Surface modification, characterization and photophysical properties of the FA conjugated DFP doped SiNPs

In order to mask the silica nanoprobe from the host's immune system and target FR overexpressing tumors, the surface of the SiNPs was further modified with maleimide-terminated PEG and then FA. The succinimidyl carboxyl group on maleimide-poly(ethylene glycol)-succinimidyl carboxymethyl (MAL-PEG-SCM, M.W. 3400) was first used to react with the amine group on the surface of the SiNPs, yielding a maleimide functional group on the surface to react with the thiol group on (S)-2-(2-(4-((2-amino-4-hydroxypteridin-6-yl)methylamino)phenyl) acetamido)-5-(2-mercaptoethylamino)-5-oxopentanoic acid (FA-SH) in the next step (Scheme V-1). Finally, the FA-conjugated SiNPs were purified by dialysis to remove unreacted molecules. The success of FA conjugation to the SiNPs was confirmed by zeta potential measurement (Figure V-5a). The zeta potential value of amine-terminated SiNPs (SNP-DFP-NH_2) decreased

from +2.8 mV to -6.4 mV after reaction of surface amino groups with MAL-PEG-SCM to form the MAL-terminated SiNPs (SNP-DFP-PEGMAL) since most of the positive charge from NH_3^+ was eliminated. After FA-SH conjugation with SNP-DFP-PEGMAL and formation of FA-terminated SiNPs (SNP-DFP-PEGFA) the zeta potential value decrease continuously to -13.8 mV, possibly because the positive charge on the surface was shielded by the FA derivative.

In addition, proton NMR spectra of the SiNPs in D_2O, as well as SCM-PEG-MAL and Tween-80 in D_2O, FA-SH in DMSO-d_6, DFP in CD_3Cl (Figure V-5c and ^1H NMR spectra in Supporting Information), confirmed the surface modification of the DFP-doped SiNPs modified by FA. A signal at δ = 6.76 ppm from the maleimide was present after the amine terminated SiNPs reacted with MAL-PEG-SCM, producing maleimide groups on the surface of the SiNPs. Then the signal from maleimide at δ = 6.76 ppm disappeared after the maleimide reacted with the thiol of FA-SH, and the signal at δ = 7.62 ppm from folic acid appeared in the proton NMR spectrum of FA-modified SiNPs. Due to the presence of PEG on the surface of the SiNPs, the FA-conjugated SiNPs dispersed well in phosphate buffered saline (PBS, 1×) solution and was quite stable. A representative TEM image and dynamic light scattering (DLS) size distribution of the FA conjugated nanoparticles dispersed in PBS is shown in Figure V-13. The average particle size was ~28 nm with a polydispersity index (PdI) value of 0.375 and no aggregation or decomposition was observed through all experiments.

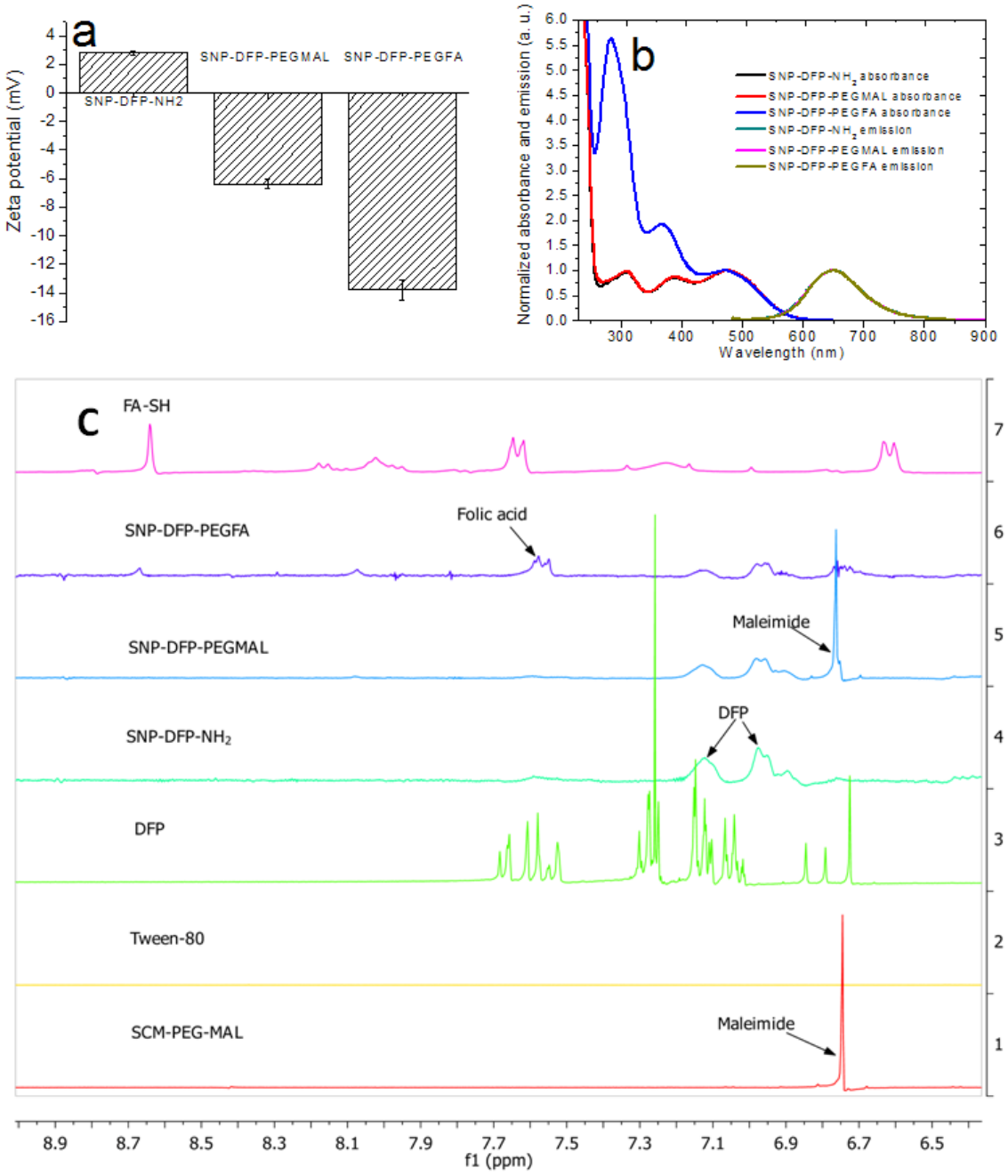

Figure V-5. (a) Zeta potential values of surface modified DFP-doped SiNPs dispersed in water. (b) Absorption and fluorescence emission spectra of surface modified DFP-doped SiNPs dispersed in PBS. (c)

^{1}H NMR spectra of different surface modified DFP-doped SiNPs dispersed in D_2O, as well as SCM-PEG-MAL and Tween-80 in D_2O, FA-SH in DMSO-d_6, and DFP in CD_3Cl.

The photostability of SNP-DFP-PEGFA in PBS was evaluated with photodecomposition quantum yield, Φ_d, of 3.7×10^{-7} which was ca. 25% of the value for DFP in Tween-80 micelles in PBS (1.3×10^{-6}). This is significant in that it indicate that the photostability of SNP-DFP-PEGFA was ca. four times higher than free DFP. It is possible that when the nanoprobe was irradiated, the silica matrix protected the dye molecules from the aqueous environment and reduced the oxidation of the dye molecules by slowing the diffusion of oxygen, an aspect of future investigation.

The linear and nonlinear photophysical and photochemical properties of the silica nanoprobe resulted in a highly desirable figure of merit ($F_M = \delta\Phi_f/\Phi_d$) value of ~ 1.1×10^9 GM in PBS, a value that is about two times higher than a previously reported high-fidelity small molecule probe.[5] The absorption and emission spectra of SNP-DFP-NH_2, SNP-DFP-PEGMAL, and SNP-DFP-PEGFA are presented in Figure V-5b, and after FA conjugation the absorption of FA in the short wavelength was presented, and, as can be seen, the emission spectrum did not change.

V.3.4 Cytotoxicity, in vitro 1PFM and 2PFM folate receptor-targeted cell imaging of the DFP SiNP nanoprobe

Before applying the FA-conjugated SiNPs for FR-targeted bioimaging, the probe's cytotoxicity with HeLa and MG63 cells was investigated using an MTS assay.[5] The results (Figure V-16) indicated that the FA-conjugated SiNPs are compatible with these cell lines (~85% cell viability) over a DFP concentration range from 0.01 – 5 μM, which was high enough for imaging. DFP concentrations were determined from the absorption of SNP-DFP-PEGFA at 472

nm (absorbance coefficient, $\varepsilon_{472nm} = 5.4 \times 10^4\ M^{-1}\cdot cm^{-1}$ in PBS). The results suggested that the FA-conjugated SiNPs will be suitable for FR-targeted 2PFM *in vitro* cell imaging.

In preparation for *in vivo* imaging studies, *in vitro* cell imaging was conducted to test the selectivity of the FA-conjugated silica nanoprobe to FRs. HeLa cells, known to overexpress FRs, and low FR expressing MG63 cancer cells were incubated with the same concentration of the FA-conjugated SiNPs for the same time. 1PFM and 2PFM images are presented in Figure V-6 demonstrating that HeLa cells (top row) incubated with FA-conjugated SiNPs (SNP-DFP-PEGFA) were much brighter than the MG 63 cells (a negative control, second row from the top) incubated with the same nanoprobe. In addition, two additional control experiments were performed. In one control, HeLa cells (third row from the top) incubated with non-FA-conjugated SiNPs (SNP-DFP-PEGMAL) under the same conditions showed no significant uptake of the probe. In the additional control experiment HeLa cells (bottom low) whose FRs were first blocked with FA and, subsequently incubated with FA-conjugated SiNPs, also demonstrated no specific uptake of the SiNPs. These results indicated that the HeLa cancer cells, which are well known to overexpress FRs, took in the FA-conjugated SiNPs, presumably by FR mediation, but those cells which do not overexpress FRs or whose FRs were blocked did not uptake the silica nanoprobe effectively.

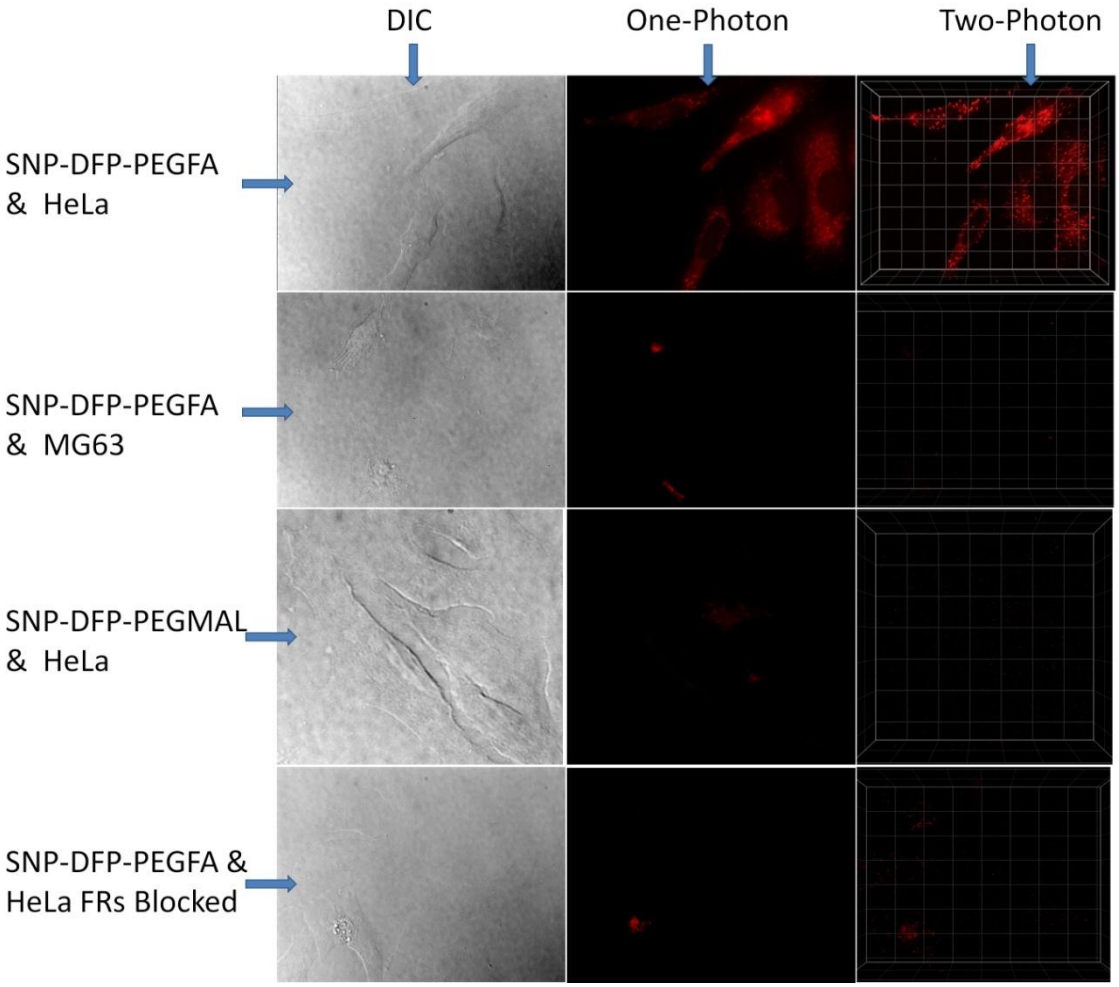

Figure V-6. Images of HeLa cells incubated with SNP-DFP-PEGFA (5 μM, 2 h) (top row), MG63 cells incubated with SNP-DFP-PEGFA (5 μM, 2 h) (second row), HeLa cells incubated with 2 mg/mL FA 1 hour first followed by incubation with SNP-DFP-PEGFA (5 μM, 2 h) (third row), HeLa cells incubated with SNP-DFP-PEGMAL (5 μM, 2 h) (bottom row). Left panel: differential interference contrast (DIC), middle panel: 1PFM image, right panel: 3D reconstruction from overlaid 2PFM images (Ex: 840 nm; Power: 90 mW, ~14% on the focal plane; Em. short-pass filter 690 nm); 10 μm grid. All images were acquired and processed with the same conditions.

V.3.5 Folate receptor-targeted in vivo tumor imaging with nanoprobes and biodistribution study

The *in vitro* studies demonstrated that the FA-conjugated SiNPs can target FRs, the SiNPs were tested for FR-targeting bioimaging in mice. Athymic nude mice bearing HeLa tumors (10 days post inoculation of 5×10^6 HeLa cells on the right thigh), which overexpress FRs, were administered with SNP-DFP-PEGFA or SNP-DFP-PEGMAL (3 nmol DFP per gram of animal body weight) via tail vein injection. The mice were imaged at different time points postinjection (p.i.), using an IVIS Spectrum imaging system; the fluorescence signals from the nanoprobes were collected in one channel with excitation at 500 nm and emission at 720 nm. The tissue background autofluorescence signals were recorded with a second channel with excitation at 605 nm and emission at 720 nm. The efficiency of the channels to separate the probe fluorescence signals from the background autofluorescence signals was checked by imaging standard samples with different concentrations of SNP-DFP-NH_2 in PBS (Figure V-17). In this experiment, two groups of mice were analyzed in the same way. The resulting overlayed images presented in Figure V-7 were corrected by subtracting the animal autofluorescence background images from the silica probe fluorescence images using the vendor software. Just after 30 min p.i., a fluorescence signal was detected in the tumor. A steady increase in the tumor fluorescence intensity in the mice injected with SNP-DFP-PEGFA was observed during the next few hours and the tumor fluorescence intensity reached its maximum at 6 h p.i. No significant fluorescence signal was detected in the tumor for the SNP-DFP-PEGMAL injected mouse. These results indicate that the FA-conjugated SiNPs accumulated in the tumor, and demonstrated that the FA-conjugated nanoprobes can be delivered to tumor sites effectively.

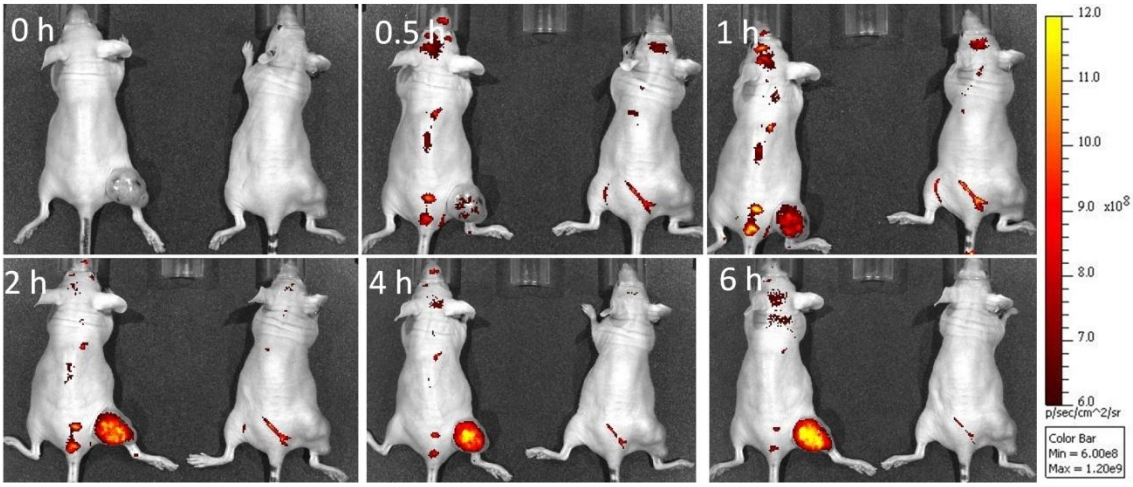

Figure V-7. Representative whole-body *in vivo* fluorescence images of a mouse bearing HeLa tumors injected with SNP-DFP-PRGFA and SNP-DFP-PEGMAL (3 nmol/g, body weight). At each time interval, the mouse on the left is the one that was injected with the DFP-containing folate SiNP conjugate while the mouse one the right was injected with a DFP-containing SiNP without folic acid derivatization.

At 6 h p.i., the mice injected with SNP-DFP-PEGFA or SNP-DFP-PEFMAL were sacrificed and their HeLa tumors and organs were harvested and imaged immediately with the IVIS spectrum imaging system using the same collection channels described above. The corrected images of the organs and tumors are showed in Figure V-18 and the SiNPs' biodistribution was determined by their relative fluorescence intensity from those organs (Figure V-8a). The biodistribution of SNP-DFP-PEGFA and SNP-DFP-PEGMAL in normal organs, e.g. liver, kidney, spleen, heart, lung, intestine, muscle, and brain were very similar between the FA-conjugated and non-conjugated probes and consistent with the biodistribution of other SiNPs reported previously.[22] The most important difference in the biodistribution was the ca. three times higher HeLa tumor uptake observed for FA-conjugated SiNPs, supporting FR-mediated

accumulation of the nanoparticles. For a better comparison and higher resolution, the excised tumors of the mice injected with SNP-DFP-PEGFA or SNP-DFP-PEGMAL were imaged and presented in Figure V-8b. The fluorescence signal intensity of the tumor from the mouse injected with SNP-DFP-PEGFA was ca. three times higher than the one from the mouse injected with SNP-DFP-PEGMAL. The efficiency of delivering the FA-conjugated nanoprobe was impressive, particularly considering that the mice used in this study were fed by a regular diet rather than a folate-free diet, which is usually necessary to increase the detection sensitivity of the folate receptor-targeted probes.[51] In addition, because the *ex vivo* tumor fluorescence signal appeared to be fairly homogenous and FRs are overexpressed by cancer cells, it is reasonable to predict that the fluorescence signal should emanate from cells distributed throughout the tumor rather than being localized in the vasculature, an aspect explored in the following section.

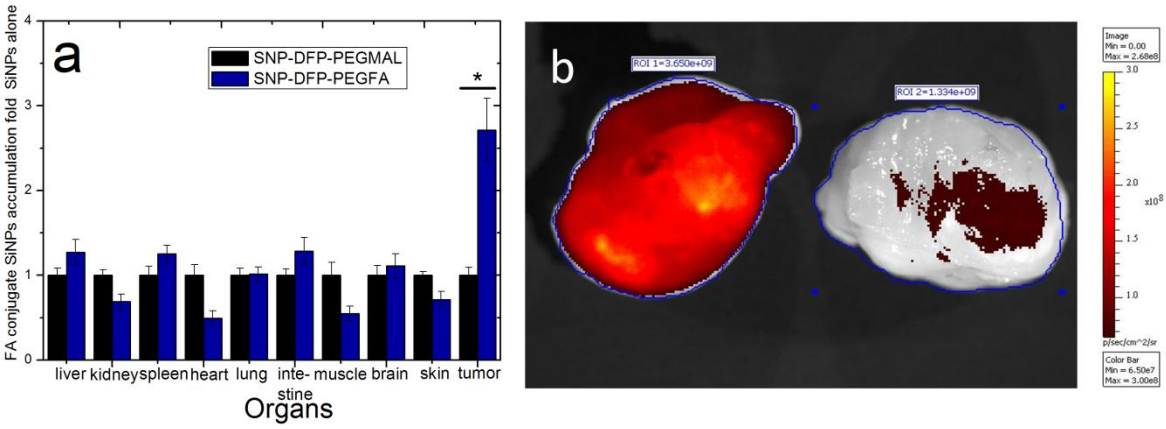

Figure V-8. (a) Comparison of the SiNPs delivery efficiency (organ accumulation) of the FA-conjugated silica nanoprobe and non-FA containing silica nanoprobe (Student's t test, n = 2 mice per group, error bars denote mean ± SEM, $*P < 0.05$) and (b) *ex vivo* image of HeLa tumor of the mice injected with SNP-DFP-PEGFA (left) and SNP-DFP-PEGMAL (right).

V.3.6 Histology studies of HeLa tumors from the mice administered with nanoprobes

After *in vivo* and *ex vivo* imaging of the tumor by the IVIS spectrum imaging system, the collected tumors were sectioned to ~20 μm thick sections. In order to determine the location of the nanoprobe in the tumor, the nuclei of the tumor were stained with Hoechst 33285 before visualizing with a Lecia 1P-FCS confocal microscope. The confocal fluorescence image of the FA-conjugated nanoprobe accumulated in the tumor together with the localized fluorescence spectrum is illustrated in Figure V-9. The 1PFM image of the tissue indicated that the FA-conjugated nanoprobe accumulated in the tumor cells (Figures V-9d and V-9f). The HeLa cancer cells internalized the nanoprobe and accumulated in specific organelles within the cancer cells (likely endosomes), and the localized fluorescence spectrum (Figure V-9e) confirmed that the localized fluorescence (pointed out by triangles in Figure V-9f) was from the internalized nanoprobe ($\lambda_{em\ max}$ = 650 nm) rather than tissue autofluorescence ($\lambda_{em\ max}$ = 524 nm), and the fluorescence signals from the folate nanoprobe was about three times higher than the autofluorescence signals.

Significantly, no fluorescence for the nanoprobe channel was observed in the HeLa tumors from the mice injected with non-folic acid-conjugated nanoprobe SNP-DFP-PEGMAL (Figure V-19). In addition, blood vessels were stained to show how far the nanoprobe penetrates into the tumor; the result shown in Figure V-20 indicated that the folate nanoprobe leaked out of the blood vessels (Figure V-20, pointed out by triangles) and spread throughout the tumor.

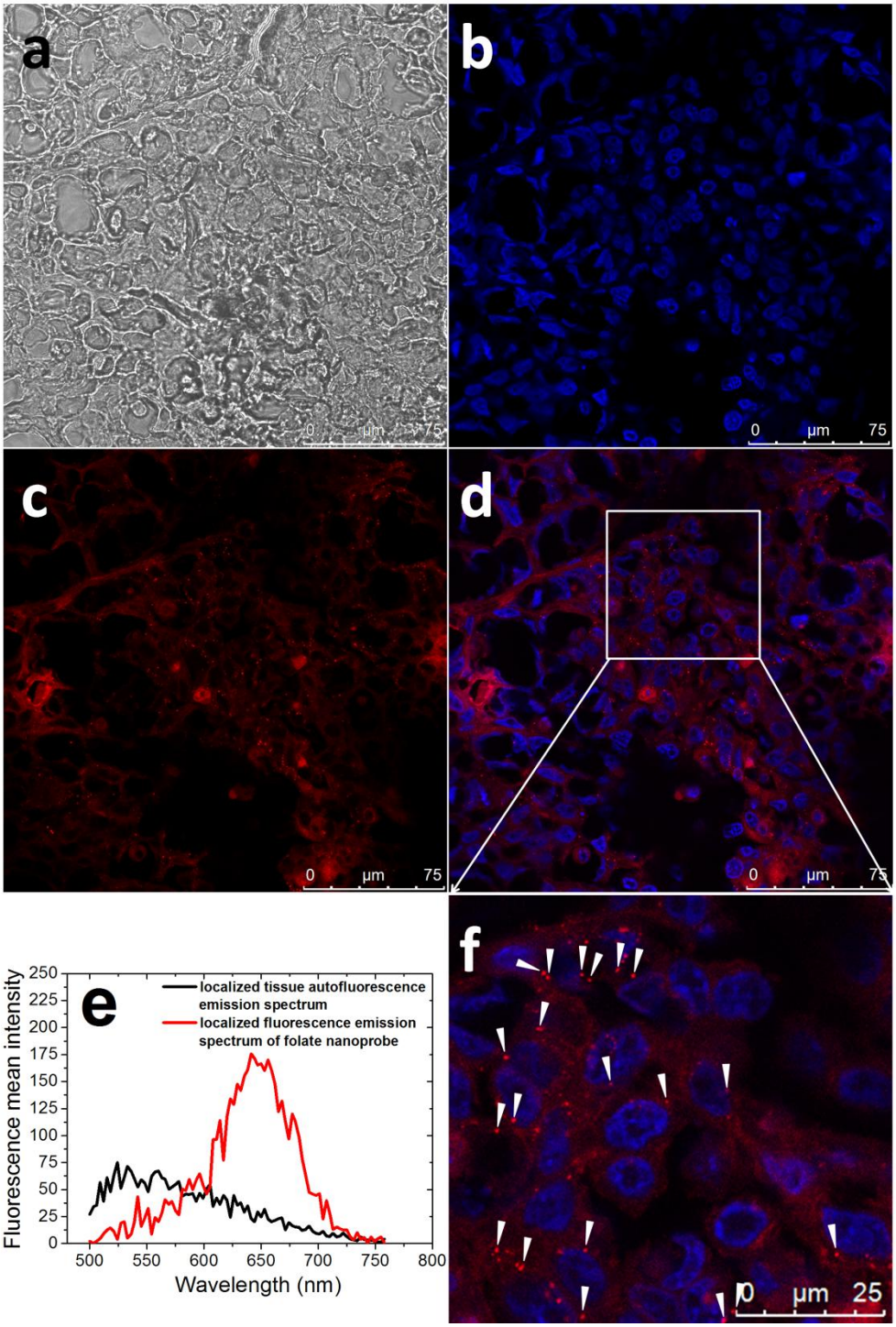

Figure V-9. One-photon confocal fluorescence images of HeLa tumor (~ 20 µm sections) from mice tail vein injected with SNP-DFP-PEGFA (3 nmol/g body weight, 6 h p.i.); a) bright field, b) image of the

nuclei of the tumor stained with Hoechst 33285 (0.2 μg/mL), Ex: 405 nm, Em: 520 – 560 nm, DM: RSP500 nm; c) image of tumor with the channel for SNP-DFP-PEGFA, Ex: 476 nm, Em: 620 - 680 nm, DM: RSP 500 nm; d) merged image of Hoechst 33285 and SNP-DFP-PEGFA; e) localized tissue autofluorescence emission spectrum and localized fluorescence emission spectrum of the folate nanoprobe, Ex: 476 nm, Em: 500 - 760 nm, DM: RSP 500 nm; f) higher magnification of (d) where the arrowheads indicate clusters of the nanoprobe taken up by the tumor cells; objective 63×, NA: 1.4; representative fields from multiple sections of two tumors are shown.

V.3.7 2PFM folate-receptor targeted imaging of HeLa tumors

The tumors excised from the nanoprobe-administered mice were whole-mounted and imaged, optical layer-by-layer, using a 2PFM imaging system. The fs laser excitation was tuned to 980 nm in order to achieve cellular-level 2PFM images of the tumors. The thick 2PFM images of the tumors are presented in Figure V-10. The 2PFM tumor images showed that the FA-conjugated nanoprobes were mainly distributed in the cytoplasm of cancer cells (a few cells are indicated by arrowheads in Figure V-10c). A deep image (ca. 350 μm) was achieved (Figure V-10e) with cellular-level visual information of a solid tumor. While the tumor from the mouse that was administered with the FA-conjugated SiNPs clearly show cells with the SiNPs (Figure V-10a), no significant signal was observed non-FA-conjugated SiNPs (Figure V-21). These results are consistent with FR-binding of the FA-conjugated SiNPs and accumulation in the tumor cells. Thus, imaging nanoprobes can be effectively and specifically delivered to tumors that overexpress FRs. These result suggest that the FA-mediated active targeting strategy is more effective that passive targeting strategies via enhanced permeability and retention (EPR).

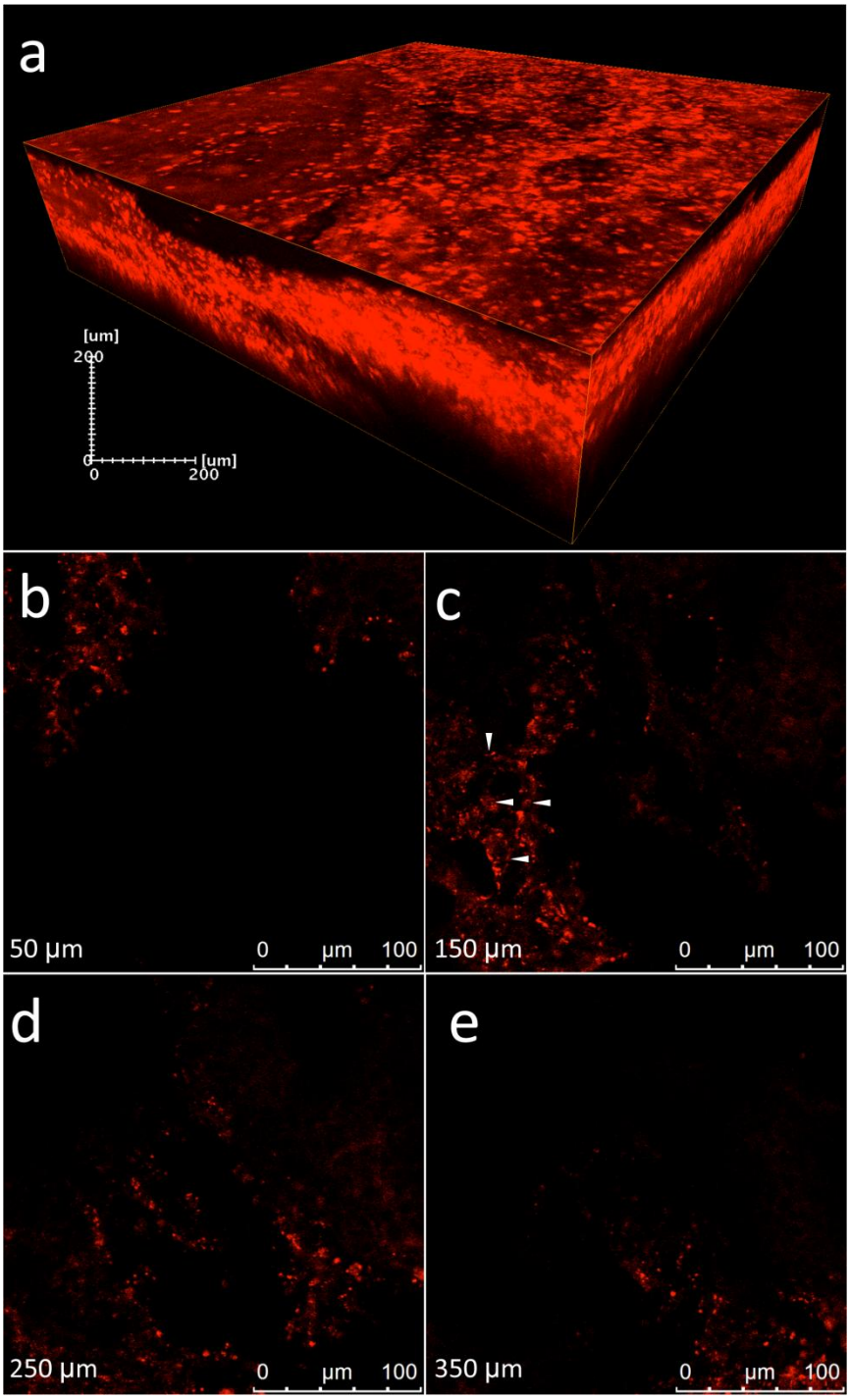

Figure V-10. a) Representative 3D two-photon fluorescence images of the HeLa tumor from a mouse that was injected with SNP-DFP-PEGFA (3 nmol/g) into the tail vein; b) 50 µm deep image, c) 150 µm deep

image, d) 250 μm deep image, e) 350 μm deep image, Ex: 980 nm; Power: 300 mW, ~ 20% on the focal plane; short-pass filter 840 nm, 20× (NA = 1.0, Lecia).

V.4 Conclusion

In this study, we have developed an aggregation-enhanced long wavelength emission, 2PA pyran derivative (DFP) that exhibited much stronger fluorescence upon aggregation than in THF solution. In order to harness the potential of the hydrophobic DFP probe for biological imaging and stabilize its aggregation, DFP-encapsulating SiNPs that target folate receptors were synthesized and characterized. In order to specifically deliver the two-photon fluorescent SiNPs to tumor, the surface of the nanoparticles was functionalized with PEG and then modified with a folic acid derivative at the outer terminus of the PEG group. Nanoparticle surface functionalization was characterized by measuring changes in the zeta potential and NMR spectra of the SiNPs. The DFP aggregate-encapsulating SiNPs exhibited enhanced fluorescence emission (twice the fluorescence quantum yield relative to unaggregated DFP). Importantly, these nanopartiles exhibited a three-fold increase in two-photon absorption relative to the DFP in solution. In addition, the photostability of the fluorescent SiNPs was ca. four times higher than the free DFP dye, resulting in an impressively high figure of merit for the new nanoparticle probe. TEM and DLS provided information regarding nanoparticle size and size distribution, indicating an average particle size of ca. 25 nm.

The cytotoxicity of the new SiNPs was assessed in two cell lines and found to be suitable for *in vitro* cell imaging. The FA-modified DFP-containing SiNPs were selectively uptaken by HeLa cells overexpressing folate receptors (FR) as determined by 1PFM and 2PFM imaging

experiments. The target specificity of the SiNPs was further demonstrated by three independent control experiments 1) using a non-FR-expressing cell line, 2) testing a non-FA labeled SiNP probe on HeLa cells, and 3) blocking FR-mediated HeLa cell binding of the SiNPs with free FA.

These FA-targeting DFP-encapsulating SiNPs were demonstrated as efficient probes for *in vivo* fluorescence bioimaging upon intravenous administration into mice bearing HeLa tumors. The real-time fluorescence image monitoring for the biodistribution of the SiNPs indicated that the SiNPs selectively accumulated in the tumor, most likely via FA-mediated active targeting. Furthermore, the nanoprobe not only targeted the tumor but also penetrated deep into the tumor parenchyma as demonstrated by cellular-level 2PFM *ex vivo* imaging of whole-tumor mounts. Thus, 2PFM of the tumor provided near cell culture-image quality up to 350 μm deep in the tumor tissue. This comprehensive study of an aggregate-enhanced emission probe sets the stage for its future use in *in vivo* biomarker 2PFM imaging, in which the probe can be deliberately modified with vectors to target various tumor biomarkers.

V.5 Experimental

V.5.1 Materials

Triethoxyvinylsilane (VTES, 97%), 1-butanol (99%), folic acid (FA), dicyclohexylcarbodiimide (DCC), *N*-hydroxysuccinimide (NHS), 2-aminoethanethiol, and the surfactant Tween-80, N' – [3-(trimethoxysilyl) – propyl] diethylenetrimaine (DETA), were obtained from Sigma-Aldrich. N-Methyl-2-pyrrolidinone (NMP, 99%), triethylamine (TEA), and dimethyl sulfoxide (DMSO) were obtained from Acros. Maleimide-poly(ethylene glycol)-succinimidyl carboxymethyl, average M.W. 3400 (MAL-PEG-SCM) was obtained from Laysan Bio Inc. Rat anti-mouse CD31 was obtained from BD Biosciences. Alexa Fluor $^{@}$ 350 goat anti-

mouse IgM was obtained from Invitrogen. The preceding chemicals or biological regents were used as received without further purification, except where otherwise noted. Thermo Slide-A-Lyzer® 10K cut off dialysis cassettes and 0.22 μm cutoff membrane filters were obtained from Fisher Inc. HeLa and MG63 cells were obtained from ATCC (America Type Culture Collection, Manassas, VA, USA). All cells were incubated in RPMI-1640 medium (Invitrogen, Carlsbad, CA, USA), supplemented with 10% fetal bovine serum (FBS, Atlanta Biologicals, Lawrenceville, GA, USA), 100 units/mL penicillin-streptomycin (Atlanta Biologicals, Lawrenceville, GA, USA), and incubated at 37 °C in a 95% humidified atmosphere containing 5% CO_2. Details of pyran derivative DFP, including preparation and characterization, will be reported elsewhere. ^{1}H NMR spectra were recorded at 300 MHz.

V.5.2 Preparation of (S)-2-(2-(4-((2-amino-4-hydroxypteridin-6-yl)methylamino)phenyl) acetamido)-5-(2-mercaptoethylamino)-5-oxopentanoic acid (FA-SH)

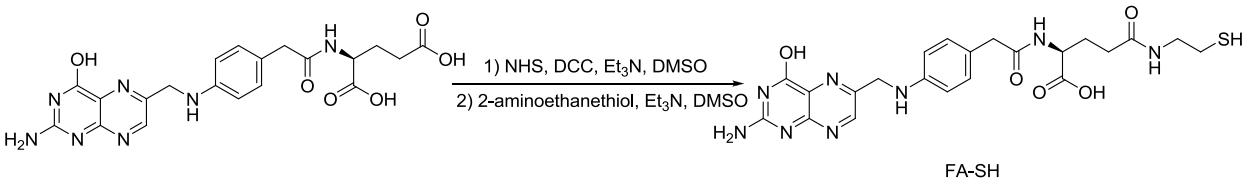

FA-SH

N-Hydroxysuccinimide ester of folic acid (NHS-FA (*γ*)) was prepared in accordance to a reported procedure.[1] Briefly, folic acid (1.0 g, 2.2 mmole) was added into a mixture of anhydrous dimethyl sulfoxide (DMSO, 30 mL) and triethylamine (TEA, 0.5 ml, 3.6 mmol). Folic acid dissolved while stirring the mixture under nitrogen and in the dark overnight. Folic acid was mixed with dicyclohexylcarbodiimide (DCC, 0.5 g, 2.4 mmole) and *N*-hydroxysuccinimide (NHS, 0.52 g, 4.5 mmole), and stirred in the dark for a further 18 h. The side product, dicyclohexylurea (DCU), precipitated and was removed by vacuum filtration. An equimolar

amount of 2-aminoethanethiol (0.170 g, 2.2 mmole) and 10 mL TEA was added to the filtrate, and the reaction was conducted under nitrogen overnight. Subsequently, 30 mL CH_2Cl_2 and 30 mL hexanes were added to the reaction mixture to precipitate the crude product that was collected by filtration. The crude product was then dissolved in 30 mL water whose pH was adjusted to 10.0 by ammonium hydroxide. The solution was washed thrice with CH_2Cl_2. After neutralization with HCl, the yellow product was precipitated and collected by filtration; 66% yd; m.p. dec. at 187 ℃. ^{1}H NMR (d-DMSO, 300 MHz) δ (TMS ppm): 12.27 (b, COOH, 1H), 8.64 (s, pteridine moiety, 1H), 8.05- 8.23 (b, NH-CO, 2H), 7.66 (d, Ar ring, 2H), 7.20 (b, NH_2, 2H), 6.65 (d, Ar ring, 2H), 4.51 (d, CH_2-N, 2H), 4.27 (m, NCH-CO-,1H), 3.31 (t, N-CH_2, 2H), 2.74 (t, CH_2-S, 1H), 2.20 (m, CH_2, 2H), 1.90-2.16 (m, CH_2, 2H, SH, 1H).

V.5.3 Preparation of DFP organic nanoparticles.

The DFP organic nanoaggregate dispersion was prepared by injecting a 0.125 mL stock solution of DFP in THF (2×10^{-4} M) into 4.825 mL of a THF/water mixture, with vigorous stirring. In all samples, the final concentration of DFD (5×10^{-6} M) was constant after stock solution injection. The relative fluorescence quantum yield values of those were measured at the same concentration of 5×10^{-6} M.

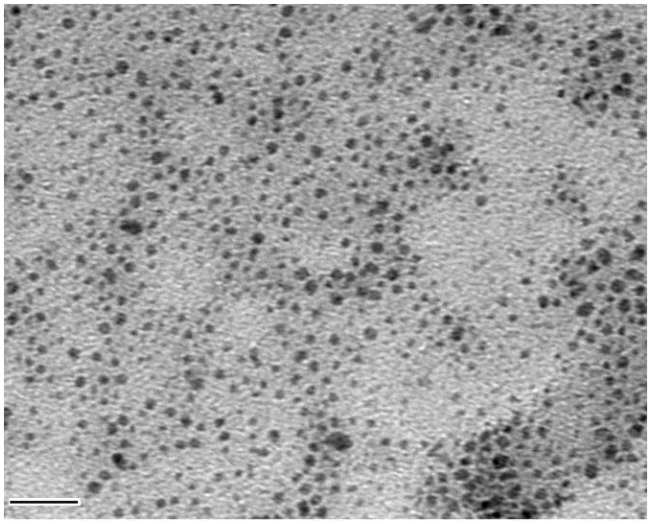

Figure V-11. TEM image of DFP nanoparticles obtained from nanoparticle suspension containing 80% volume fraction of water in THF, Scar bar: 100 nm.

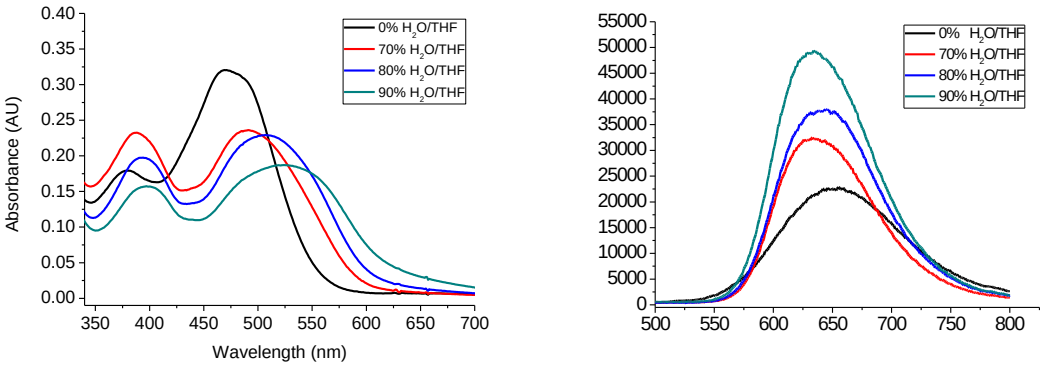

Figure V-12. a) UV-vis absorption spectral changes of DFP (5×10^{-6} mol·L^{-1}) as a function of the water fraction in THF; b) fluorescence emission spectral changes of DFP (5×10^{-6} mol·L^{-1}) as a function of the water fraction in THF.

V.5.4 Spectroscopic measurements and determination of quantum yield.

Steady-state absorption spectra were obtained with an Agilent 8453 UV-vis spectrophotometer in 10 mm path length quartz cuvettes. Steady-state fluorescence emission spectra and fluorescence quantum yield measurements were carried out using a PTI QuantaMaster spectrofluorimeter. The fluorescence quantum yields were recorded by using cresyl violet in methanol ($\Phi_f = 0.54$)[53] as standard since its emission was similar to DFP. The optical density of the standard was less than 0.1. The values of fluorescence quantum yields, $\Phi_{f(sample)}$, were calculated according to equation V-1:

$$\Phi_{f(sample)} = \Phi_{f(ref)} \frac{OD_{(ref)} I_{(sample)} n^2_{(sample)}}{OD_{(sample)} I_{(ref)} n^2_{(ref)}} \quad \text{(V-1)}$$

where Φ_f is the quantum yield, I is integrated emission signal, OD is optical density at the excitation wavelength, and n is the refractive index; subscript 'ref' stands for standard (reference sample, 'sample' stands for samples (DFP).

V.5.5 Synthesis of dye-encapsulating amine terminated SiNPs.

The amine and PEG terminated nanoparticles, with or without encapsulating the fluorenyl derivative DFP, were synthesized according to the method described by Prasad *et al.* with moderate modification.[28] Briefly, the nanoparticles were prepared by coprecipitating the dyes with polymeric organically modified silica sol in the nonpolar core of Tween-80/1-butanol micelles in deionized water. NMP was used as a hydrophilic solvent, which has unlimited water miscibility as well as suitable solubility for DFP. First, 1.0 g of VTES in 10 mL NMP was hydrolyzed and condensed in the presence of 200 μL ammonium hydroxide (28.0–30%) at room temperature for 16 h to obtain a clear solution of prepolymerized silica sol. Then, the

prepolymerized silica sol was filtered with a membrane filter (0.22 μm pore size) for further SiNP preparation. Micelles were prepared with 0.2 g of Tween-80 and 0.4 mL of 1-butanol in 10 mL of deionized water. To obtain dye-encapsulation in SiNPs, 100 μL of the sol solution was homogeneously mixed with 0.38 mL of NMP solutions without or with DFP (0 mg, 0 wt %; 0.9 mg, 10 wt %; 1.8 mg, 20 wt %; 2.7 mg, 30 wt %), followed by addition of 0.4 mL of the NMP solution by one-shot syringe injection into the prepared micelle dispersions to induce nanoprecipitation under vigorous magnetic stirring. After 30 min, 20 μL EDTA was added to functionalize the surface of the nanoparticles with amine. To ensure completion of sol-gel condensation within the coprecipitated nanoparticles, the mixtures were further stirred at room temperature for 24 h. Nanoparticle purification was conducted by dialyzing the dispersion against deionized water in a 10 kDa cutoff cellulose membrane to remove Tween-80 and 1-butanol for 48 h. The dialyzed solution was then filtered through a 0.22 μm cutoff membrane filter. The resulting nanoparticles were stored at 4 ℃ for later experiments.

V.5.6 Conjugation of amine-terminated SiNPs with MAL-PEG-SCM.

To 10 mL of DFP-doped silica nanoparticles dispersed in deionized water, 0.5 mL PBS (20×, pH = 7.4) and 10 mg MAL-PEG-SCM (M. W. 3400) in 300 μL water were added. The mixture was stirred for 30 min in the dark. The unreacted MAL-PEG-SCM polymer was removed by dialyzing the dispersion against deionized water in a 10 kDa cutoff cellulose membrane for 48 h. Finally, the dialyzed solution was filtered through a 0.22 μm cutoff membrane filter and stored at 4 °C for later experiments.

V.5.7 Surface modification of MAL-terminated SiNPs with FA.

To 2 mL of the MAL terminated SiNPs dispersed in deionized water, 0.1 mL PBS (20×, pH = 7.4) and (S)-2-(2-(4-((2-amino-4-hydroxypteridin-6-yl)methylamino)phenyl) acetamido)-5-(2-mercaptoethylamino)-5-oxopentanoic acid (FA-SH) (1 mg/mL in DMSO, 500 μL) was added, and the mixture was stirred for 1 h. The unreacted FA-SH and DSMO were removed by dialyzing the reaction mixture against deionized water in a 10 kDa cutoff cellulose membrane for 48 h. Finally, the dialyzed solution was filtered through a 0.22 μm cutoff membrane filter and stored at 4 ℃ for subsequent experiments.

V.5.8 Characterization of dye-encapsulating SiNPs

Transmission electron microscopy (TEM) images were obtained using a JEOL-JEM 1011 transmission electron microscope (JEOL, Ltd., Japan.) operating at 100 kV in bright field for the nanoparticles. A drop of SiNPs dispersed in water was placed on a holey carbon film copper grid and left to evaporate. The zeta potential measurement and particle size analysis by a light scattering method were conducted using the Zetasizer Nano-ZS90 (Malvern Instruments). ^{1}H NMR spectra of SiNPs dispersed in D_2O were recorded at 300 MHz.

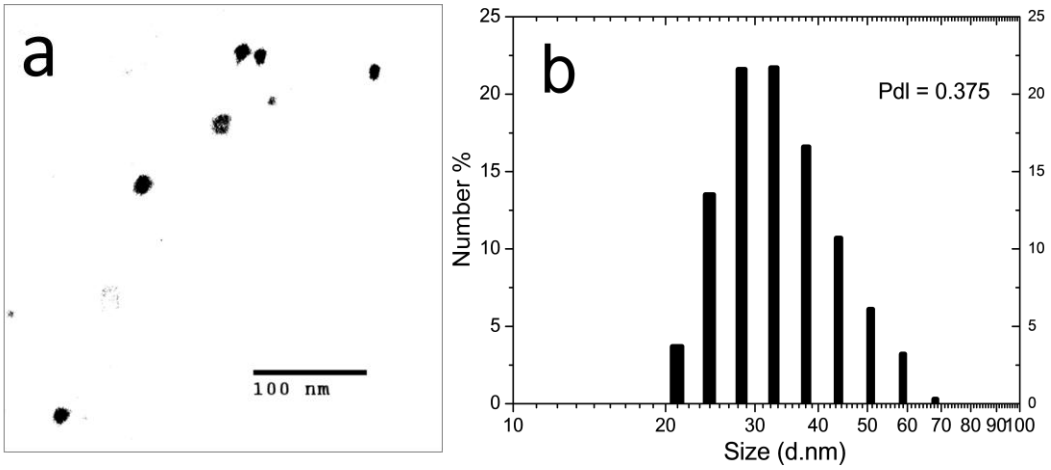

Figure V-13. A representative TEM image (a) and DLS size distribution (b) of the FA conjugated nanoparticles in PBS.

V.5.9 Determination of two-photon absorption cross sections.

The 2PA spectra of DFP in THF and $CHCl_3$ and 20 wt% SiNPs (SNP-DFP-PEGMAL) in PBS, were determined over a broad spectral region by a typical z-scan method.[3] We used a femtosecond regenerative Ti:sapphire amplifier (Coherent Legend-HE), which is seeded by a Ti:sapphire femtosecond oscillator (Coherent Mira 900). An optical parametric amplifier (OPA) (Coherent OperA-Solo) pumped by the Coherent Legend-HE provided laser pulses of 100 fs duration with a broadly adjustable wavelength. The tuning range of 700–1200 nm was used in this experiment. The z-scan measurements were performed in 1 mm quartz cuvettes with DFP at ~ 10^{-2} M in THF and SNP-DFP-PEGMAL at ~ 3×10^{-4} M in PBS. In addition, the scattering affect of the nanoparticles was checked by non-dye labeled nanoparticles with the same concentration and no significant signal was observed from the blank particles at this concentration. The uncertainty in the measured cross sections was ca. 15%.

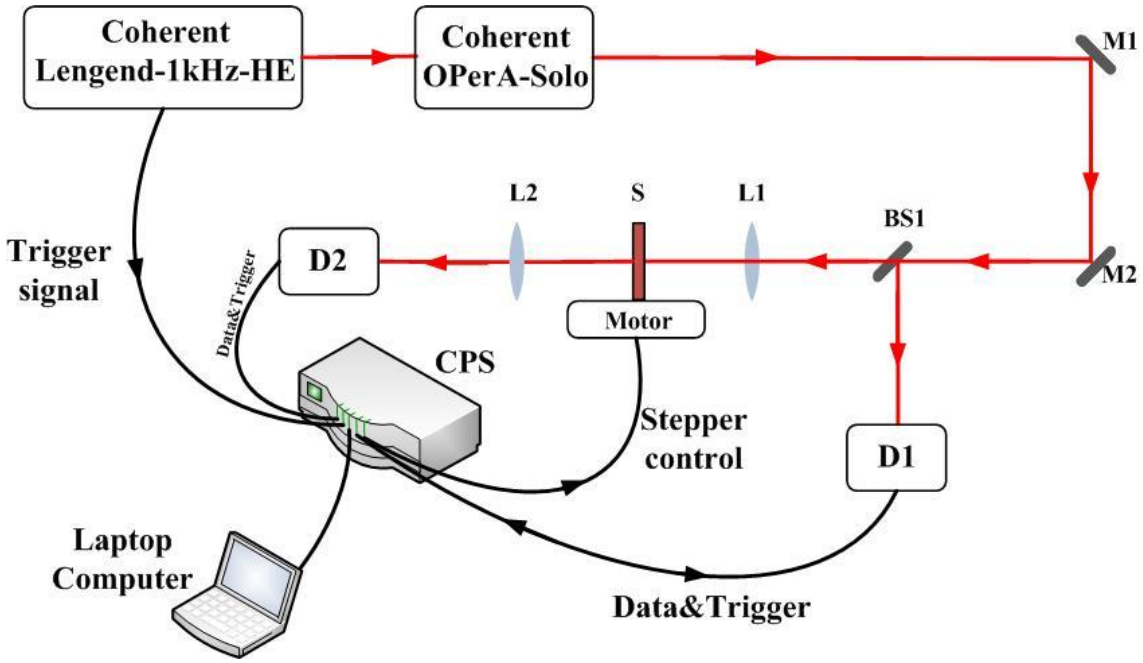

Figure V-14. Z-Scan setup for measuring absolute two-photon absorption cross sections.

V.5.10 Photostability measurement.

The photostability of dye-doped SiNPs and free dye DFP encapsulated in Tween-80 micelles in PBS were determined by the absorption method previously described.[54] A solution of SNP-DFP-PEGFA in PBS or DFP encapsulated in Tween-80 micelles in PBS was irradiated in 1 cm path length quartz cuvettes with a 501 nm Argon laser at 10 mW. The values of photodecomposition quantum yields, Φ_d, were calculated according to equation V-2, and the results are the average of ten pairs of adjacent absorbance maxima. The normalized absorbance maxima of two solutions according to the bleaching time are presented in Figure V-15,

$$\Phi_d = \frac{(A_1 - A_0)N_A}{10^3 \times \varepsilon \times I \times (1 - 10^{-(A_1+A_0)/2}) \times (t_1 - t_0)} \qquad \text{(V-2)}$$

where Φ_d is the photobleaching decomposition quantum yield, A_1 is absorbance maxim at t_1, A_0 is absorbance max at t_0, N_A is Avogadro's number, ε is molar absorbance, t_1-t_0 is time exposed (s), and I is the intensity of laser in photon·cm^{-2}·s^{-1}.

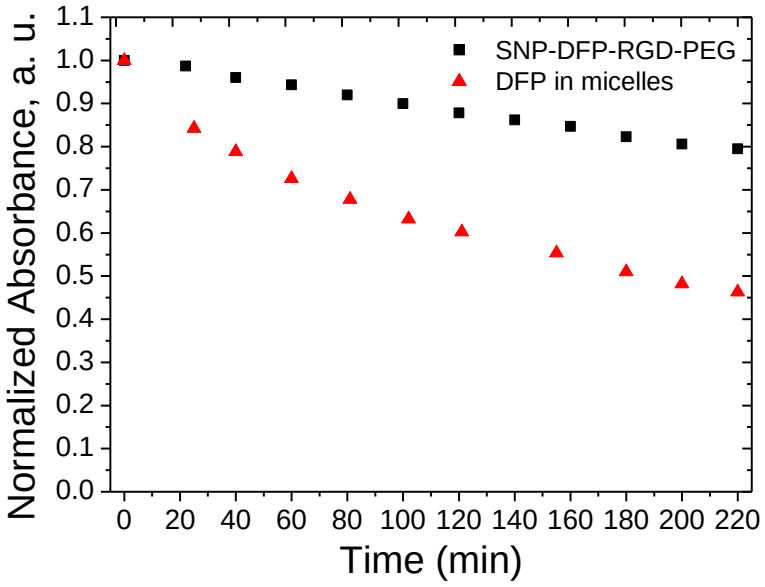

Figure V-15. Photobleaching of SNP-DPF-PEGFA and DFP encapsulated in Tween-80 micelles in PBS at 501 nm with a power of 10 mW.

V.5.11 Cytotoxicity Assay.

To assess the cytotoxicity of silica nanoprobes, 1×10^3 per well of HeLa or MG63 cells in 96-well plates were incubated in 90 μL of RPMI-1640 medium without phenol red, supplemented with 10% FBS and 100 units / mL penicillin-streptomycin for 24 h. The cells were then incubated with various amounts of SiNPs containing a certain amount of DFP (0.01, 0.1, 0.5, 1, and 5 μM) for an additional 20 h. Subsequently, 20 μL of CellTiter 96® AQueous One Solution reagent was added to each well, followed by further incubation for 4 h at 37 °C. The relative viability of the cells incubated with the silica nanoprobes to untreated cells was determined by

measuring the MTS-formazan absorbance on a microplate reader (Spectra Max M5, Molecular Devices, Sunnyvale, CA, USA) at 538 nm with subtraction of the absorbance of the cell-free nanoprobe at 538 nm. The results from three individual experiments were averaged. The cell viability data are presented in Figure V-16.

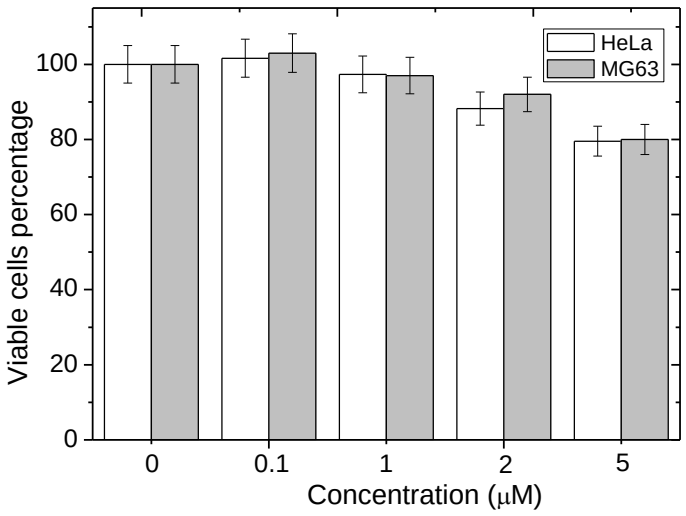

Figure V-16. Viability of HeLa and MG63 cells, incubated with SNP-DFP-PEGFA. Error bars represent standard error of the mean of 3 replicates.

V.5.12 Uptake of SiNPs by cancer cells.

HeLa or MG63 cells were placed onto poly-D-lysine coated glasses in 24-well plates (15,000 cells per well), and the cells were incubated for 48 h before incubating with dye-doped SiNPs. Stock solution of dye-doped SiNPs suspended in water was prepared as ~50 μM solution. The solution was diluted to 0.1, 1, and 5 μM solutions by complete growth medium, RPMI-1640, and freshly placed over the cells for a 2 h period. After incubation, the cells were washed with PBS (3–5×) and fixed using 3.7% formaldehyde solution for 15 min at 37 °C. To reduce

autofluorescence, a fresh solution of $NaBH_4$ (1 mg / mL) in PBS (pH = 8.0), which was prepared by adding few drops of 6N NaOH solution into PBS (pH = 7.2), was used for treating the fixed cells for 15 min (2×). The plates were then washed twice with PBS and once with water. After this, the glass coverslips were mounted by Prolong gold mounting medium for microscopy.

V.5.13 Animal model and in vivo and ex vivo imaging.

Eight-week-old female athymic nude mice were obtained from Harlan Laboratories (Indianapolis, IN). HeLa cells (5×10^6 cells) were inoculated subcutaneously into the right thighs of mice. Imaging studies were performed 10 days after the tumor inoculation; SiNPs dispersed in PBS (300 μM, ~ 0.2 mL, 3 nmol/g body weight) or vehicle (PBS, ~ 0.2 mL) were injected to the mice via the tail vein. At different times after the injection of SiNPs or vehicle, the mice were imaged using an IVIS Spectrum imaging system (Caliper Life Sciences) while under anesthesia. Fluorescence images were recorded by two channels. One channel, excitation at 500 nm, and emission at 720 nm, was used to record the fluorescence from the SiNPs, while the other channel, excitation at 605 nm and emission at 720 nm, was used to record background tissue autofluorescence. The resulting images were processed by subtracting the background tissue autofluorescence from the fluorescence from the SiNPs with software of the IVIS Spectrum imaging system. After *in vivo* imaging, the mice were euthanized with i.v. injections of xylazine and the tissue samples were collected, fixed in 4% paraformaldehyde, and cryprotected in PBS solution for *ex vivo* one- and two-photon fluorescence microscopy imaging. Two mice were examined for each sample.

V.5.14 1PFM cell, tissue and ex vivo 2PFM imaging

Conventional single-photon fluorescence cell images were obtained using an inverted microscope (Olympus IX70) equipped with a QImaging cooled CCD (Model Retiga EXi) and excitation with the filtered emission of a 100 W mercury lamp. In order to improve the fluorescence background-to-image ratios, one-photon confocal fluorescence images of the fixed cells were taken using a custom made filter cube for dye-doped SiNPs. The specifications of the filter cube were tailored to match the excitation wavelength of probes and to capture most of its emission profile. 1PFM imaging of *ex vivo* tissue sections was performed on a Leica TCS SP5 II Tandem Scanner upright multiphoton laser scanning microscopy system. Frozen tumors were sectioned by a freeze microtome (Lecia, CM1900) to ~ 20 μm thick sections. For labeling the of endothelia of blood vessels, MEC13.3 antibody (1:50 dilution in PBS) was used to react with CD31, and a labeled goat anti-mouse IgM antibody Alexa Fluor$^{@}$ 350 (1 μg/mL in PBS) was used to label the primary antibody MEC13.3. The nuclei of the sectioned tissues were stained with Hoechst 33285 (0.2 μg/mL in PBS). The section tissues were imaged and examined by laser-scanning confocal microscopy (Lecia, TCS SP5). 2PFM cell imaging was performed using a modified Olympus Fluoview FV300 microscope system coupled to a tunable Coherent Mira 900F Ti: sapphire laser (76 MHz, modelocked, 200 femtosecond pulse width, tuned to 840 nm). A short-pass emission filter (cutoff 690 nm) was placed in the microscope scanhead to avoid background irradiance from the excitation source. Consecutive layers, separated by approximately 0.15 μm for cell imaging, were recorded to create a 3D reconstruction from overlaid 2PFM images. Two-photon induced fluorescence was collected with a 60× microscope objective (UPLANSAPO 60×, NA = 1.35, Olympus). 2PFM thick tissue imaging was performed

using a Lecia TCS SP5 microscope system coupled to a tunable Coherent Chameleon Vision S (80 MHz, modelocked, 75 femtosecond pulse width, tuned to 980 nm). A short-pass emission filter (cutoff 840 nm) was placed before the CCD camera to avoid background irradiance from the excitation source. Consecutive layers, separated by approximately 0.5 μm for thick tumor imaging, were recorded to create a 3D reconstruction from overlaid 2PFM images. Two-photon induced fluorescence was collected with a water immersion high NA/low magnification objective lens HC X APO L20× (NA = 1.0, Leica) with the magnification changer in the CCD camera mode (3× magnification was used).

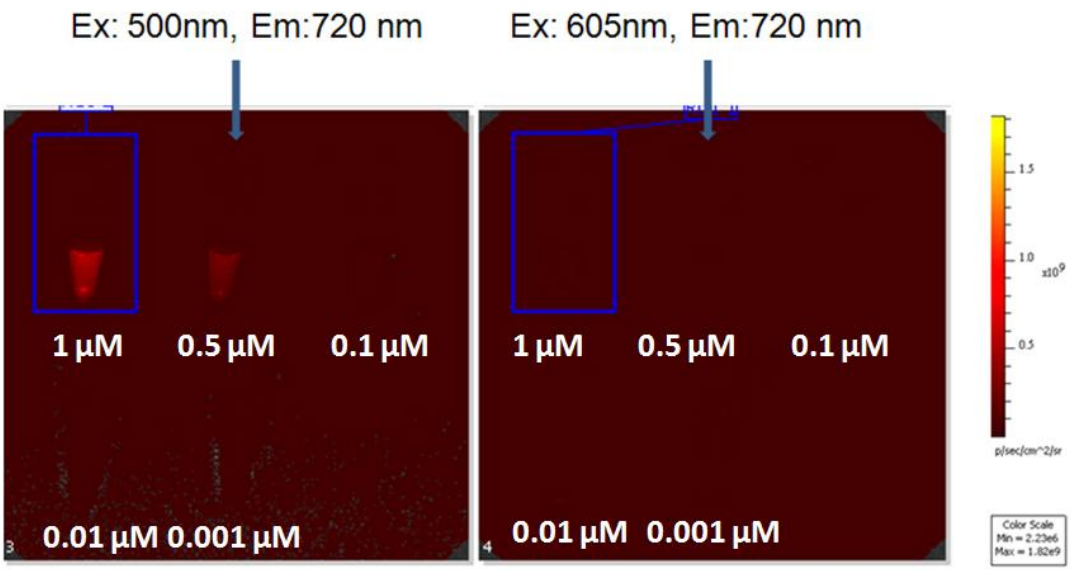

Figure V-17. Standard samples with different concentration of SNP-DFP-NH_2 in PBS (1, 0.5, 0.1, 0.01, and 0.001 μM). Filter sets for the images of standard samples in tubes are: left 500/720 and right 605/720.

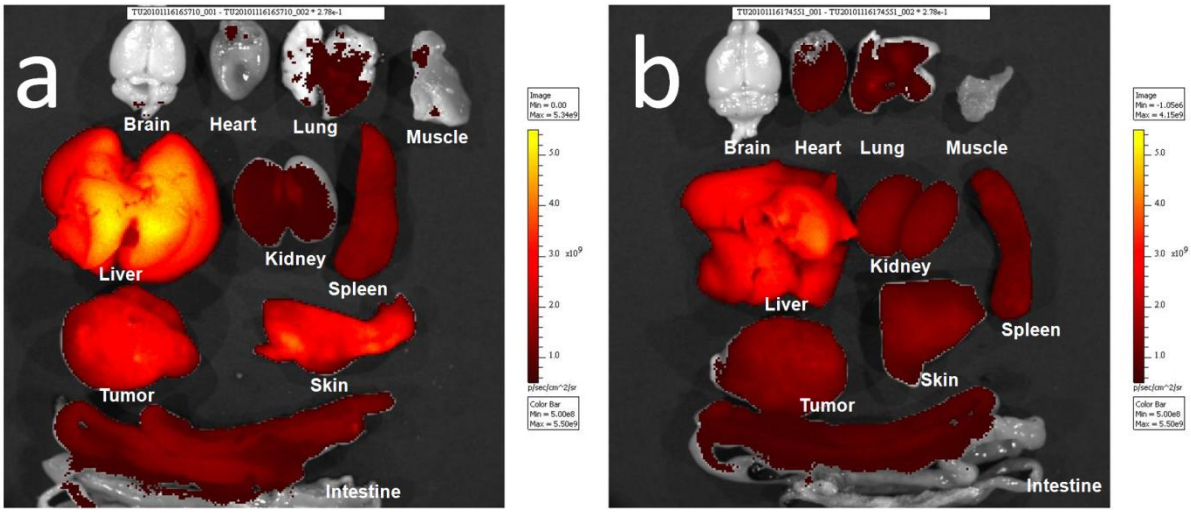

Figure V-18. *Ex vivo* images of the HeLa tumor and organs of the mice injected with (a) SNP-DFP-PEGFA and (b) SNP-DFP-PEGMAL.

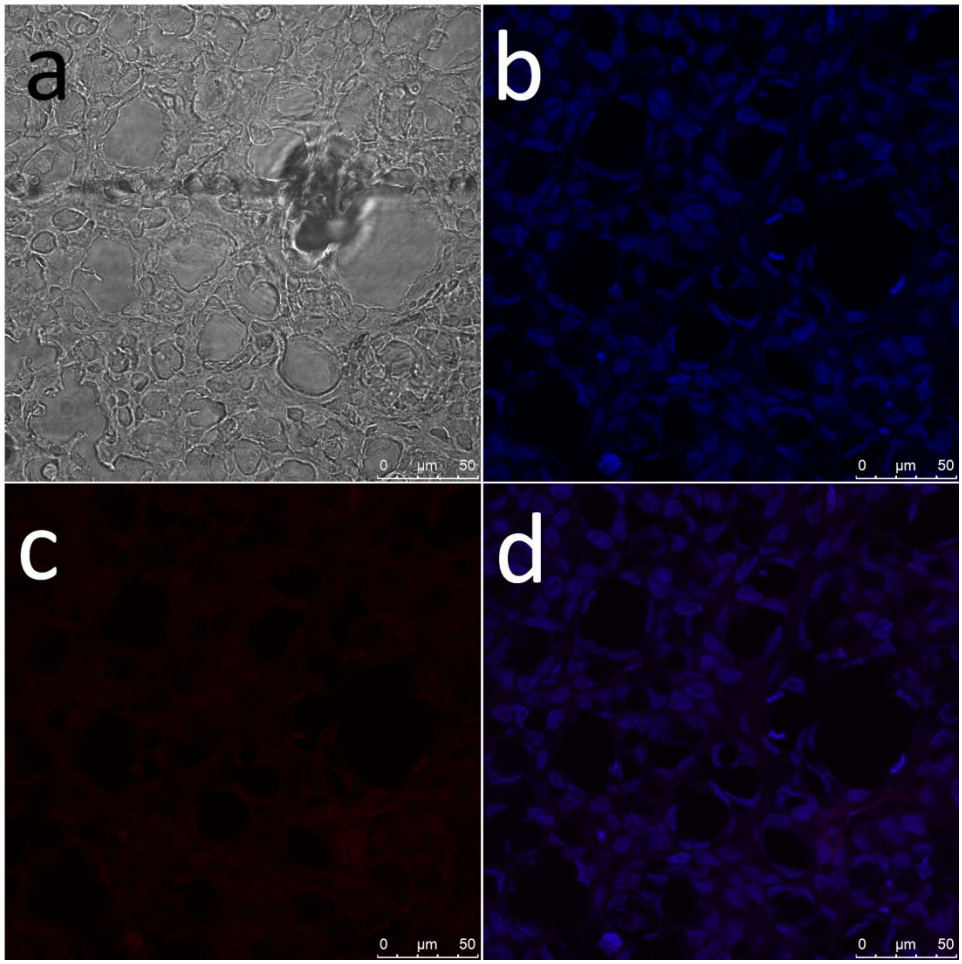

Figure V-19. One-photon confocal images of HeLa tumor tissue sections (~20 µm thick sections) from mice tail vein injected with SNP-DFP-PEGMAL (3 nmol/g body weight, 6 h p.i.); a) bright field, b) image of the nuclei of the tumor stained with Hoechst 33285 (0.2 µg/mL), Ex: 405 nm, Em: 520 – 560 nm, DM: RSP500 nm; c) image of tumor with the channel for SNP-DFP-PEGFA, Ex: 476 nm, Em: 620 - 680 nm, DM: RSP 500 nm; and d) merged image; objective 63×, NA: 1.4. Representative fields from multiple sections of two tumors are shown.

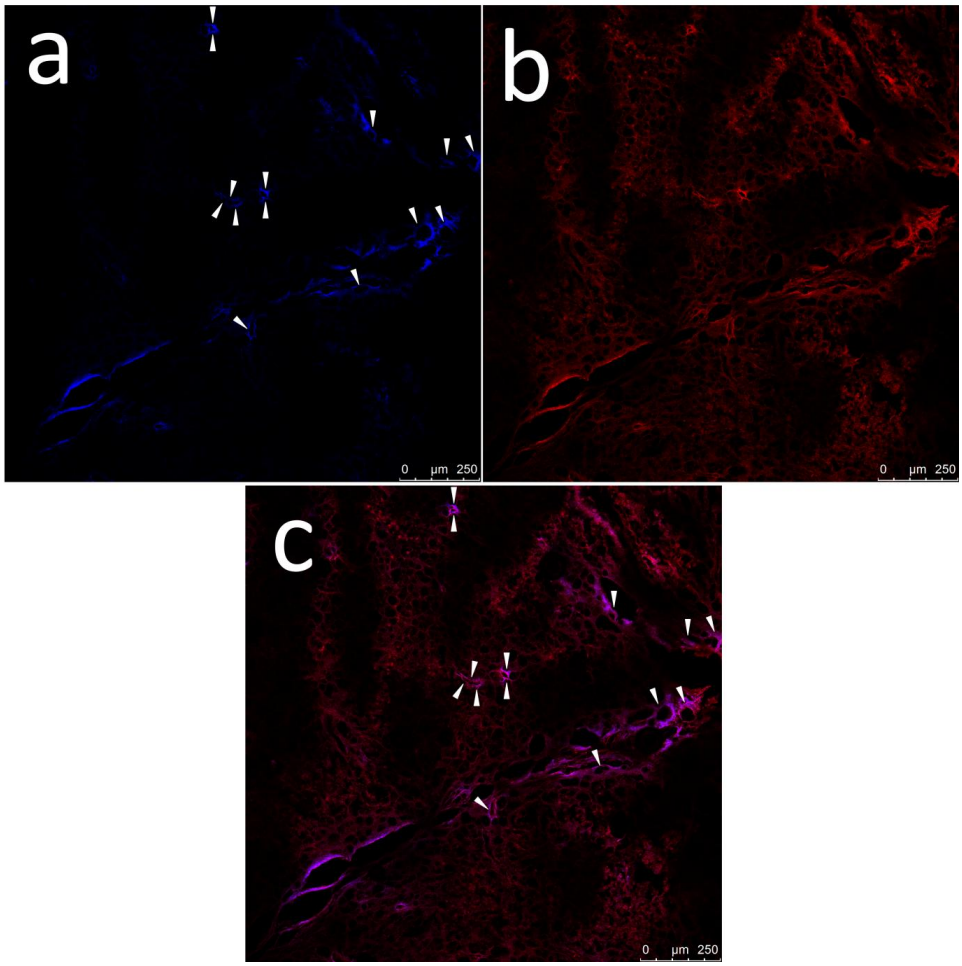

Figure V-20. One-photon confocal images of HeLa tumor (~ 20 µm sections) from mice tail vein injected with SNP-DFP-PEGFA (3 nmol/g body weight, 6 h p.i.); a) image of the CD31, primary antibody MEC13.3 (1 : 50 dilution in PBS), secondary antibody Alexa Fluor 350 goat anti-mouse IgG antibody (1 µg/mL), Ex: 351nm, Em: 450 – 560 nm; b) image of tumor with the channel for SNP-DFP-PEGFA, Ex: 476 nm, Em: 620 - 680 nm, DM: RSP 500 nm; c) merged image; Objective 10×, NA: 0.4; Representative fields from multiple sections of two tumors are shown.

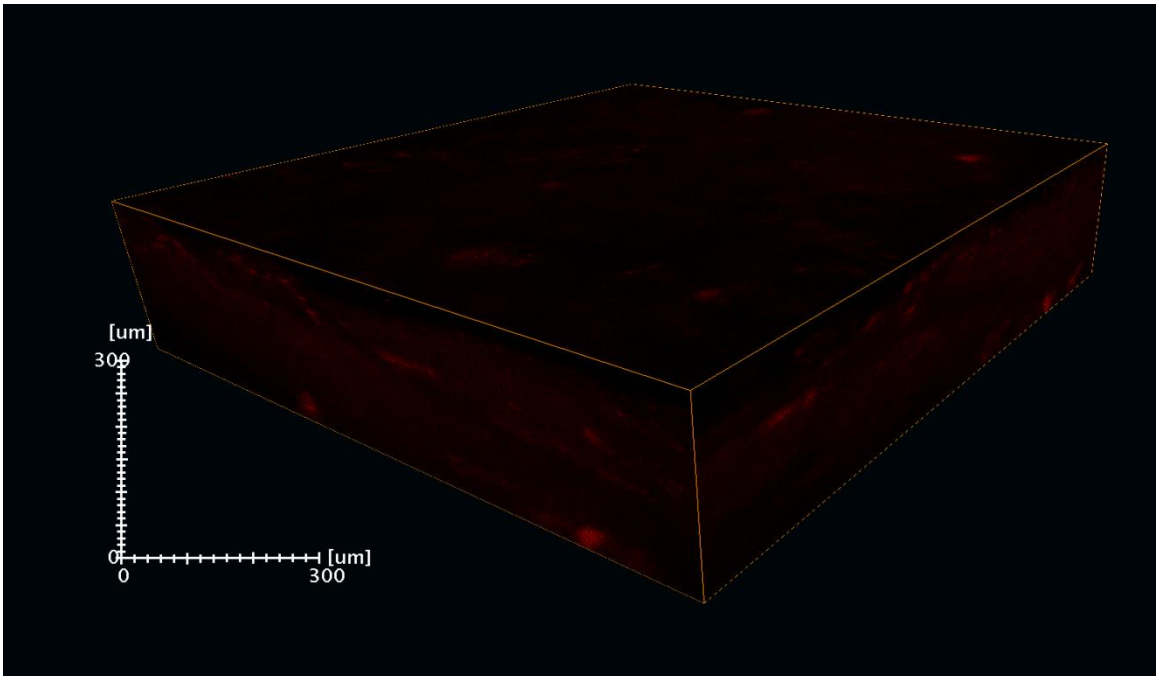

Figure V-21. Representative thick 3D-two-photon fluorescence image of the HeLa tumor from a mouse that was injected with SNP-DFP-PEGMAL (3 nmol/g) into the tail vein. Ex: 980 nm; Power: 300 mW, ~20% on the focal plane; short-pass filter 840 nm, 20× (N.A. 1.0, Lecia).

V.6 References

[1] Pawley, J. B. Handbook of biological confocal microscopy, Third Edition, Springer, New York, 2005.

[2] Prasad, P. N. Introduction to biophotonics, John Wiley & Sons, Hoborken, New Jersey, 2003.

[3] Weissleder, R. *Nature Review Cancer* **2002**, *2*, 11-18.

[4] Yang, M.; Baranov, E.; Jiang, P.; Sun, F.; Li, X.; Li, L.; Hasegawa, S.; Bouvet, M.; Tuwaijri, M.; Chishima, T.; Shimada, H.; Moossa, A. R.; Penman, S.; Hoffman, R. M. *Proc. Natl. Acad. Sci. USA* **2002**, *97*, 1206-1211.

[5] Wang, X.; Nguyen, D. M.; Yanez, C. O.; Rodriguez, L.; Ahn, H.; Bondar, M. V.; Belfield, K. D. *J. Am. Chem. Soc.* **2010**, 132, 12237-12239.

[6] Zoumi, A.; Yeh, A.; Tromberg, B. J. *Proc. Natl. Acad. Sci. USA* **2002**, *99*, 11014-11019.

[7] Svoboda, K.; Yasuda, R. N. *Neuron* **2006**, *50*, 823–839.

[8] Pavlova, I.; Hume, K. R.; Yazinski, S. A.; Peters, R. M.; Weiss, R. S.; Webb, W.W. *Proc. Soc. Photo. Opt. Instrum. Eng.* **2010**, 7569: 756918.

[9] Kelloff, G. F.; Krohn, K. A.; Larson, S. M.; Weissleder, R.; Mankoff, D. A.; Hoffman, J. M.; Link, J. M. *Clin. Cancer Res*. **2005**, *11*, 7967-7985.

[10] Master, B. R.; So, P. T. C. *Handbook of Biomedical Nonlinear Optical Microscopy*; Oxford University Press: New York, 2008.

[11] Helmchen F.; Denk, W. *Nat. Methods* **2005**, *2*, 932-940.

[12] Wang, B. G.; Känig, K.; Halbhuber, K. J. *J. Microsc.* **2010**, *238*, 1-20.

[13] Nguyen, D. M.; Wang, X.; Ahn, H.; Rodriguez, L.; Bondar, M. V.; Belfield, K. D. *ACS Appl. Mater. Interfaces* **2010**, *2*, 2978–2981.

[14] Diaspro, A. *Confocal and Two-Photon Microscopy, Foundations, Applications, and Advances*; Wiley-Liss: New York, 2002.

[15] Morales, A. R.; Schafer-Hales, K. J.; Marcus, A. I.; Belfield, K. D. *Bioconjugate Chem.* **2008**, *19*, 2559-2567.

[16] Morales, A. R. Yanez, C. O.; Schafer-Hales, K. J.; Marcus, A. I.; Belfield, K. D. *Bioconjugate Chem.* **2009**, *20*, 1992-2000.

[17] Morales, A. R.; Luchita, G.; Yanez, C. O.; Bondar, M. V.; Przhonska, O. V.; Belfield, K. D. *Org. Biomol. Chem.* **2010**, *8*, 2600-2608.

[18] Yao, S.; Ahn, H.; Wang, X.; Fu, J.; Van Stryland, E. W.; Hagan, D. J.; Belfield, K. D. *J. Org. Chem*. **2010**, *75*, 3965-3974.

[19] Andrade, C. D.; Yanez, C. O.; Rodriguez, L.; Belfield, K. D. *J. Org. Chem.* **2010**, *75*, 3975-3982.

[20] Rosenholm, J. M.; Meinander, A.; Peuhu, E.; Niemi, R.; Eriksson, J. E.; Sahlgren, C.; Lindén, M. *ACS Nano* **2009**, *3*, 197-206.

[21] Nakamura, M.; Shono, M.; Ishimura, K. *Anal. Chem.* **2007**, *79*, 6507-6514.

[22] Kumar, R.; Roy, I.; Ohulchanskky, T. Y.; Vathy, L.; Bergey, E. J.; Sajjad, M.; Prasad, P. N. *ACS Nano* **2010**, *4*, 699-708.

[23] Wang, X.; Yao, S.; Ahn, H.; Zhang, Y.; Bondar, M. V.; Torres, J. A.; Belfield, K. D. *Biomed. Opt. Express* **2010**, *1*, 453–462.

[24] Kim, S.; Zheng, Q.; He, G. S.; Bharali, D. J.; Pudavar, H. E.; Baev, A.; Prasad, P. N. *Adv. Funct. Mater.* **2006**, 16, 2317-2323.

[25] Luo, J.; Xie, Z.; Lam, J. W. Y.; Cheng, L.; Chen, H.; Qiu, C.; Kwok, H. S.; Zhan, X.; Liu, Y.; Zhu, D.; Tang, B. Z. *Chem. Commun.* **2001**, *18*, 1740-1741.

[26] An, B.; Kwon, S.; Jung, S. D.; Park, S. Y. *J. Am. Chem. Soc.* **2002**, *124*, 14410–14415.

[27] An, B.; Kwon, S.; Park, S. Y. *Angew. Chem. Int. Ed.* **2007**, *46*, 1978-1982.

[28] Lim, S.; An, B.; Jung, S. D.; Chung, M.; Park, S. Y. *Angew. Chem. Int. Ed.* **2004**, *116*, 6506-6510.

[29] Kim, S.; Pudavar, H. E.; Boniu, A.; Prasad, P. N. *Adv. Mater.* **2007**, *19*, 3719-3795.

[30] Tong, H.; Hong, Y.; Dong, Y.; Ren, Y.; Häussler, M.; Lam, J. W. Y.; Wong, K. S.; Tang, B. Z. *J. Phys. Chem. B* **2007**, *111*, 2000-2007.

[31] Pasult, G.; Veronese, F. M. *Adv. Drug Del. Rev.* **2009**, *61*, 1177-1188.

[32] Harris, J. M.; Chess, R. B. *Nature Reviews Drug Discovery* **2003**, *2*, 214-221.

[33] Davis, M. E.; Chen, Z.; Shin, D. M. *Nature Reviews Drug Discovery* **2008**, *7*, 771-782.

[34] Xiong, J.; Stehle, T.; Zhang, R.; Joachimiak, A.; Frech, M.; Goodman, S. L.; Arnaout, M. A. *Science* **2002**, *296*, 151-155.

[35] Brigger, I.; Dubernet, C.; Couvreur, P. *Adv. Drug Del. Rev.* **2002**, *54*, 631-651.

[36] Low, P. S.; Antony, A. C. *Adv. Drug Del. Rev.* **2004**, *56*, 1055–1231.

[37] Sun, C.; Veiseh, O.; Gunn, J,; Fang, C.; Hansen, S.; Lee, D.; Sze, R.; Ellenbogen, R. G.; Olson, J.; Zhang, M. *Small* **2008**, *4*, 372-379.

[38] Yang, S.; Lin, F.; Tsai, K.; Wei, M.; Tsai, H.; Wong, J.; Shieh, M. *Bioconjugate Chem.* **2010**, *21*, 679-689.

[39] Liu, Y.; Li, K.; Pan, J.; Feng, S. *Biomaterials* **2010**, *31*, 330-338.

[40] Bharali, D. J.; Lucey, D. W.; Jyakumar, H.; Pudavar, H. E.; Prasad, P. N. *J. Am. Chem. Soc.* **2005**, *127*, 11364-11371.

[41] Low, P. S.; Henne, W. A.; Doorneweerd, D. D. *Acc. Chem. Res.* **2008**, *41*, 120-129.

[42] Yu, G.; Yin, S. W.; Liu, Y. Q.; Chen, J. S.; Xu, X. J.; Sun, X. B.; Ma, D. G.; Zhan, X. W.; Peng, Q.; Shuai, Z. G.; Tang, B. Z.; Zhu, D. B.; Fang, W. H.; Luo, Y. *J. Am. Chem. Soc.* **2005**, *127*, 6335−6346.

[43] Kim S.; Ohulchanskyy, T. Y.; Pudavar, H. E.; Pandey, R. K.; Prasad, P. N. *J. Am. Chem. Soc.* **2007**, *129*, 2669−2675.

[44] Zhao, X.; Bagwe, R. P.; Tan, W. *Adv. Mater.* **2004**, 16, 173-176.

[45] Bharali, D. J.; Klejbor, I.; Stachowiak, E. K.; Dutta, P.; Roy, I.; Kaur, N.; Bergey, E. J.; Prasad, P. N.; Stachowiak, M. K. *Proc. Natl. Acad. Sci. USA* **2005**, *102*, 11539-11544.

[46] Roy, I.; Ohulchanskyy, T.Y.; Bharali, D. J.; Pudavar, H. E.; Mistretta, R. A.; Kaur, N.; Prasad, P. N. *Proc. Natl. Acad. Sci. USA* **2005**, *102*, 279-284.

[47] Kumar, R.; Roy, I.; Ohulchanskyy, T. Y.; Goswami, L. N.; Bonoiu, A. C.; Bergey, E. J.; Tramposch, K. M.; Maitra, A.; Prasad, P. N. *ACS Nano* **2008**, *2*, 449-456.

[48] Horn, D.; Rieger, J. *Angew. Chem. Int. Ed.* **2001**, 40, 4330-4361.

[49] Sheik-Bahae, M.; Said, A. A.; Wei, T. H.; Hagan, D. J.; Van Stryland, E.W. *IEEE J. Quant. Electr.* **1990**, *26*, 760 – 769.

[50] Kim, S.; Huang, H.; Pudavar, H. E.; Cui, Y.; Prasad, P. N. *Chem. Mater.* **2007**, *19*, 5650–5656.

[51] Gravier, J.; Schneider, R.; Frochot, C.; Bastogne, T.; Schmitt, F.; Didelon, J.; Guillemin, F.; Barberi-Heyob, M. *J. Med. Chem.* **2008**, *51*, 3867-3877.

[52] a) Hu, X.; Chen, X.; Liu, S. Shi, Q.; Jing, X. *J. Polym. Sci. A: Polym. Chem.* **2008**, *46*, 1852-1861. b) Chan, P.; Kurisawa, M.; Chung, J. E.; Yang, Y. *Biomaterials* **2007**, *28*, 540-549.

[53] Lakowicz, J. R. Principles of Fluorescence Spectroscopy; Plenum Press: New York, NY, 1999, pp53.

[54] Corredor, C. C.; Belfield, K. D.; Bondar, M. V.; Przhonska, O. V.; Yao, S. One- and two-photon photochemical stability of linear and branched fluorene derivatives. *J. Photonchem. Photobiol. A: Chem.* **2006**, *184*, 105-112.

CHAPTER VI: FUTURE WORK

Photodynamic therapy (PDT) is a promising and well established noninvasive modality for treating certain types of tumors. The major drawback of this therapeutic treatment is often lack of method to find the accurate tumor location and detect if the photosensitizers were efficiently delivered to subcutaneous tumor tissue for effective light irradiation.

A promising approach to address both issues is to develop so called theranostic agents, which are multi-functional constructs that target and deliver therapeutic construct and diagnostic imaging agent to pathological sites simultaneously. The hypothesis is that well-designed water soluble and biocompatible multi-functional nanomaterial-based theranostic with targeting moieties can accurately deliver the imaging agent and therapeutic construct to pathological sites. Norborne-based amphiphilic block copolymers can form nanoscale micelles or particles and are promising candidates as delivery agents. Here the challenge is how to achieve high quality images and effective localized irradiation for singlet oxygen generation *in vivo*. For the imaging segment, the theranostic agents can be functionalized with highly efficient two-photon absorbing moieties for two-photon fluorescence microscopy (2PFM) and two-photon fluorescence lifetime imaging microscopy (2PFLIM) or polymer stabilized magnetic nanoparticles for magnetic resonance imaging (MRI). These techniques are all well known for their ability of collect *in vivo* deep tissue images with 3D resolution. So, the following two areas are proposed for future work:

I. In vivo bioimaging.

The application of biocompatible and biodegradable nanoprobes for targeting bioimaging is an interesting area for early cancer digenesis. However, safety and efficiency needs be investigated before clinical application while their bio-distribution and clearance pathway in live animals also needs elucidation.

II. In vivo photodynamic therapy research.

A series of aggregation-enhanced emission dyes have developed, and, perhaps, can be employed as energy donors for photosensitizes in multiphoton photodynamic therapy to achieve a deep tissue penetration. Certain biomolecules, such as peptides, can be used to functionalize the nanomaterials to enhance their targeting and tissue penetration efficiency. Thus, appropriately functionalized block copolymer scaffolds can be prepared that incorporate 2PA dyes, photosensitizes, and peptide targeting agents. Amphiphilic block copolymers may be able to be constructed that form micelles that induced aggregation of the 2PA dyes (designed for aggregate-enhanced 2PA and emission), affording two-photon based theranostic probes with unprecedented efficiency.

APPENDIX A ^{1}H AND ^{13}C NMR SPECTRA OF NEW COMPOUNDS IN CHAPTER II

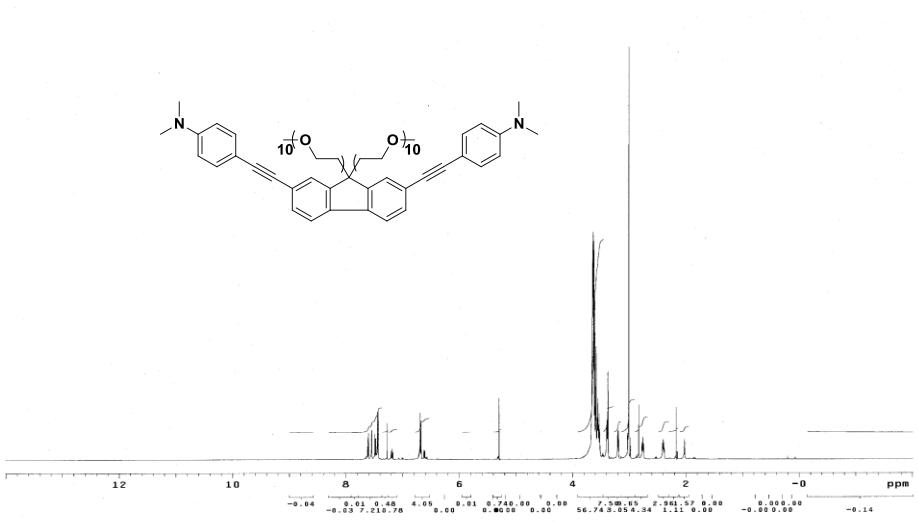

Figure A1. ^{1}H NMR spectrum of LT1 in $CDCl_3$.

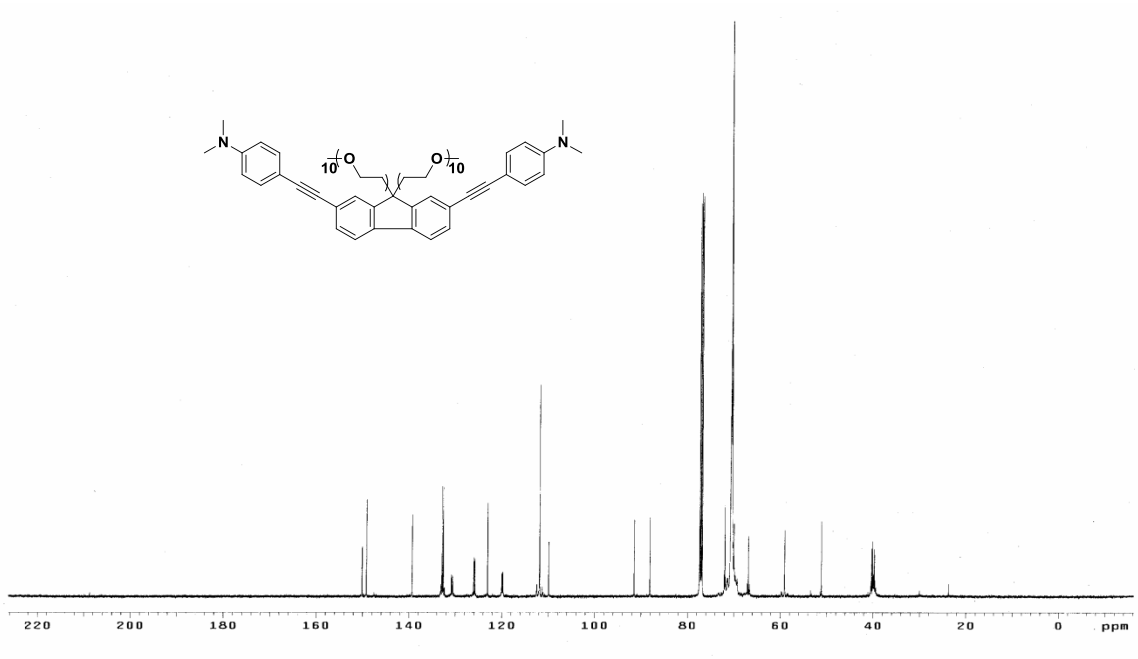

Figure A2. ^{13}C NMR spectrum of LT1 in $CDCl_3$.

APPENDIX B ^{1}H NMR SPECTRA OF THE MATERIALS IN CHAPTER V

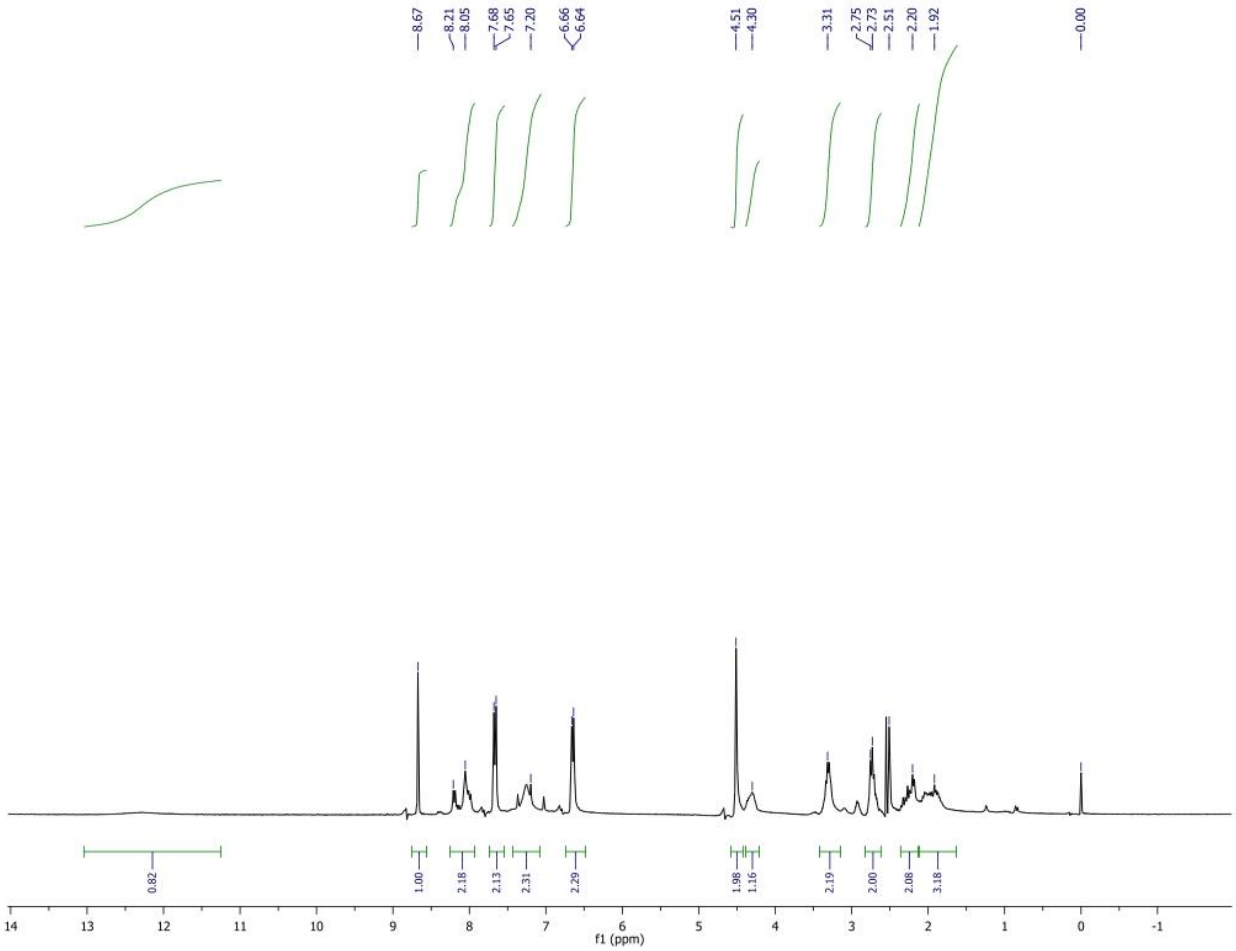

Figure B1. ^{1}H NMR spectrum of FA-SH in DMSO-d_6.

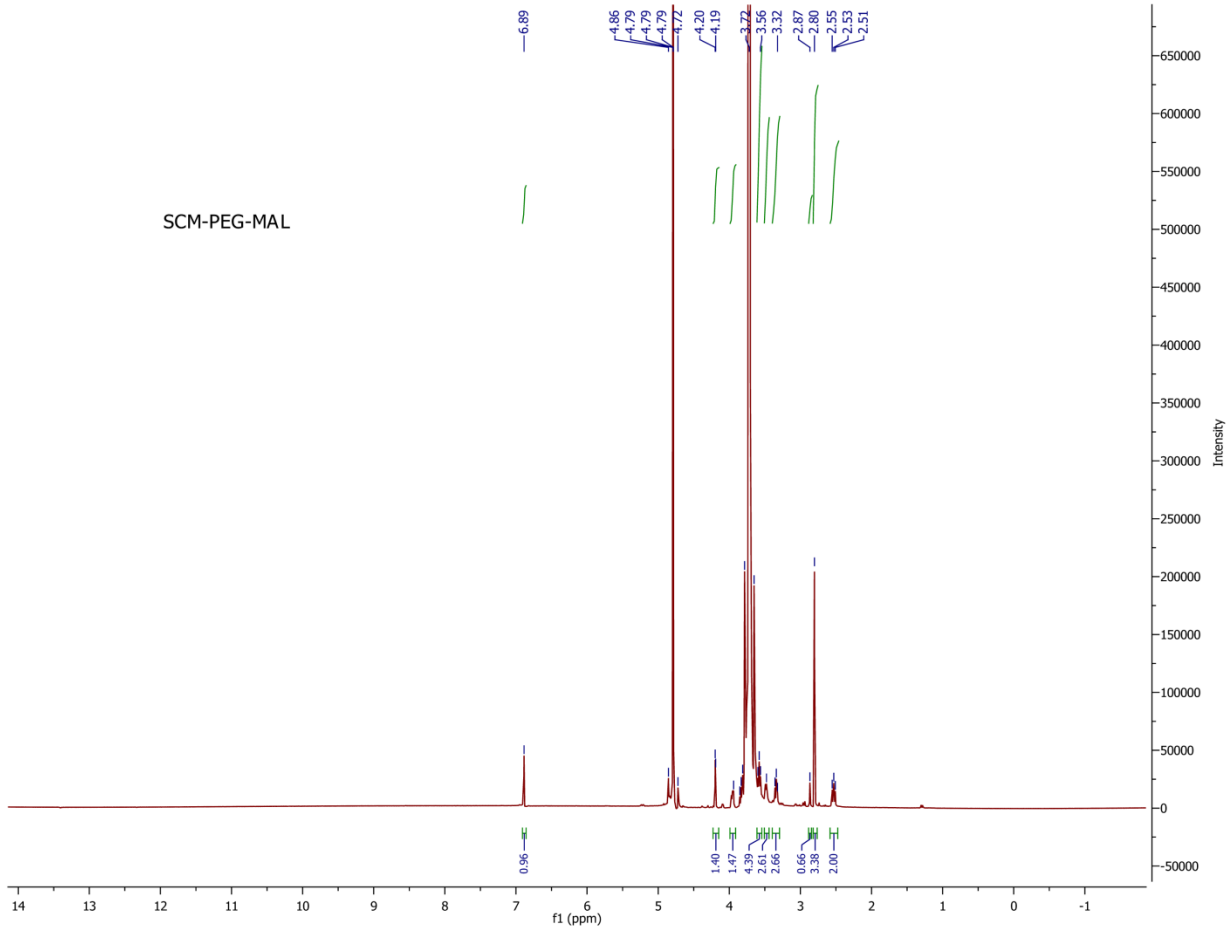

Figure B2. ^{1}H NMR spectrum of SCM-PEG-MAL in D_2O.

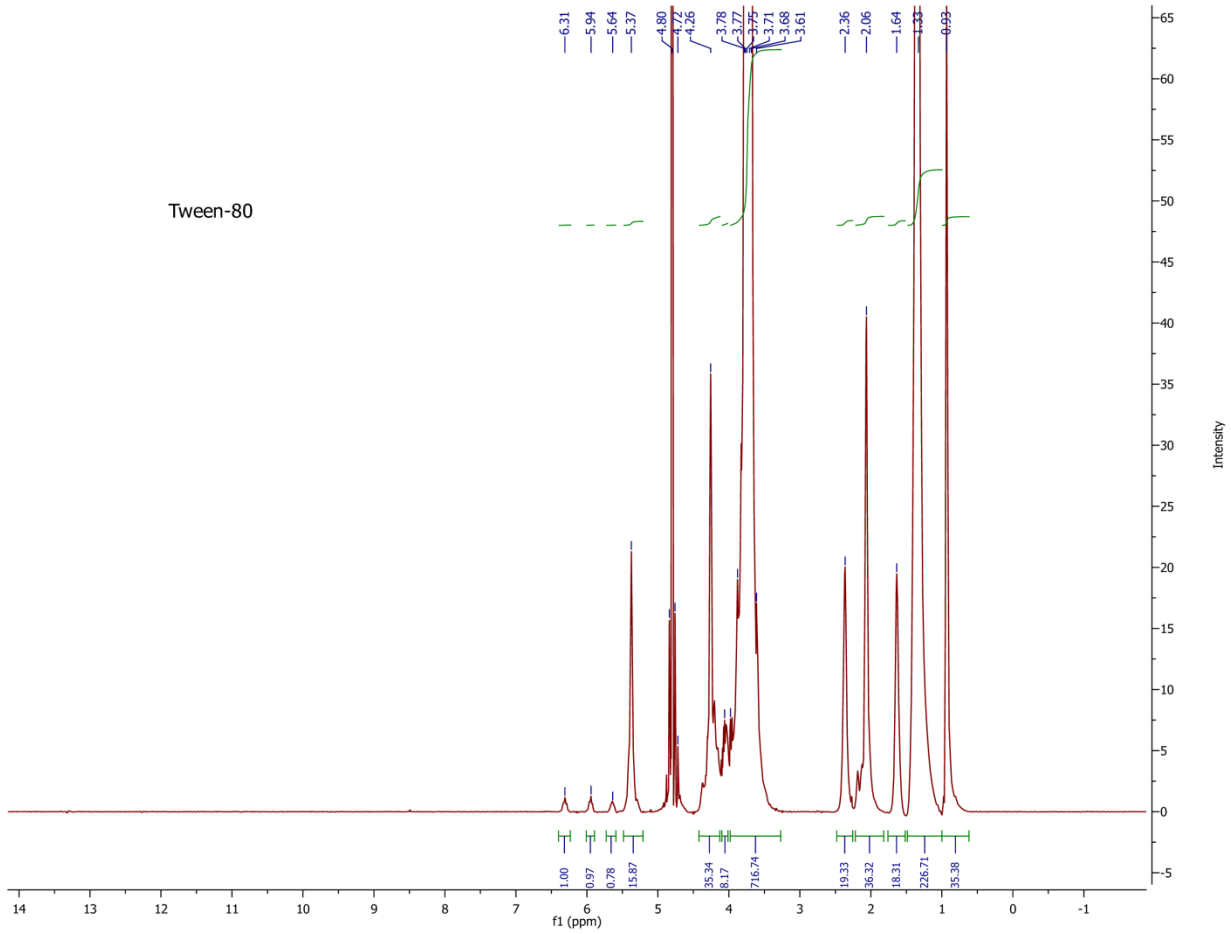

Figure B3. ^{1}H NMR spectrum of Tween-80 in D_2O.

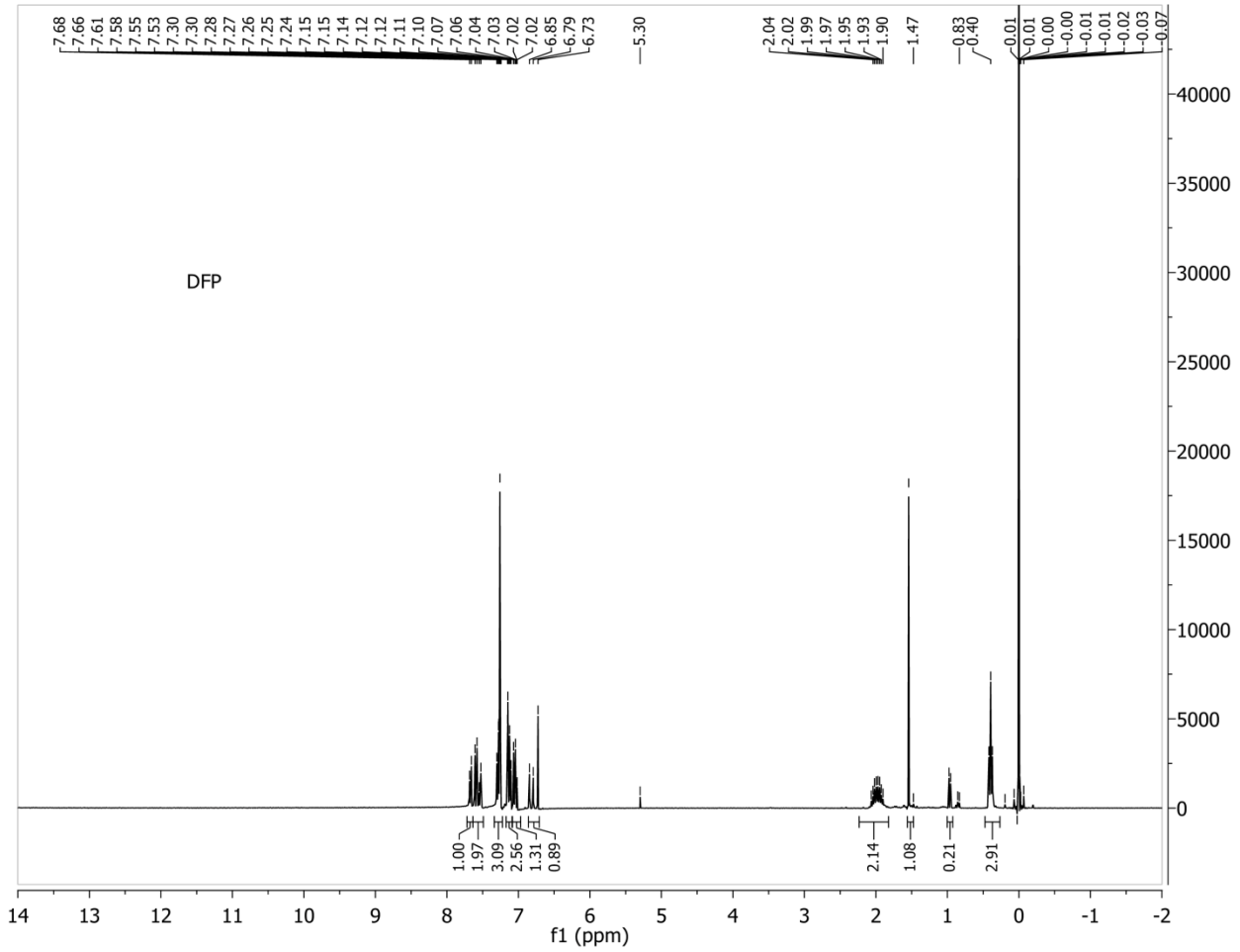

Figure B4. ^{1}H NMR spectrum of DFP in $CDCl_3$.

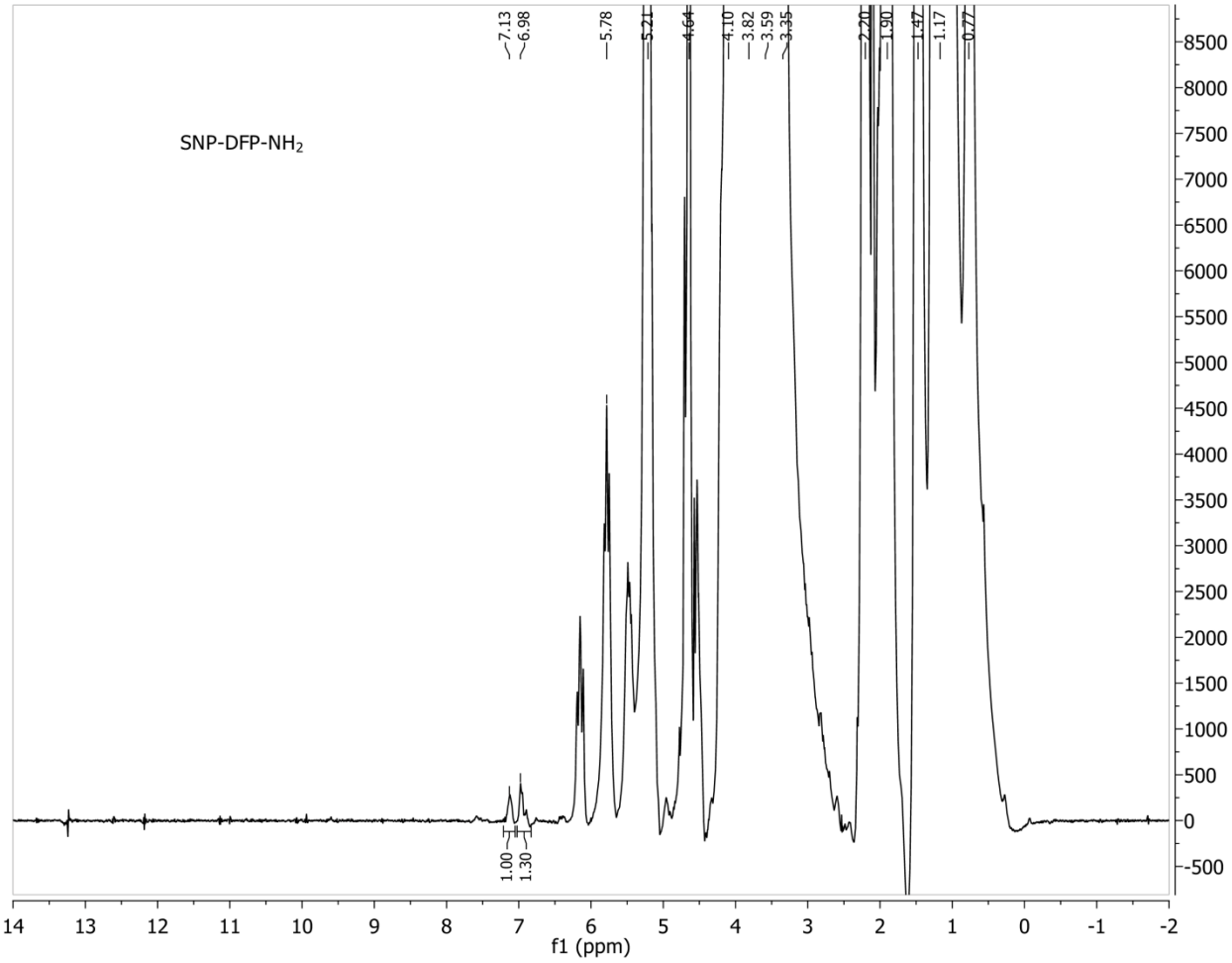

Figure B5. ^{1}H NMR spectrum of SNP-DFP-NH_2 in D_2O.

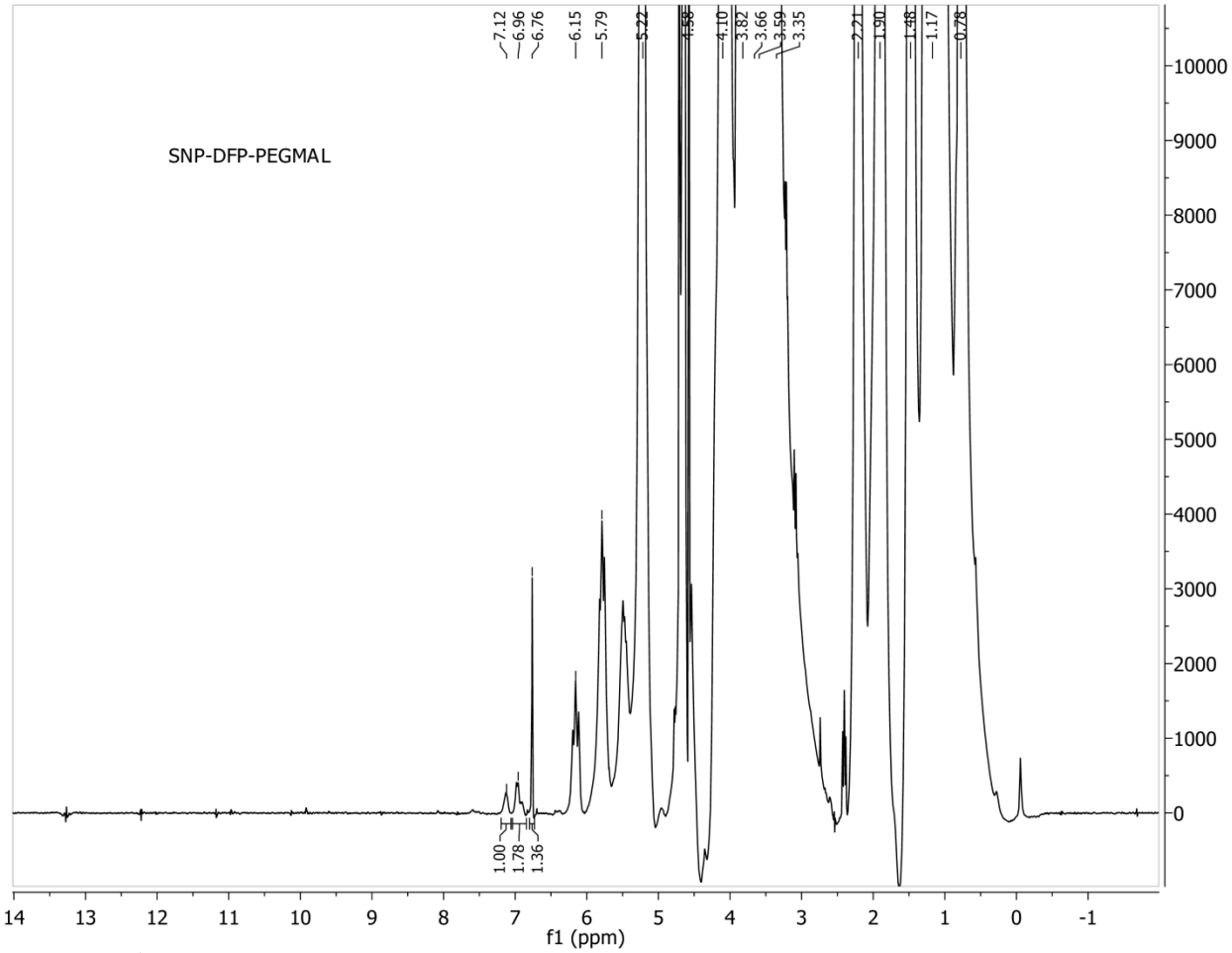

Figure B6. ^{1}H NMR spectrum of SNP-DFP-PEGMAL in D_2O.

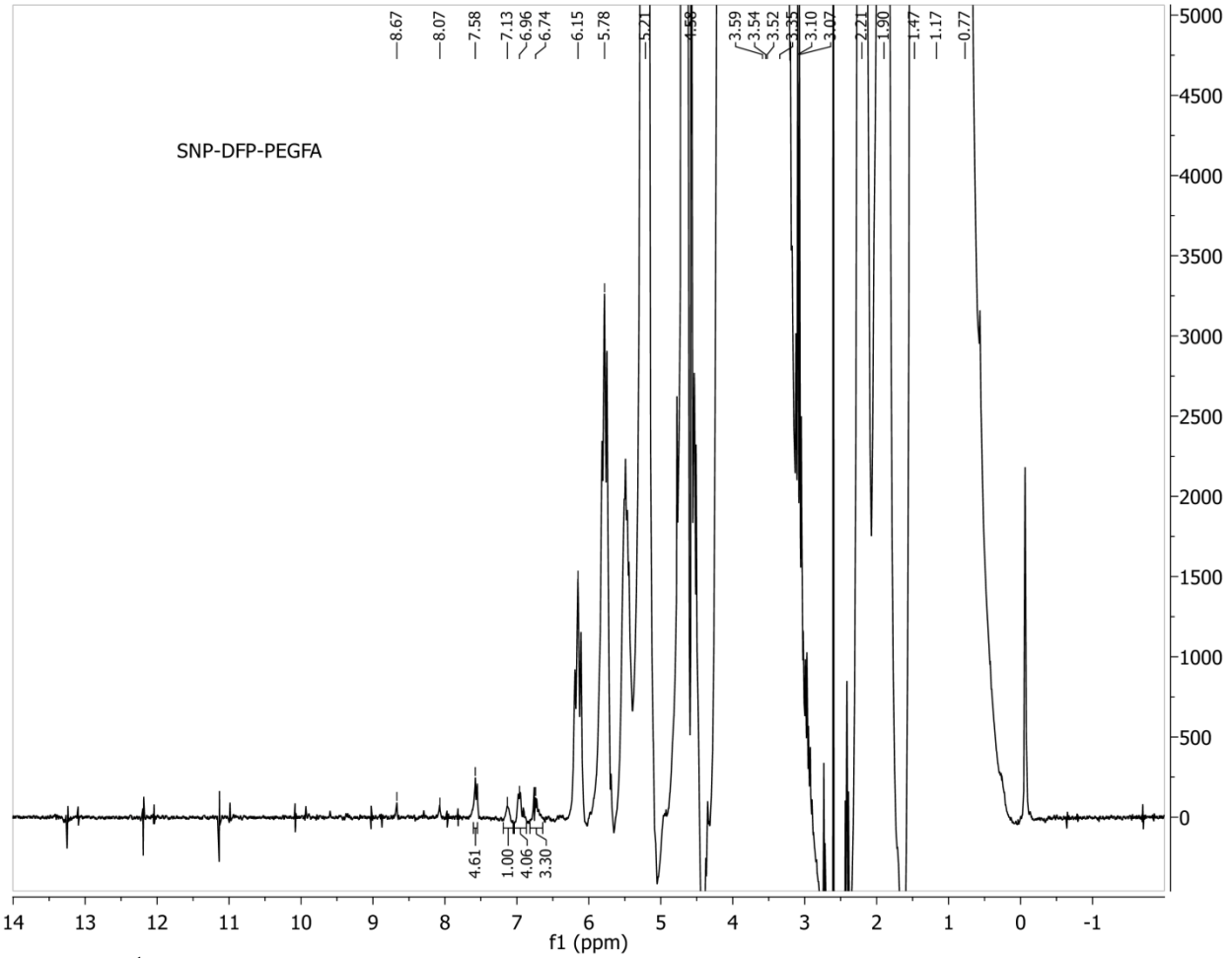

Figure B7. ^{1}H NMR spectrum of SNP-DFP-PEGFA in D_2O.

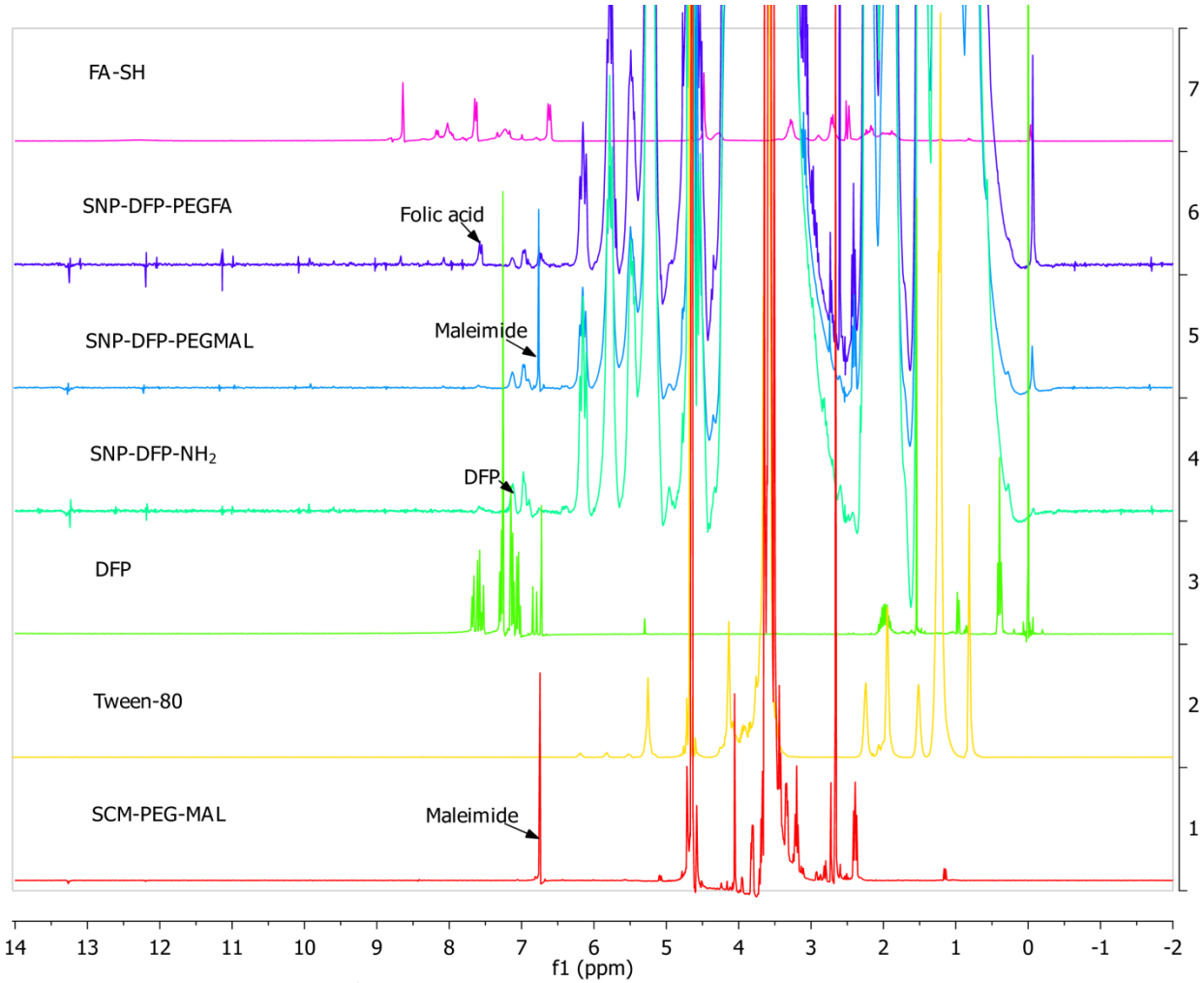

Figure B8. Stacked plot of the ^{1}H NMR spectra of the materials.